STUDY ON ENERGY STORAGE ABILITY OF ZnO/TiO_2 FOR PHOTOCATALYTIC DEGRADATION OF ISOPROPANOL

Ratchawan Jarumanee

A Thesis Submitted in Partial Fulfillment of the Requirements
for the Degree of Master of Science
The Petroleum and Petrochemical College, Chulalongkorn University
in Academic Partnership with
The University of Michigan, The University of Oklahoma,
Case Western Reserve University, and Institut Français du Pétrole
2017

บทคัดย่อและแฟ้มข้อมูลฉบับเต็มของวิทยานิพนธ์ตั้งแต่ปีการศึกษา 2554 ที่ให้บริการในคลังปัญญาจุฬาฯ (CUIR)
เป็นแฟ้มข้อมูลของนิสิตเจ้าของวิทยานิพนธ์ที่ส่งผ่านทางบัณฑิตวิทยาลัย
The abstract and full text of theses from the academic year 2011 in Chulalongkorn University Intellectual Repository(CUIR)
are the thesis authors' files submitted through the Graduate School.

Thesis Title: Study on Energy Storage Ability of ZnO/TiO_2 for Photocatalytic Degradation of Isopropanol

By: Ratchawan Jarumanee

Program: Petrochemical Technology

Thesis Advisors: Prof. Pramoch Rangsunvigit
Asst. Prof. Pailin Ngaotrakanwiwat

Accepted by The Petroleum and Petrochemical College, Chulalongkorn University, in partial fulfillment of the requirements for the Degree of Master of Science.

..... College Dean
(Prof. Suwabun Chirachanchai)

Thesis Committee:

.....
(Prof. Pramoch Rangsunvigit)

.....
(Asst. Prof. Pailin Ngaotrakanwiwat)

.....
(Assoc. Prof. Siriporn Jongpatiwut)

.....
(Assoc. Prof. Paisan Kongkachuichay)

ABSTRACT

5871016063: Petrochemical Technology Program
Ratchawan Jarumanee: Study on Energy Storage Ability of ZnO/TiO_2 for Photocatalytic Degradation of Isopropanol.
Thesis Advisors: Prof. Pramoch Rangsunvigit, and Asst. Prof. Pailin Ngaotrakanwiwat 84 pp.
Keywords: Photocatalytic degradation/ Photocatalyst/ TiO_2/ Isopropanol/ Energy storage

The photocatalytic degradation of isopropanol under UV irradiation was studied by using p-n junction of ZnO/TiO_2 photocatalysts prepared by sol-gel technique. Their energy storage ability was tested with their photocatalytic activity where there was no UV illumination. That was investigated by illumination the system with UV light for 2 h and off for 2 h until 8 h. The composition and surface structure of the catalyst were characterized by X-ray diffraction (XRD), scanning electron microscopy (SEM), surface area analysis, and particle size analysis. The change in the isopropanol concentration was observed by using gas chromatography. The result showed that the degradation efficiency of the ZnO doped on TiO_2 layer films was higher than the single-TiO_2 thin film, about 74.0% and 48.0%, respectively. Moreover, acetone was found during the photocatalytic degradation process of isopropanol. The effects of isopropanol solution pH, ZnO loading, and ZnO calcination temperature were studied. ZnO calcined at 600ºC and 15 mol% at unadjusted pH was suitable for both photocatalytic activity and energy storage. The photocatalytic degradation rates of isopropanol for the first and second illumination were about 21.0% and 20.8%, respectively. With no illumination, the highest degradation of isopropanol was about 14.8%.

บทคัดย่อ

รัชวรรณ จารุมณี : การศึกษาความสามารถในการกักเก็บพลังงานของตัวเร่งปฏิกิริยาเชิงแสงซิงค์ออกไซด์บนไททาเนียมไดออกไซด์เพื่อสลายไอโซโพรพานอล (Study on Energy Storage Ability of ZnO/TiO_2 for Photocatalytic Degradation of Isopropanol) อ. ที่ปรึกษา : ศ. ปราโมช รังสรรค์วิจิตร และ ผศ.ดร.ไพลิน เงาตระการวิวัฒน์ 84 หน้า

เพื่อทำศึกษาการสลายตัวเชิงแสงของไอโซโพรพานอลภายใต้แสงอัลตราไวโอเลต โดยใช้ตัวเร่งปฏิกิริยาเชิงแสงชนิดพี-เอ็น ของซิงค์ออกไซด์บนไททาเนียมไดออกไซด์ โดยใช้วิธีการสังเคราะห์ด้วยเทคนิคโซลเจล และศึกษาความสามารถในการเก็บสะสมพลังงานของตัวเร่งปฏิกิริยาเชิงแสงซึ่งทดสอบโดยวัดความว่องไวของการสลายตัวในสภาวะที่ไม่มีแสงอัลตราไวโอเลต ในการศึกษาจะเปิดแสงอัลตราไวโอเลตเป็นเวลา 2 ชั่วโมง และไม่มีแสงเป็นเวลา 2 ชั่วโมง จนครบ 8 ชั่วโมง โดยที่ความเข้มข้นของไอโซโพรพานอลตรวจวัดด้วยโครมาโทกราฟีแบบแก๊ส อีกทั้งทำการวิเคราะห์ลักษณะโครงสร้าง และพื้นที่ผิวของตัวเร่งปฏิกิริยาเชิงแสงโดยใช้กล้องจุลทรรศน์อิเล็กตรอนแบบส่องกราด เครื่องเอกซ์เรย์ดิฟแฟรกชัน เครื่องวิเคราะห์คุณลักษณะพื้นที่ผิว และเครื่องวัดขนาดอนุภาค จากผลการศึกษาพบว่าการสลายไอโซโพรพานอลโดยใช้ซิงค์ออกไซด์บนไททาเนียมไดออกไซด์มีประสิทธิภาพมากกว่าไททาเนียมไดออกไซด์ ซึ่งมีค่าร้อยละการสลายเท่ากับ 74.0 และ 48.0 ตามลำดับ และยังตรวจพบสารอะซิโตนในระหว่างปฏิกิริยาการสลายไอโซโพรนอล นอกจากนี้ได้ศึกษาผลของการเปลี่ยนแปลงของค่าแสดงความเป็นกรด-เบสของสารละลายไอโซโพรพานอล ปริมาณของซิงค์ออกไซด์ และอุณหภูมิแคลไซน์ ต่อความความสามารถในการกักเก็บพลังงานของตัวเร่งปฏิกิริยาเชิงแสง สภาวะที่เหมาะสมในการศึกษา ความความสามารถในการกักเก็บพลังงานของตัวเร่งปฏิกิริยาเชิงแสงคือซิงค์ออกไซด์แคลไซน์ที่อุณหภูมิ 600 องศาเซลเซียส และปริมาณซิงค์ออกไซด์ 15 ร้อยละโดยโมล ในสภาวะที่ไม่มี การปรับค่าพีเอช อัตราการสลายตัวเชิงแสงของไอโซโรพานอล ในการให้แสงครั้งแรกและครั้งที่สองมีค่าประมาณ 21.0% และ 20.8% ตามลำดับ ในสภาวะไม่มีแสง อัตราการย่อยสลายสูงสุดของไอโซโพรพานอล มีค่าประมาณ 14.8%

ACKNOWLEDGEMENTS

I would like to express my sincere thanks to my thesis advisor, Prof. Pramoch Rangsunvigit, for his invaluable help and constant encouragement throughout the course of this research. I am most grateful for his discussions and advices. I would not have achieved this far and this thesis would not have been completed without all support that I have always received from him.

I would like to thank my co-advisors, Asst. Prof. Pailin Ngaotrakanwiwat for suggestions, guidances, and all their helps.

I would also like to thank to the thesis committees, Assoc. Prof. Siriporn Jongpatiwut and Assoc. Prof. Paisan Kongkachuichay.

In addition, I would like to thank the entire faculty and staff at the Petroleum and petrochemical College, Chulalongkorn University and Department of Chemical Engineering, Burapha University for their kind assistance and cooperation.

Unforgettably, I am grateful for the partial scholarship and partial funding of the thesis work provided by the Petroleum and Petrochemical College, and the Center of Excellence on Petrochemical and Materials Technology, Thailand. And this research was partially supported by The 90th Anniversary of Chulalongkorn University Fund (Ratchadaphiseksomphot Endowment Fund), Chulalongkorn University, Thailand and National Research Council of Thailand.

Finally, I most gratefully acknowledge my parents and my friends for all their support throughout the period of this research.

TABLE OF CONTENTS

		PAGE
Title Page		i
Abstract (in English)		iii
Abstract (in Thai)		iv
Acknowledgements		v
Table of Contents		vi
List of Tables		ix
List of Figures		x
CHAPTER		
I	**INTRODUCTION**	1
II	**THEORETICAL BACKGROUND AND LITERATURE REVIEW**	4
	2.1 Principle of Photocatalysis	4
	2.2 Titanium Dioxide (TiO_2)	9
	2.2.1 Structure of TiO_2	10
	2.2.2 Photocatalytic Degradation Mechanism of Titanium Dioxide	11
	2.2.3 Doping of Titanium Dioxide	13
	2.3 Photocatalytic Degradation Mechanism of Zinc Oxide	16
	2.4 Isopropanol	19
	2.5 Oxidation Energy Storage of TiO_2	23
	2.5.1 p-n Junction Model	26
	2.5.2 Mediation Model	27
	2.6 Sol-Gel Method for Thin Film Preparation	30

CHAPTER **PAGE**

III EXPERIMENTAL 34

3.1 Chemicals and Equipment 34

3.1.1 Chemicals 34

3.1.2 Equipment 34

3.2 Experimental Procedures 35

3.2.1 ZnO doped on TiO_2 Bilayer Films 35

3.2.2 Photocatalytic Activity 35

3.2.3 Physical Characterization 36

3.3 Analytical Techniques 36

3.3.1 Gas Chromatography 36

3.3.2 XRD Spectrometer 36

3.3.3 SEM Spectrometer 36

3.3.4 Surface Area Analyzer 36

3.3.5 Particle Size Analyzer 37

IV RESULT AND DISCUSSION 38

4.1 Catalyst Characterization 38

4.1.1 Scanning Electron Microscopy 38

4.1.2 Particle Size Analysis 40

4.1.3 Brunauer-Emmett-Teller Surface Area Analysis 42

4.1.4 X-ray Diffraction 42

4.2 Photocatalytic Activity 45

4.2.1 Photocatalytic Activity of TiO_2, ZnO, 400ZnO/TiO_2, 500ZnO/TiO_2, and 600ZnO/TiO_2 Films 46

4.3 Energy Storage 50

4.3.1 Energy Storage of TiO_2 Films 50

4.3.2 Energy Storage of ZnO Films 51

4.3.3 Effects of UV Exposure Time of the 600ZnO/TiO_2 Bilayer Film on the Oxidation Energy Storage 52

CHAPTER **PAGE**

4.3.4 pH Effects on the ZnO/TiO_2 Bilayer Film Activity on the Photocatalytic Reaction 54
4.3.5 pH Effects on the ZnO/TiO_2 Bilayer Film Activity on the Oxidation Energy Storage 56
4.3.6. Effects of ZnO Loading of the $600ZnO/TiO_2$ Bilayer Film on the Oxidation Energy Storage 57
4.3.7 Effects of ZnO Calcination Temperature of the ZnO/TiO_2 Bilayer Film on the Oxidation Energy Storage 63
4.3.8 Photocatalytic degradation of TiO_2, $400ZnO/TiO_2$, $500ZnO/TiO_2$, $600ZnO/TiO_2$, and ZnO Films on the Oxidation Energy Storage 68

V **CONCLUSIONS AND RECOMMENDATIONS** 70
5.1 Conclusions 70
5.2 Recommendations 70

REFERENCES 71

APPENDICES 81
Appendix A Standard X-ray Diffraction Powder Patterns of TiO_2 81
Appendix B Standard X-ray Diffraction Powder Patterns of ZnO 82
Appendix C Calculation sample of ZnO loadings on TiO_2 layer 83

CURRICULUM VITAE 84

LIST OF TABLES

TABLE		PAGE
4.1	Effect of calcination temperatures on the physical properties of ZnO	42
4.2	Crystallite size of ZnO/TiO_2 bilayer films estimated using the XRD technique and Scherrer's equation	44
4.3	Reaction rates of isopropanol by the ZnO/TiO_2 bilayer films with different pH	57
4.4	Reaction rates of isopropanol by the ZnO/TiO_2 bilayer films with different ZnO loading	62
4.5	Reaction rates of isopropanol by the ZnO/TiO_2 bilayer films with different ZnO calcinations temperature	68

LIST OF FIGURES

FIGURE **PAGE**

2.1 Schematic representation of semiconductor energy band. 5

2.2 Basic processes of charge carrier generation upon the light irradiation of a semiconductor particle; E_{ph}: energy of irradiated photon, A: electron acceptor, D: electron donor. 5

2.3 Schematic diagram of photocatalytic degradation of organic effluent. 6

2.4 Schematic conventional cells for anatase (a), rutile (b) and brookite (c). 10

2.5 Modification of titania photocatalyst by using metal doping. 13

2.6 Mechanism of TiO_2 photocatalysis: hv_1: pure TiO_2; hv_2: metal-doped TiO_2 and hv_3: nonmetal-doped TiO_2. 14

2.7 Schematic diagram of electron-hole separation process. 17

2.8 Molecular structure of isopropanol. 20

2.9 p-n junction of semiconductor. 24

2.10 Negative and positive barrier of semiconductor. 24

2.11 Depletion region of semiconductor. 25

2.12 p-n junction model for the oxidative energy storage photocatalysts. 26

2.13 Band gaps and band positions of a) n-type semiconductors and b) p-type semiconductors used for composite photocatalyst heterojunction. 27

2.14 Mediation model for the oxidative energy storage photocatalysts. 28

2.15 Schematic simplify diagram of sol-gel method associate with dip-coating. 31

2.16 Schematic of the spin coating process. 32

4.1 SEM micrographs of TiO_2 film at (a) 400X and (b) 10,000X magnification, respectively. 39

FIGURE **PAGE**

4.2 SEM micrographs of ZnO/TiO_2 film at (a) 400X and (b) 10,000X magnification, respectively. 39

4.3 ZnO particle size diameters with different calcination temperature. 40

4.4 SEM micrographs of (a) 400ZnO, (b) 500ZnO, and (c) 600ZnO at 70,000X magnification. 41

4.5 XRD patterns of TiO_2, ZnO and ZnO/TiO_2 bilayer films. 43

4.6 XRD patterns of 400, 500 and 600ZnO/TiO_2 bilayer films. 44

4.7 XRD patterns of ZnO/TiO_2 bilayer films with different ZnO loading. 45

4.8 Photocatalytic degradation of isopropanol in unadjusted pH by the TiO_2, ZnO, 400ZnO/TiO_2, 500ZnO/TiO_2, and 600ZnO/TiO_2 films with the UV illumination for 8 h. 46

4.9 Photocatalytic degradation of isopropanol per catalyst loading weight in unadjusted pH as a function of operating time by the TiO_2, ZnO, 400ZnO/TiO_2, 500ZnO/TiO_2, and 600ZnO/TiO_2 films with the UV illumination for 8 h. 48

4.10 Changes of isopropanol concentration and acetone from isopropanol degradation as a function of operating time over the (a) TiO_2, (b) 400ZnO/TiO_2, (c) 500ZnO/TiO_2 and (d) 600ZnO/TiO_2 films with the UV illumination for 8 h. 49

4.11 Isopropanol photocatalytic degradation mechanism. 50

4.12 Photocatalytic degradation of isopropanol in unadjusted pH as a function of operating time by the TiO_2 film with and without UV illumination. 51

4.13 Photocatalytic degradation of isopropanol at unadjusted pH as a function of operating time by the ZnO film with and without UV illumination. 52

4.14 Photocatalytic degradation of isopropanol at unadjusted pH by the 600ZnO/TiO_2 film, UV irradiation for 1 h and turn off 1 h until 8 h. 53

FIGURE **PAGE**

4.15 Photocatalytic degradation of isopropanol at unadjusted pH by the 600ZnO/TiO_2 film, UV irradiation for 2 h and turn off 2 h until 8 h. 53
4.16 Photocatalytic degradation of isopropanol at unadjusted pH by the 600ZnO/TiO_2 film, UV irradiation for 3 h and turn off 3 h until 12 h. 54
4.17 pH effect of 600ZnO/TiO_2 film on the photocatalytic degradation of isopropanol at various pH with the UV illumination for 8 h. 55
4.18 Concentration of isopropanol at various time compared with isopropanol initial concentration by the ZnO/TiO_2 bilayer films with different pH. 56
4.19 Photocatalytic degradation of isopropanol at unadjusted pH by the 600ZnO/TiO_2 film, 4 mol% ZnO, with and without UV illumination. 59
4.20 Photocatalytic degradation of isopropanol at unadjusted pH by the 600ZnO/TiO_2 film, 8 mol% ZnO, with and without UV illumination. 59
4.21 Photocatalytic degradation of isopropanol at unadjusted pH by the 600ZnO/TiO_2 film, 15 mol% ZnO, with and without UV illumination. 60
4.22 Photocatalytic degradation of isopropanol at unadjusted pH by the 600ZnO/TiO_2 film, 19 mol% ZnO, with and without UV illumination. 60
4.23 Concentration of isopropanol at various time compared with isopropanol initial concentration by the ZnO/TiO_2 bilayer films with different ZnO loading with and without UV illumination. 61
4.24 Photocatalytic degradation of isopropanol at unadjusted pH by the 400ZnO/TiO_2 film, 15 mol% ZnO, with and without UV illumination. 64

FIGURE **PAGE**

4.25 Photocatalytic degradation of isopropanol at unadjusted pH by the 500ZnO/TiO_2 film, 15 mol% ZnO, with and without UV illumination. 65

4.26 Photocatalytic degradation of isopropanol at unadjusted pH by the 600ZnO/TiO_2 film, 15 mol% ZnO, with and without UV illumination. 65

4.27 Photocatalytic degradation of isopropanol at unadjusted pH by the 700ZnO/TiO_2 film, 15 mol% ZnO, with and without UV illumination. 66

4.28 Concentration of isopropanol at various time compared with isopropanol initial concentration by the ZnO/TiO_2 bilayer films with different ZnO calcination temperature with and without UV illumination. 67

4.29 Photocatalytic degradation of isopropanol per catalyst loading weight on the oxidation energy storage in unadjusted pH by the TiO_2, 400ZnO/TiO_2, 500ZnO/TiO_2, 600ZnO/TiO_2, and ZnO films with the UV irradiation. 69

CHAPTER I
INTRODUCTION

In recent years, development of industries especially semiconductor manufacturing and other high-tech electronic industries are enlarged, and these industries are connected with discarding of a vast number of organic pollutants, which are harmful to microbes, aquatic system, and human health (Tian *et al*., 2009). Isopropanol is a commonly used in solvent semiconductor industry and present at high concentrations in wastewater. Wastewater containing organic solvent that is not decomposed deteriorates the quality of water in the environment, while its volatile nature results in air pollution that affects the health of factory workers and residents in the neighborhood. Moreover, isopropanol and its metabolite, acetone, act as central nervous system depressants (Burkhart and Kulig, 1990).

Many methodologies have been applied in the treatment of organic compounds such as biological treatment, reverse osmosis, ozonation, filtration, adsorption on solid phases, incineration, and coagulation (Garcia *et al*., 2008). However, each of them has its own limitations; deadly toxic volatiles products (Vinita *et al*., 2010), ghastly smell, quite expensive, and do not eliminate the organic compounds utterly but just transform one phase to another (Zelmanov and Semiat, 2008). In recent era, photocatalytic oxidation/degradation process has been found as an effective and alternative way for treatment of the organic compounds (Huang *et al*., 2008). Several studies have used this technique to chemically convert isopropanol into nontoxic compounds such as water (H_2O) and carbon dioxide (CO_2) (Zhao and Yang, 2003).

Among the photocatalysts, titanium dioxide (TiO_2) has been attracted for the degradation of environmental contaminants because of remarkable photocatalytic activity, non-toxicity, low cost, and good chemical stability (Pelaez *et al*., 2012). However, the uses of TiO_2 as a photocatalyst have some limitations, which are the recombination of photo-generated charged carriers; therefore, some researchers have attempted to modify TiO_2 by doping it with metals/metal oxide loading (Adriana, 2008). Furthermore, TiO_2 functions only under light irradiation that cannot be applied for indoor air and water purification. To overcome these limitations, researchers have developed photocatalysts with energy storage abilities. The oxidation energy storage has

been reported by p-n junction concept, which utilizes the contact between a p-type semiconductor such as $Ni(OH)_2$, Cu_2O, V_2O_5 with TiO_2 as a redox-active n-type semiconductor. The oxidative energy of photocatalysts is stored in a p-type semiconductor, and it is possible to retain the removal of some toxic compounds without illumination. Takahashi and Tatsuma (2005) revealed that the stored oxidative energy can be discharged electrochemically or used for chemical oxidation of various species. Xiong *et al*. (2009) and similar work carried out by Yamasonee and Bandara (2008) reported that the system may be potentially applied to portable devices charged at daytime and used at night without extra storage cells. A photocatalyst with reductive energy storage ability has been developed by doping TiO_2 as an n-type semiconductor with a redox active n-type such as WO_3, MoO_3 or $H_3PW_{12}O_{40}$ (phosphotungstic acid; PWA). The reductive energy of photocatalysts is stored in an n-type semiconductor, and it utilizes to keep anti-corrosion and bactericidal effects in the dark. Tatsuma *et al*. (2002) revealed that the reductive energy can be stored by WO_3, and the reductive energy can be retained for a certain period even after the light was turned off. Takahashi *et al*. (2003) suggested that MoO_3 exhibited larger charging and discharging capacities and greater ability for oxygen reduction than did WO_3, and it might be used as bactericidal materials under humid conditions. However, TiO_2 is an n-type semiconductor, in which the electrons in its conduction band are mobile, whereas the holes in its valence band are much less mobile, so that the storage of the oxidative energy of TiO_2 should be more difficult than that of the reductive energy. Hence, the oxidative energy storage has been challenging in recent years.

Chavadej *et al*. (2008) studied photocatalytic degradation of isopropanol by using Pt/TiO_2 as a photocatalyst. They reported that the photodegradation activity of TiO_2 doped with platinum was better than using titania or platinum alone. Apart from that, the photocatalytic activity of TiO_2 was improved by a metal dopant such as V, Fe, Cr, and Pt. Moreover, they found that acetone was detected as an intermediate product. Yamashita *et al*. (2001) also suggested that the contact between the n-type TiO_2 and the p-type doped TiO_2 introduced the p-n junction that drove electron and hole. Shifu *et al*. (2008) studied photocatalytic activity of p-ZnO/n-TiO_2 that is similar to other works by Giuseppe *et al*. (2001) and Ming *et al*. (2009). These studies revealed that, when the p-type ZnO and n-type TiO_2 were integrated, a p-n junction was formed. At equilibrium,

inner electric field made the p-type semiconductor ZnO region to have negative charge, while the TiO_2 region had positive charge. Under near UV illumination, electron-hole pairs may be created, and the photogenerated electron-hole pairs are separated. The holes flowed into the ZnO region, while the electrons moved to the TiO_2 region. As a result, the separation of electron-hole pairs was efficiently generated leading to the enhancement of photocatalytic activity.

As mentioned previously, it is important to understand how this p-n junction concept can reserve energy. Therefore, the main goal of this research is to prepare a p-n junction of TiO_2 as an n-type semiconductor with ZnO as a p-type semiconductor by sol-gel method. Moreover, the photodegradation of isopropanol by using ZnO/TiO_2 as the oxidative energy storage photocatalyst with and without UV illumination, and intermediate product of isopropanol photodegradation will be investigated.

CHAPTER II
THEORETICAL BACKGROUD AND LITERATURE REVIEW

2.1 Principle of Photocatalysis

Photocatalysis is a technical term conventionally defined as "the acceleration of the rate of a chemical reaction, induced by the absorption of light by a catalyst or co-existing molecule" (Serpone and Salinaro, 1999; Braslavsky, 2007). Basic photochemical principles of heterogeneous photocatalysis have been reported in many literatures and found that organic molecules came into contact with a catalyst surface under irradiation, inducing a series of oxidation and reduction (redox) reactions and degrading pollutant molecules (Ohtani, 2014). The heterogeneous photocatalysis is a discipline, which includes a large variety of reactions: organic synthesis, water splitting, photoreduction, hydrogen transfer, O_2^{18}-O_2^{16} and deuterium-alkane isotopic exchange, metal deposition, etc. (Gaya and Abdullah, 2008). These different reactions are related with many applications, air and water treatment, active surfaces, green chemistry, and energy conversion (Coronado *et al*., 2008). Normally, it is accepted that the degradation of pollutants consists of many kinds of reaction after illumination of semiconductor particles (Kisch, 2013).

Semiconductor heterogeneous photocatalysis has enormous potential to treat organic contaminants in water and air. This process is known as advanced oxidation process (AOP) and is suitable for the oxidation of a wide range of organic compounds. Basically, when light is absorbed by a semiconductor photocatalyst, electronic excitations take place, which can be exploited in chemical or electrical work. The material absorbs light when the energy of incident photons is equal or larger than band gap energy of the semiconductor. Thus, an electron is excited from valence band (VB) into its conduction band (CB) and leaving hole behind (Roland, 2014). The schematic representation of semiconductor energy band is shown in Figure 2.1.

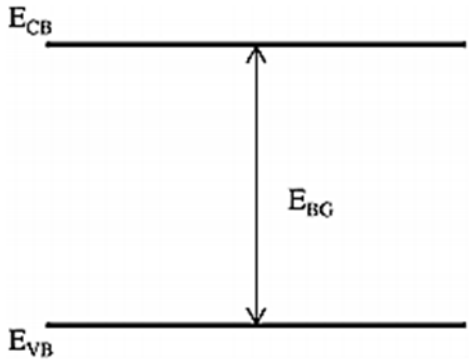

Figure 2.1 Schematic representation of semiconductor energy band (Angelo *et al*., 2013).

The semiconductor energy band consists of valence band (E_{VB}) and conduction band (E_{CB}). The energy difference between the conduction and valence edges is called the band gap energy of the semiconductor (E_{BG}).

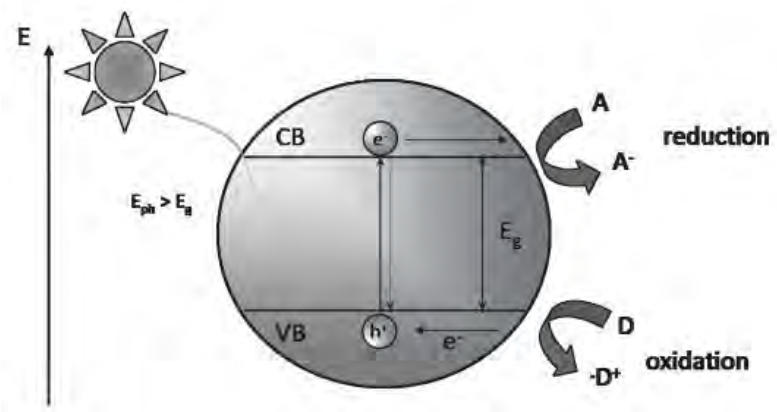

Figure 2.2 Basic processes of charge carrier generation upon the light irradiation of a semiconductor particle; E_{ph}: energy of irradiated photon, A: electron acceptor, D: electron donor. (Roland, 2014).

The basic three steps of photocatalytic reactions are 1) photoexcitation of charge carriers; 2) charge carrier separation and diffusion to the photocatalyst surface; and 3) oxidation and reduction reaction on the catalyst surface. During step (2), recombination can occur via different mechanism. The major pathway is already

mentioned relaxation of photoexcited electrons back to the valence band, which can directly happen from the conduction band. For example, if the photogenerated charge carriers are not used in photocatalytic reactions, they will recombine. The basic principles of these processes are depicted in Figure 2.2 (Roland, 2014).

In the photocatalyst reaction, redox potential of photogenerated valence band hole must be sufficiently positive to generate $OH^{\bullet}$ radicals, which can subsequently oxidize the organic pollutant followed by Eq. (2.1)

$$H_2O + h^+_{vb} \rightarrow OH^{\bullet} + H^+ \qquad (2.1)$$

Photocatalytic degradation (PCD) process is gaining importance in the area of wastewater treatment; especially for wastewater containing small amounts of refractory organic substances. The process has several advantages over competing processes. There are: (1) complete mineralization, (2) no waste disposal problem, (3) low cost, and (4) only mild temperature and pressure conditions are necessary (Mills *et al*., 1993).

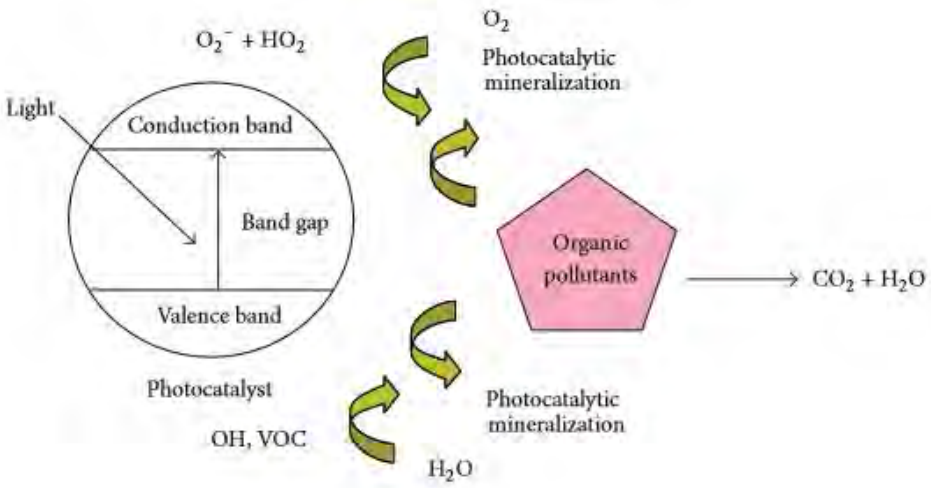

Figure 2.3 Schematic diagram of photocatalytic degradation of organic effluent (Gnanaprakasam *et al*., 2015).

As mentioned previously, the photocatalytic degradation involves several steps such as adsorption-desorption, electron-hole pair production, recombination of electron pair, and chemical reaction. The general mechanism of photocatalytic degradation of organic molecules is explained in Figure 2.3.

When the photocatalyst is irradiated with photon of energy equal to or more than its band gap energy, generation of excited high-energy states of electron and hole pairs occurs. It results in the promotion of an electron in the conduction band (e^-_{cb}) and formation of a positive hole in the valence band (h_{vb}^+), as shown in Eq. (2.2).

$$\text{Photocatalyst} + h_v \rightarrow e^-_{cb} + h^+_{vb} \qquad (2.2)$$

where h_v is the energy essential to transfer the electron from valence band to conduction band. The e^-_{cb} and h^+_{vb} are powerful oxidizing and reducing agents, respectively. Both of them can migrate to catalyst surface, where they can enter in a redox reaction with other species present on the surface. The electrons generated through irradiation could be readily trapped by O_2 absorbed on the photocatalyst surface or dissolved O_2 to give superoxide radicals ($O_2^{-\bullet}$), as shown in Eq. (2.3).

$$e^-_{cb} + O_2 \rightarrow O_2^{-\bullet} \qquad (2.3)$$

Consequently, $O_2^{-\bullet}$ could react with H_2O to produce hydroperoxy radical ($HO_2^\bullet$) and hydroxyl radical ($OH^\bullet$), which are strong oxidizing agents to decompose the organic molecule, as shown in Eq. (2.4).

$$O_2^{-\bullet} + H_2O \rightarrow HO_2^\bullet + OH^\bullet \qquad (2.4)$$

Simultaneously, the photoinduced hole could be trapped by surface hydroxyl group (or H_2O) on the photocatalyst surface to give hydroxyl radicals ($OH^\bullet$), as shown in Eq. (2.5).

$$h^+_{vb} + OH^- \rightarrow {}^\bullet OH_{ad}$$

$$h^{+}_{vb} + H_2O \rightarrow {}^{\bullet}OH + H^{+} \quad (2.5)$$

Finally, the organic molecules will be oxidized to yield carbon dioxide and water by reacting with hydroxyl radical ($OH^{\bullet}$) due to its electrophilic nature (electron preferring), the $OH^{\bullet}$ can non-selectively oxidize almost all electron rich organic molecules as follows:

$$OH^{\bullet} + \text{organic molecules} + O_2 \rightarrow CO_2 + H_2O \quad (2.6)$$

Meanwhile, recombination of positive hole and electron could take place which could reduce the photocatalytic activity as follows: (Gnanaprakasam *et al*., 2015)

$$e^{-}_{cb} + h^{+}_{vb} \rightarrow \text{photocatalyst} \quad (2.7)$$

Bhatkhande *et al*. (2001) reviewed the chemical effects of various variables on the rate of degradation of different pollutants. They discussed that effect of operation parameters, which could influence the photocatalytic degradation of organic pollutants, such as adsorption, intensity of light, pH, temperature, and presence of anions, cations. Effects of adsorption also were analyzed, and it was concluded that the substances, which were readily adsorbed, were degraded at a faster rate, indicating that the reaction was a surface phenomenon. And the effects of pH was negligible so pH adjustment was not required. They suggested that a light source and catalyst also affected the cost of the operation. Solar radiation was obviously an attractive proposition.

Zhao *et al*. (2005) reviewed progress in the TiO_2 photocatalytic degradation of organic pollutants by visible light. They focused on metal semiconductor, which operates at ambient conditions. Under such conditions, the dyes not only are decolored, but also mineralized. As the TiO_2 semiconductor is relatively large band gap and can be excited only by high energy UV radiation, extending the response of TiO_2-based material to the visible region can be achieved in many ways such as dye sensitization,

non-metal or transition metal ions doping, and surface modification. However, the removal efficiency of organic pollutants from water or air in visible region is low.

Akpan and Hameed (2009) reviewed the effect of operating parameters including pH, oxidizing agents, and catalyst loading on the photocatalytic degradation of textile dyes, dopant content, and calcination temperature by using TiO_2-based photocatalysts. The finding revealed the various operational parameters affected the effectiveness or activities of TiO_2-based photocatalysts. The reaction should be undertaken at the proper pH. Oxidizing agents, calcination temperature, and catalyst loadings were found to exert their individual influence on the photocatalytic degradation of any dyes. And it was also discovered that the sol-gel method was widely used.

Umar and Aziz (2013) reviewed the degradation of organic pollutants in water by using semiconducting oxide photocatalysts. The process is capable of removing a wide range of organic pollutants such as pesticides, herbicides, and micropollutant such as endocrine disrupting compounds. Especially, the TiO_2 has been most commonly because of its ability to break down organic pollutants and even complete mineralization. However, this application is constrained such as wide band gap (3.2 eV), lack and inability for high proton efficiency to utilize wider solar spectra. And they suggested that the use of solar radiation has to be improved by virtue of the design of the photoreactor in order to reduce the cost of treatment.

2.2 Titanium Dioxide (TiO_2)

Titanium dioxide (TiO_2) is a material with a huge technological relevance because of its numerous applications (e.g. pigments, sensors, catalyst). Strong oxidation and reduction power of photoexcited TiO_2 was realized from the discovery of Honda-Fujishima effect in 1972, who reported photoinduced decomposition of water by solar light on TiO_2 electrodes. Thus, this solid has been attracting the interest of the scientific community mainly and remaining as the most widely used photocatalyst. In fact, this oxide has been considered as a synonym of photocatalyst, because more than 67% of the articles about photocatalysis are still based on the use of TiO_2. The reasons for this prominent position of TiO_2 as a photoactive material rely

mainly on its particular physicochemical characteristics, thermally stable, non-toxic, optical and electrical properties, and capable of promoting oxidation of organic compounds, although other aspects, like its biocompatibility and its availability at a relatively low cost, have also facilitated the extensive use of this semiconductor (Coronado *et al*, 2008).

Photocatalytic reactions at the surface of TiO_2 have been attracting much attention in view of their practical applications to environmental cleaning such as self-cleaning of tiles, glasses, and windows. The TiO_2 represents an effective photocatalyst for water and air purification and for self-cleaning surfaces. Additionally, it can be used as antibacterial agent because of strong activity and superhydrophilicity (Fujishima and Zhang, 2006).

2.2.1 Structure of Titanium Dioxide

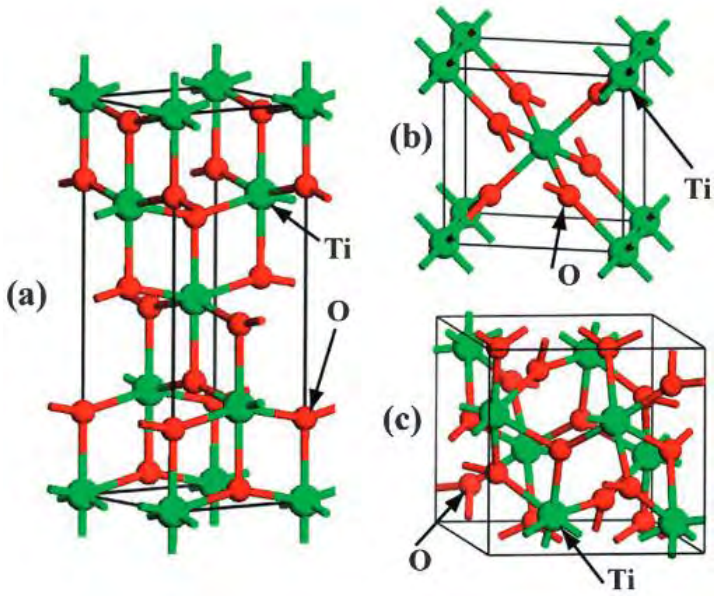

Figure 2.4 Schematic conventional cells for anatase (a), rutile (b) and brookite (c). The big green spheres represent Ti atoms and the small red spheres represent O atoms (Zhang *et al*., 2007).

Titanium dioxide (TiO_2) or titania exists in four mineral forms, viz: anatase, rutile, brookite, and metastable TiO_2 or TiO_2 (B) that can be prepared without using special synthesis conditions (Gianluca *et al*., 2008). Anatase type TiO_2 has a crystalline structure that corresponds to the tetragonal system (with dipyramidal habit) and is used mainly as a photocatalyst under UV irradiation. Rutile type TiO_2 also has a tetragonal crystal structure (with prismatic habit). This type of titania is mainly used as white pigment in paint. As the different arrangements, rutile is denser (4.250 $cm^3.g^{-1}$) than anatase (3.894 $cm^3.g^{-1}$). In case of brookite type, TiO_2 has an orthorhombic crystalline structure. It consists of chains of edge-sharing octahedra connected to each other by vertices. This type of TiO_2 is closely related to that of anatase, but it presents a different array of octahedral chains, which results in less dense crystals, so it is not often used for experimental investigations (Chen and Mao, 2007). These three crystal structures are represented in Figure 2.4. And TiO_2 (B) is a monoclinic mineral and is a versatile material that has applications in various products such as paint pigment, sunscreen lotions, electrochemical electrodes, capacitors, solar cells, and even food coloring agent, and in toothpastes (Meacock *et al*., 1997). Only rutile and anatase will be focused because both of them are inexpensive, chemically stable, harmless and photocatalytic application (Lan *et al*., 2013).

2.2.2 Photocatalytic Degradation Mechanism of Titanium Dioxide

Due to TiO_2 shows relatively high reactivity and chemical stability under ultraviolet light (λ<387 nm), whose energy exceeds the band gap of 3.2 eV in the crystalline phase, so it has been the most studied semiconductor for photocatalytic applications (Adriana, 2008).

In the basic mechanism, photocatalysis reaction is activated by absorption of a photon with sufficient energy by equal to or higher than 3.2 eV resulting in initiating excitation related to charge separation event (gap band). It results in the promotion of an electron from the valence band to the conduction band, thus generating hole in the valence band. The ultimate goal of the process is to have a reaction between the activated electrons with an oxidant to produce an oxidized product. The photogenerated electrons could reduce the dye or react with electron acceptors such as O_2 adsorbed on the Ti(III)-surface or dissolved in water, reducing it

to superoxide radical anion ($O_2^{-\bullet}$). The photogenerated holes can oxidize the organic molecule (R) to form R^+, or react with OH^- or H_2O oxidizing them into $OH^\bullet$ radicals. Together with other highly oxidant species (peroxide radicals), they are reported to be responsible for the heterogeneous TiO_2 photodecomposition of organic substrates as dyes. The resulting $OH^\bullet$ radicals, being a very strong oxidizing agent (standard redox potential +2.8 eV) can oxidize most azo dyes, electron poor aromatics, or quinones to the mineral end-products. According to this, the relevant reactions at the semiconductor surface causing the degradation of organic molecules can be expressed as follows (Konstantinou and Albanis, 2004):

$$TiO_2 + h\nu\ (UV) \rightarrow TiO_2\ (e^-_{cb} + h^+_{vb}) \quad (2.8)$$

$$TiO_2\ (h^+_{vb}) + H_2O \rightarrow TiO_2 + H^+ + OH^\bullet \quad (2.9)$$

$$TiO_2\ (h^+_{vb}) + OH^- \rightarrow TiO_2 + OH^\bullet \quad (2.10)$$

$$TiO_2\ (e^-_{cb}) + O_2 \rightarrow TiO_2 + O_2^{-\bullet} \quad (2.11)$$

$$O_2^{-\bullet} + H^+ \rightarrow HO_2^\bullet \quad (2.12)$$

$$R + OH^\bullet \rightarrow \text{degradation products} \quad (2.13)$$

$$R + h^+_{vb} \rightarrow \text{oxidation products} \quad (2.14)$$

$$R + e^-_{cb} \rightarrow \text{reduction products} \quad (2.15)$$

The presence of dissolved oxygen is extremely important during photocatalytic degradation as it can make the recombination process on TiO_2 (e^-_{cb} /h^+_{vb}) difficult, which results in maintaining the electroneutrality of the TiO_2 particles (Boroski *et al*., 2009). In other words, it is important for effective photocatalytic degradation of organic pollutants that the reduction process of oxygen and the oxidation of pollutant proceed simultaneously to avoid the accumulation of electron in the conduction band and thus reduce the rate of recombination of e^-_{cb} and h^+_{vb} (Hoffmann *et al*., 1995).

2.2.3 Doping of Titanium Dioxide

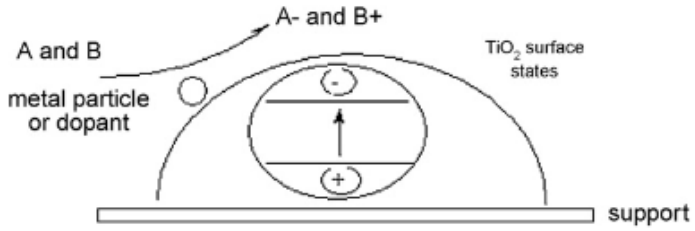

Figure 2.5 Modification of titania photocatalyst by using metal doping (Gaya and Abdullah, 2008).

Doping of photocatalyst could improve the photocatalyst efficiency in the following ways: (1) band gap energy narrowing (Sathishkumar *et al*., 2013); (2) formation impurity energy levels (Cao *et al*., 2013); (3) oxygen vacancies; (4) unique surface are for the adsorption of organic molecules (Wu *et al*., 2010); and (5) electron trapping (Barakat *et al*., 2013). In general, catalyst with smaller band gap energy is preferred to be an effective photocatalyst to generate more electron hole pairs. Band gap narrowing, introduction of impurity energy level, and oxygen-deficient sites can result in a catalyst with higher photocatalytic activity even under visible light. Thus, doping prevents recombination of electrons and holes and gets better the photocatalytic activity by trapping the photoinduced electrons.

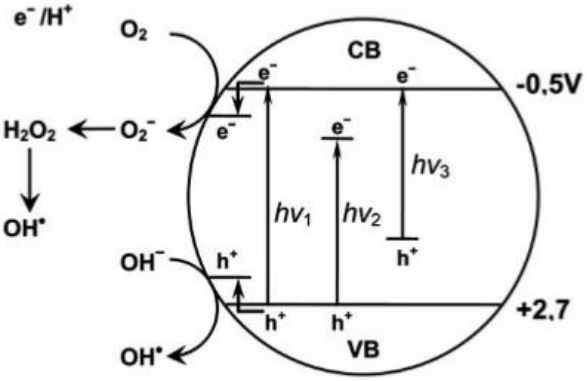

Figure 2.6 Mechanism of TiO_2 photocatalysis: hv_1: pure TiO_2; hv_2: metal-doped TiO_2 and hv_3: nonmetal-doped TiO_2 (Adriana, 2008).

The mechanism of photoactivity of pure TiO_2 and TiO_2 doped with metal and nonmetal species are represented in Figure 2.6. In the case of pure TiO_2, the photocatalytic mechanism is initiated by the absorption of the photon hv_1 with energy equal to or greater than the band gap of TiO_2 producing an electron-hole pair on the surface of TiO_2 nanoparticle. An electron is promoted to the conduction band (CB) while a positive hole is formed in the valence band (VB). Excited-state electrons and holes can recombine and dissipate the input energy as heat, get trapped in metastable surface states, or react with electron donors and electron acceptors adsorbed on the semiconductor surface or within the surrounding electrical double layer of the charged particles. The photoactivity of metal-doped TiO_2 can be explained by a new energy level produced in the band gap of TiO_2 by the dispersion of metal nanoparticles in the TiO_2 matrix. An electron can be excited from the defect state to the TiO_2 conduction band by photon with energy equals hv_2. Additional benefit of transition metal doping is the improved trapping of electrons to inhibit electron-hole recombination during irradiation. Decrease of charge carriers recombination results in enhanced photoactivity (Hoffmann *et al*., 1995).

Zhao and Yang, (2003) reviewed using of photocatalytic oxidation (PCO) to destruct volatile organic compounds in indoor air. They discussed that TiO_2 is widely used as a photocatalyst in various reactors due to its superior characteristics. For the PCO application, TiO_2 anatase is superior to rutile because the conduction band

location for anatase is more favorable for driving conjugate reactions involving electrons, and very stable surface peroxide group can be formed at the anatase but not on the rutile surface. And they also suggested that, intermediates produced during the PCO process can occupy the active site of the catalyst surface and result in deactivation of catalyst, so activity of the catalyst dropped.

Gaya and Abdullah (2008) reviewed an overview of the dramatic trend in the use of the TiO_2 photocatalyst for remediation and decontamination of wastewater. They mentioned that titania has played a much larger role than another semiconductor photocatalysts. Extensive literature analysis has shown many possibilities in improving the efficiency of photodecomposition over titania by combining the photoprocess with either physical or chemical operations. The resulting combined processes revealed a flexible line of action for wastewater treatment technologies. The choice of treatment method usually depends upon the composition of the wastewater.

Sun *et al*. (2008) studied the degradation of orange G (OG) on nitrogen-doped TiO_2 photocatalysis under visible light and sunlight irradiation. The result showed that not only the N-doped TiO_2 caused the new absorption band but also the photosensitized oxidation mechanism originated from the azo dyes themselves and contributed to the higher visible light activity. Therefore, the N-doped TiO_2 catalyst had higher the degradation OG than undoped TiO_2 catalyst under visible light. In contrast, the undoped TiO_2 catalyst exhibited high photocatalytic activity under sunlight irradiation.

Amini and Ashrafi (2016) studied photocatalytic degradation of rhodamine B (RB), methylene blue (MB), and acridine orange (AO) under solar light irradiation using TiO_2 and ZnO nanoparticles. The results showed that the degradation of RB in the absence of photocatalyst was very slow. When the TiO_2 catalyst was added, the degradation was complete faster. But the activity decreased when using the ZnO as catalyst. They suggested that the TiO_2 is chemically inert and stable with respect to photocorrosion and chemical corrosion, while the ZnO is unstable. The degradation of MB for two catalysts was complete in the same time but in absence light, the removal is not obvious. For pH effect, they found that the TiO_2 followed order pH 5 > 7 > 9 and 9 > 7 > 5 for the ZnO. And the degradation of AO by using

these catalysts, degradation percentage of AO increased almost linearly with time. They concluded that the TiO_2 and ZnO were found to be an effective catalyst for the destruction of industrial dyes.

2.3 Photocatalytic Degradation Mechanism of Zinc Oxide

Although TiO_2 currently represents to be a benchmark photocatalyst for the degradation of organic dyes and pollutants mainly due to its excellent performance; however, the photocatalytic activity of TiO_2 is limited because of the easily recombination of photogenerated electrons and holes. Moreover, TiO_2 shows lower absorbance value. Composite of semiconductor to promote the separation efficiency of photogenerated charge and extend the range of excite spectrum have been investigated.

One of the most popular metal oxides is zinc oxide (ZnO), which is a wide band-gap n-type semiconductor with unique properties such as good transparency, high electron mobility, and high electrochemical stability. It has been widely used in chemical sensor, surface acoustic wave device, and photoanode films of solar cell. Very highly reducing electrons and oxidizing holes are photogenerated on ZnO under UV light irradiation. Besides holes, h^+, the main oxidizing species in water are hydroxyl radicals, $OH^\bullet$. Other oxidizing species such as singlet oxygen, hydroperoxyl radicals and superoxide ions play a minor role in photocatalytic transformations in liquid-liquid reactions (Coronado *et al.*, 2008). In addition, Zn^{2+} is a very important oxidation state. The presence of Zn^{2+} can act as the following mechanism (Rauf *et al.*, 2011).

$$Zn^{2+} + e^- \rightarrow Zn^+ \quad (2.16)$$

$$Zn^+ + O_2(abs) \rightarrow Zn^{2+} + O_2^{-\bullet} \quad (2.17)$$

$$Zn^+ + h^+ \rightarrow Zn^{2+} \quad (2.18)$$

$$Zn^{2+} + h^+ \rightarrow Zn^{3+} \quad (2.19)$$

$$Zn^{2+} + OH^\bullet \rightarrow Zn^{2+} + OH^\bullet \quad (2.20)$$

$$Zn^{3+} + e^- \rightarrow Zn^{2+} \quad (2.21)$$

Although ZnO presents higher electron mobility than TiO_2, which should favor electron transport, its chemical stability is poor, giving rise to filter effect, that is, a layer of inactive organic-Zn^{2+} insoluble complexes.

ZnO is sometimes preferred over TiO_2 for degradation of organic pollutants due to its high quantum efficiency, especially for the production of peroxides. The photodegradation mechanism of organic pollutants in ZnO has been claimed to be similar to that of TiO_2. Furthermore, according to the band edge position, as the conduction band of TiO_2 is lower than that of ZnO, the former can act as a sink for the photogenerated electrons. The photogenerated electrons of the ZnO conduction band will be transferred to the conduction band of TiO_2, while the photogenerated electrons of TiO_2 will remain in the conduction band of TiO_2. Since the holes move in the opposite direction from the electrons, the photogenerated holes of the TiO_2 valence band will be transferred to the valence band of ZnO, which makes charge separation more efficient as shown in Figure 2.7 (Shifu *et al*., 2008).

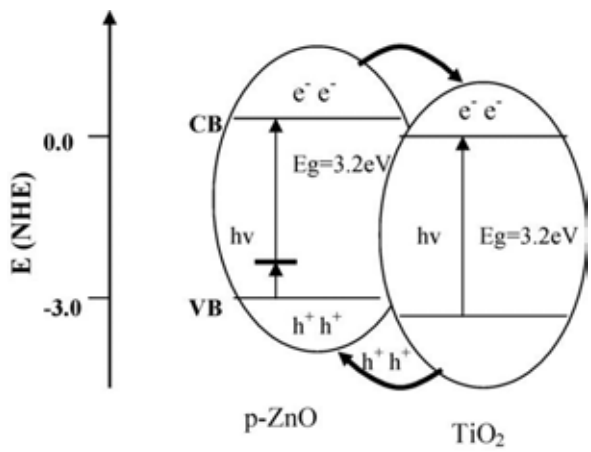

Figure 2.7 Schematic diagram of electron-hole separation process (Shifu *et al*., 2008).

Perez-Gonzalez *et al*. (2015) studied photocatalytic activity and properties of TiO_2-ZnO thin film to degrade methylene blue. The results are explained in terms of the $(TiO_2)_{1-x}$-$(ZnO)_x$, with x value in range 0.00 to 1.00. From the experiment, they discussed that the degradation activity of film increased with the TiO_2 content. The BET surface and the crytallinity showed opposite behaviors as a function of x value.

Therefore, x = 0.00 showed the lowest BET surface area and the highest crystallinity, resulting in the best photocatalytic performance. However, ZnO has been reported to show greater degradation activity than TiO_2 for specific organic dyes. They concluded that the high crystallinity seemed to be the most relevant factor for the degradation activity because it indicated low surface defects, low amorphous content and reduces the recombination rate.

Sakthivel *et al*. (2003) studied solar photocatalytic degradation of acid brown 14 by using ZnO and TiO_2 as photocatalysts. The results showed that the rate of degradation of two catalysts increased with increasing initial dye concentration then drastically decreased due to maximum concentration value exceeded. The rate of degradation of these catalysts increased linearly with catalyst loading, but the higher amount of catalysts can result in decreasing the efficiency. For both ZnO and TiO_2, the adsorption of dye was high at low pH range. The degradation rate of TiO_2 was high at low pH, in contrast to ZnO. The acid brown 14 was converted completely into colourless and degraded by using ZnO was faster than TiO_2. They concluded that ZnO was the most active photocatalyst in the degradation of acid brown 14 using sunlight as an energy source because it absorbed large fraction of solar spectrum.

Liao *et al*. (2004) studied photocatalytic activity of ZnO doped TiO_2 by sol-gel method and $SO_4^{2-}/TiO_2/ZnO$ modified by sulfating the dry gels ZnO/TiO_2 with H_2SO_4 solution. In this study, they used zinc sulfate as precursor of zinc. The results showed that the addition of zinc could enhance the activity of catalyst, and if the catalyst was a mixture of anatase and rutile TiO_2, the activity was also improved. They found that the stronger the acidity, the catalytic activity was higher. The photocatalytic activity decreased with the increase in the calcination temperature. And they also compared the activities of several catalysts before and after sulfating, the result showed that the activity of $SO_4^{2-}/TiO_2/ZnO$ was higher than that of TiO_2 doped by single ZnO or TiO_2 treated with single H_2SO_4. They concluded that the sulfating ZnO/TiO_2 with sulfuric acid resulted to dramatic enhancement.

Zhang *et al*. (2007) studied preparation of photocatalytic nano-ZnO/TiO_2 film with vacuum vaporized and sol-gel methods. The oxidation efficiency of the ZnO/TiO_2 was higher than the pure TiO_2 film and ZnO film. Therefore, the ZnO/TiO_2 film can largely enhance the photocatalytic degradation efficiency of organic compounds.

Moreover, ZnO increased concentration of free electrons in TiO_2. Effect of pH showed that the photocatalytic oxidation of organic compounds increased with the pH value.

Konyar *et al*. (2012) studied effect of sintering on photocatalytic efficiencies of self-supporting ZnO/TiO_2 composite plates, which was fabricated at a molar ratio of ZnO:TiO_2 = 1:1. Then, the plates were sintered in air at range 600-700°C to retain ZnO and TiO_2. The results showed that the surface area was decreased with increasing the sintering temperature. Moreover, when the sintering temperature increases, the amount of pure ZnO and TiO_2 decreased while the amount of photocatalytically inactive phases, such as Zn_2TiO_4 or $Zn_2Ti_3O_8$, increased. The decrease in the surface area values resulted in low degradation efficiency. They concluded that heat treatment at temperature as low as 600°C reduced the interdiffusion between ZnO and TiO_2.

2.4 Isopropanol

Isopropanol, isopropyl alcohol, or 2-propanol is a compound with chemical formula C_3H_8O and has a molecular structure as shown in Figure 2.8.

It is a sharp, colorless, and flammable liquid with a characteristic alcoholic odor and completely miscible (mixes completely) with most solvents, including water. It is also commonly used in cosmetics, skin and hair products, perfumes, pharmaceuticals, lacquers, dyes, cleaners, antifreezes, and other chemicals (www.dow.com/webapps/msds/msdssearch.aspx). Moreover, it is a common organic reagent present at high concentrations in the wastewater and volatile in nature. This organic compound poses direct or indirect harm to irritate and burn the skin and eyes, prolonged contact can cause a skin rash, itching, dryness, and redness and may be toxic to kidneys, liver, skin, central nervous system. Repeated high exposure can cause headache, dizziness, loss of coordination, unconsciousness, and even death. And it is a dangerous fire hazard (nj.gov/health/eoh/rtkweb/documents/fs/1076.pdf).

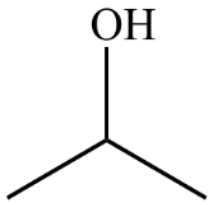

Figure 2.8 Molecular structure of isopropanol (www.chemicalbook.com /Chemical ProductProperty_EN_CB8854102.htm).

In addition, isopropanol is the major organic ingredient in wastewater of semiconductor manufacturing industry. The efficiency of traditional wastewater treatment processes using physical-chemical or microorganism decomposition approaches is limited. Wastewater containing organic solvents that are not decomposed deteriorates the quality of water in the environment, while its volatile nature results in air pollution that affects the health of factory workers and residents in the neighborhood (Chen and Mao, 2007). Isopropanol and its metabolite, acetone, act as central nervous system depressants (Burkhart and Kulig, 1990). Besides, isopropyl alcohol wastewater contains many other refractory and complex organic compounds, e.g., fluoride and suspended solids, which not only introduce direct or indirect contamination to environment but also are harmful to human health (Lin and Kiang, 2003).

Furthermore, it was found that acetone was solely detected as an intermediate product from the photocatalytic degradation of isopropanol. The isopropanol is degraded to form acetone, and acetone is further oxidized into carbon dioxide and water as shown in Eqs. (2.22) and (2.23), respectively (Chavadej *et al*., 2008).

$$CH_3CHOHCH_3 + 2OH^{\bullet} \rightarrow (CH_3)_2CO + 2H_2O \quad (2.22)$$

$$(CH_3)_2CO + OH^{\bullet}/{}^{\bullet}O_2^{-} \rightarrow \text{other intermediates} \rightarrow CO_2 + H_2O \quad (2.23)$$

Bickley *et al*. (1973) used rutile TiO_2 and studied the photocatalyzed oxidation (PCO) in isopropanol vapor. The isopropanol quickly reacted to form acetone and H_2O. Acetone was then displaced by H_2O and appeared in the gas stream.

Adsorbed acetone was photocatalytically oxidized at a distinctly slower than isopropanol oxidized to acetone. Instead, acetone oxidized to strongly adsorbed intermediate, and the continuation of PCO was observed by O_2 uptake. The authors concluded that CO_2 decreased in O_2 uptake rate on samples pretreated at higher temperatures was due to lower concentrations of surface OH groups, which played a role in the PCO process by increasing O_2 photoadsorption. Moreover, no reaction occurred in the absence of UV light and only a small amount of acetone was formed in the absence of O_2 in the gas stream.

Chavadej *et al*. (2008) studied the photocatalytic degradation of 2-propanol by using platinum, titania, and platinum loaded on titania as photocatalysts. The result showed that the activity of either platinum or titania alone was greatly low in the photocatalytic degradation but increased for platinum loaded on titania. Increasing of the catalyst dosage and initial concentration of 2-propanol resulted in increasing the rate of degradation. The degradation rate increased with decreasing pH solution because of better adsorption of 2-propanol on the surface of catalyst. However, it increased again in the pH of solution was around 12 because the hydroxyl radical formation rate increased. Moreover, a high dissolved oxygen level gave a much higher degradation rate, since it can act as electron scavenger. And in this work, acetone was detected as an intermediate product.

Chen *et al*. (2009) studied photocatalytic properties of nanostructured $PbSnO_3$ photocatalysts with particulate and tubular morphologies for isopropyl alcohol (IPA) degradation under visible light irradiation. The gaseous IPA was gradually oxidized through an acetone intermediate to CO_2. The results revealed that the photocatalytic activities for IPA degradation over these catalysts were in the order of nanoparticle > nanotube > bulk material, which was consistent with that of BET surface areas. And they found that the degradation of IPA over these catalysts was only driven by light irradiation. They concluded that the larger surface area means much more active sites and better crystallinity which resulted in the increase of photocatalytic activity since it could reduce electron-hole recombination rate.

Salazar and Nanny (2010) investigated the aqueous photocatalytic degradation of small polar organic compounds (SPOCs) that bear hydrogen-bonding capabilities but do not readily adsorb on the TiO_2 catalyst like isopropanol and acetone.

This study suggested that small aliphatic alcohols and ketones may adsorb to the TiO_2 catalyst in contact with their aqueous solution through the formation of hydrogen bonds with the surface hydroxyl groups**.** The result showed that the fastest degradation rates of acetone and isopropanol occurred at conditions where the rate of hydroxyl radical production was more favorable such as in alkaline pH**.**

Wang and Egerton (2013) compared the effect of chromium on photo-oxidation of propan-2-ol, for which hydroxyl radicals were the catalytically active intermediates and stearic acid oxidation, which proceeds via direct hole transfer. For the photo-oxidation of propan-2-ol, the amount of acetone product increased linearly with time, and the effect of increasing amount of chromium dopant was less than 0.01% that was little affected but decreased significantly for more than 0.1% of chromium. By contrast, photocatalytic oxidation of stearic acid decreased with increasing concentration of chromium. They suggested that the initial increase in the propan-2-ol oxidation activity was associated with the oxidation state of Cr greater than 3 but that at higher chromium concentrations the activity for both stearic acid and propan-2-ol are decreased because of increased recombination induced by Cr^{3+} ions that substitute for Ti^{4+} in the rutile lattice.

Lu *et al*. (2016a) studied photodegradation of gaseous isopropyl alcohol (IPA) at ppb level in internal-illuminated monolith photoreactor (IMR) by using TiO_2 and Ag/TiO_2 as photocatalysts. The experimental results showed that, increasing the contents of Ag on TiO_2, the removal efficiency was increased because of the higher surface barrier. As a result, the electron-hole pair separation enhanced due to their space charge layer became narrower than TiO_2. However, if the presence of Ag was too much, it can be resulted in a decrease in the photocatalytic ability. Possible reasons were the electrostatic interaction between negatively charged Ag sites, and the excessive coverage of Ag can mask the incident light on TiO_2 surface.

2.5 Oxidative Energy Storage Model of TiO_2

TiO_2 has been widely used in our every daylife as a pollution abatement catalyst for various applications based on its oxidative and reductive energy converted from light energy. However, the uses of TiO_2 as a photocatalyst still have some limitation to activate the formation of photo-excited electrons and holes. Some researchers attempted to modify TiO_2 by doping it with both metallic and non-metallic substances in order to reduce band gap energy of the metal oxide, so its photocatalytic activity under the visible light can be obtained (Luo *et al*., 2011). Additionally, the use of TiO_2 as a catalyst for pollution abatement in the absence of both UV and visible light, which can be applied for indoor air quality, is still challenging. In this regard, the concept of using TiO_2 in combination with other lower band gap metal oxides, capable of functioning as a kind of energy storage substance, has been developed (Tatsuma *et al*., 2001).

Working mechanism of the mixed metal oxides can be described as following. In the presence of light, TiO_2 will be photo-excited and electrons/holes are generated. Some of electron can be transferred to the lower band gap metal oxide and stored in intermediate compound form. Then, in the dark, electron from the intermediate compound will be released and transferred back to the system. In other words, stored electron in the lower band gap metal oxide compound will serve as a source of electron for catalytic activity of the system in the dark. Moreover, the electron can also interact with oxygen in ambient, leading to the mixed metal oxides also work under versatile illumination condition including UV irradiation, visible light illumination and, in the dark (Ngaotrakarnwiwat, 2013).

Recently, the energy storage of photocatalyst has been attracting and investigated by doping an active semiconductor or p-n junction semiconductor. When an n-type semiconductor (TiO_2) is joined with a p-type semiconductor, a p-n junction is formed. The region, where the p-type and n-type semiconductors, are joined is called p-n junction, as shown in Figure 2.9. At equilibrium, the inner electric field makes the p-type semiconductor region have the negative charge, while the TiO_2 region have the positive charge (Dai *et al*., 2013).

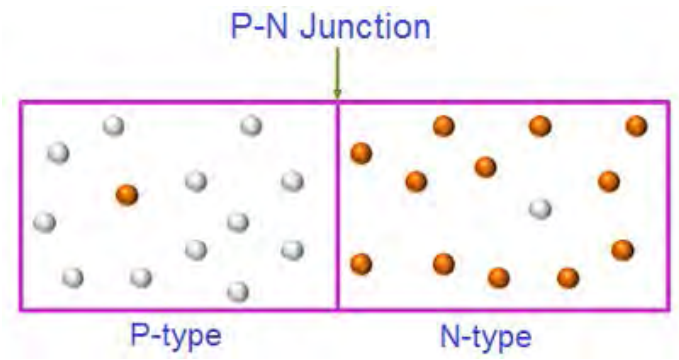

Figure 2.9 p-n junction of semiconductor (www.physics-and-radio-electronics .com).

Each free electron that is crossing the junction from the n-side to fill the hole in the p-side atom creates a negative ion at p-side. Similarly, each free electron that left the parent atom at the n-side to fill the hole in the p-side atom creates a positive ion at the n-side. Negative ion has more number of electrons than protons. Hence, it is negatively charged. Thus, a net negative charge is built at the p-side of p-n junction. Likewise, positive ion has more number of protons than electrons. Hence, it is positively charged. So, a net positive charge is built at n-side of the p-n junction.

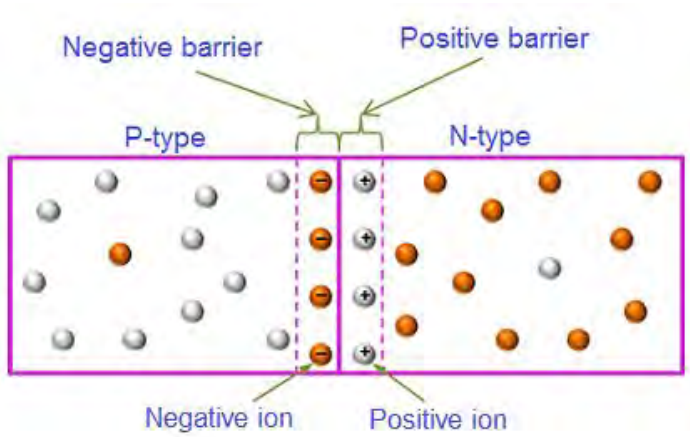

Figure 2.10 Negative and positive barrier of semiconductor (www.physics-and-radio-electronics.com).

The net negative charge at the p-side of the p-n junction prevents further flow of free electrons crossing from the n-side to the p-side because the negative charge

present at the p-side of the p-n junction repels the free electrons. Comparably, the net positive charge at the n-side of the p-n junction prevents further flow of holes from the p-side to n-side.

Thus, immobile positive charge at the n-side and immobile negative charge at the p-side near the junction acts like a barrier or wall and prevents further flow of free electrons and holes, as shown in Figure 2.10. The region near the junction where flow of charges carriers are decreased over a given time and finally results in empty charge carriers or full of immobile charge carriers is called depletion region. The depletion region is also called as depletion zone, depletion layer, space charge region, or space charge layer. The depletion region acts like a wall between p-type and n-type semiconductor and prevents further flow of free electrons and holes, as shown in Figure 2.11 (www.physics-and-radio-electronics.com).

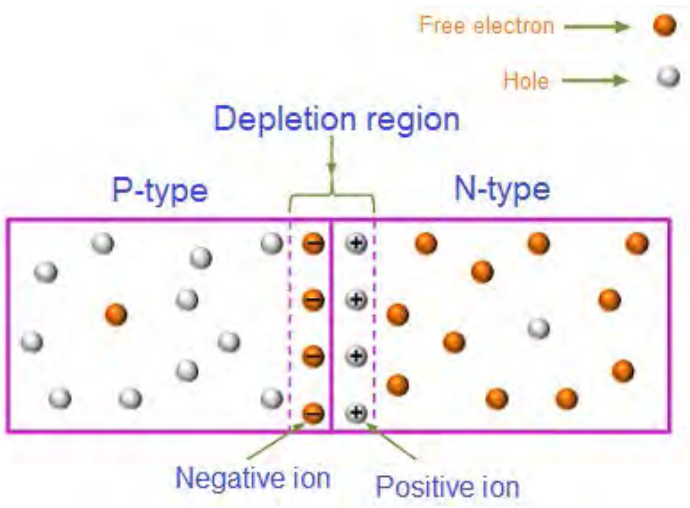

Figure 2.11 Depletion region of semiconductor (www.physics-and-radio electronics.com).

Two kinds of models for storing the oxidative energy of TiO_2 were proposed, p-n junction model and mediation model.

2.5.1 p-n Junction Model

In the former, a redox-active p-type semiconductor is combined with TiO_2 to form a p-n junction, as shown in Figure 2.12.

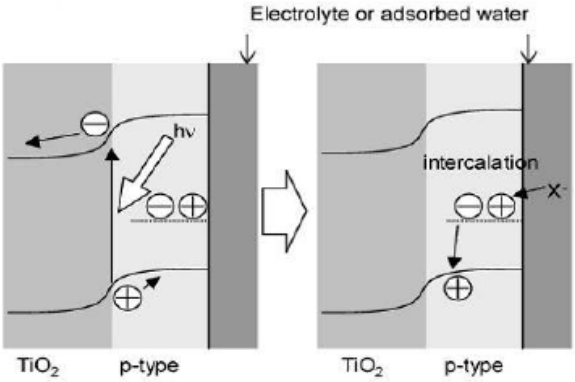

Figure 2. 12 p- n junction model for the oxidative energy storage photocatalysts (Takahashi and Tatsuma, 2005).

Semiconductors consist of a p-type and an n-type, where the n-type has a high electron concentration, and the p-type has a high hole concentration. The connection of the two types resulting in the move of excess electrons in the n-type material to the p-type side and the excess holes from the p-type material to the n-type side. An n-type semiconductor like TiO_2 adsorbs photon having energy equal to or higher than its band gap energy. With each photon of the required energy (i.e. wavelength), electrons rise to the unoccupied conduction band, leading to excited state conduction band electron and leaving the positive valence band holes (h^+) at the valence band. Later, the electrons then transfer from the p-type (electron donor) to the valence band of the n-type (electron acceptor) semiconductor at the junction between the p- and n-type semiconductors. The holes at the p-type are not stable and need intercalation (x^-) from an electrolyte for stabilization, as shown in Figure 2.12. The energy storage of TiO_2 with the p-type semiconductor takes place with the below model. The p-n heterojunction photocatalyst accelerates the separation of electron-hole pairs. Therefore, the p-n heterojunction photocatalyst has attracted much attention in recent years (Takahashi and Tatsuma, 2005).

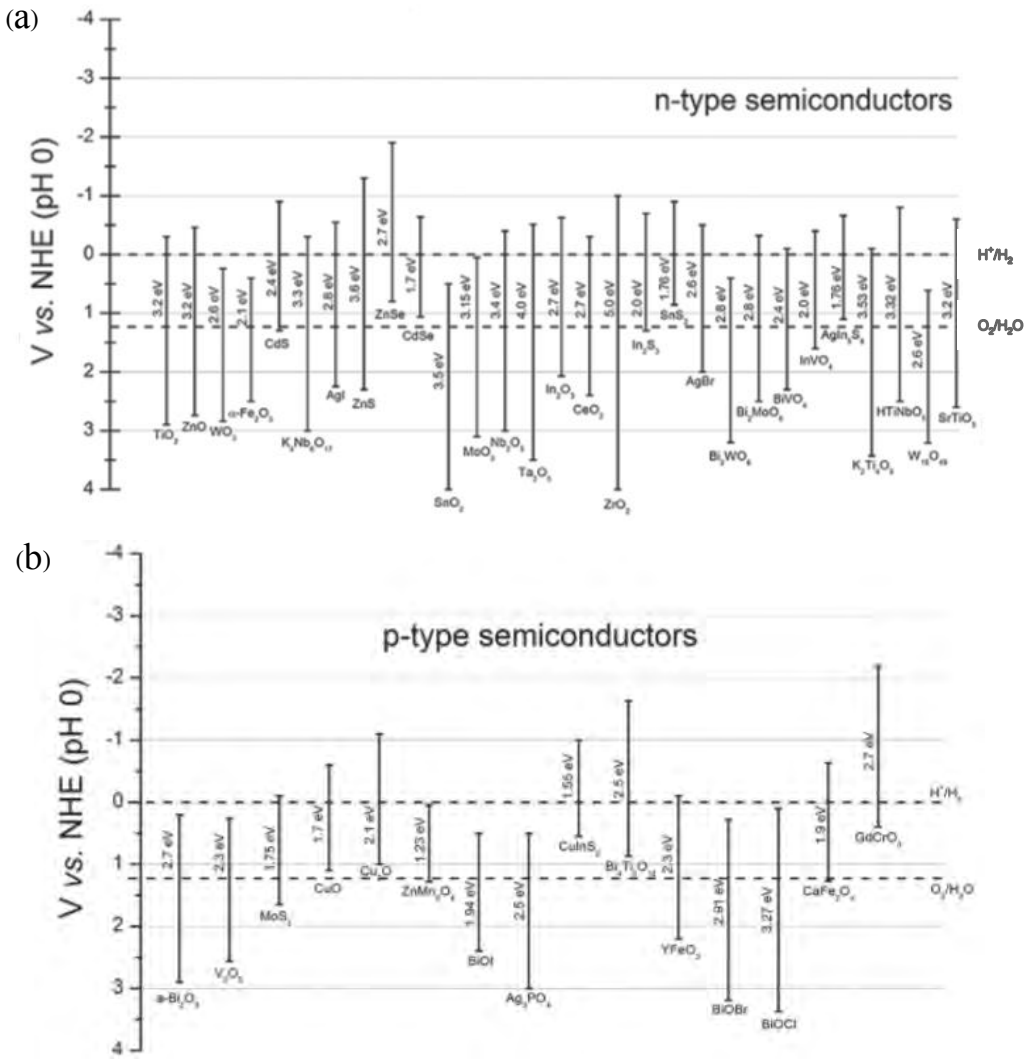

Figure 2.13 Band gaps and band positions of a) n-type semiconductors and b) p-type semiconductors used for composite photocatalyst heterojunction and values taken from references given in the article (Roland, 2014).

2.5.2 <u>Mediation Model</u>

In the mediation model, an oxidant likes O_2, which is photocatalytically produced by the oxidation of water adsorbed on TiO_2, diffuses and oxidizes a redox-active material.

The first step of the mediation model resembles the p-n junction model. That is a TiO_2 photocatalyst absorbs photon having energy equal to or higher than its band gap energy. With each photon of the required energy (i.e. wavelength), electrons

rise to the conduction band, leading to excited state conduction band electrons and leaving the positive valence band holes (h^+) at the valence band. On the other hand, unlike the p-n junction model, the electrons from the mediation (H_2O_2) then transfer to the valence band of TiO_2 for electrical neutrality, and the electrons of redox active material are transferred to mediation. As the result of the redox active material is wided in stability, intercalation (x^-) from an electrolyte for stabilization, as shown in Figure 2.14. The energy storage of TiO_2 with a redox active metal takes place with the below mechanism (Takahashi and Tatsuma, 2005).

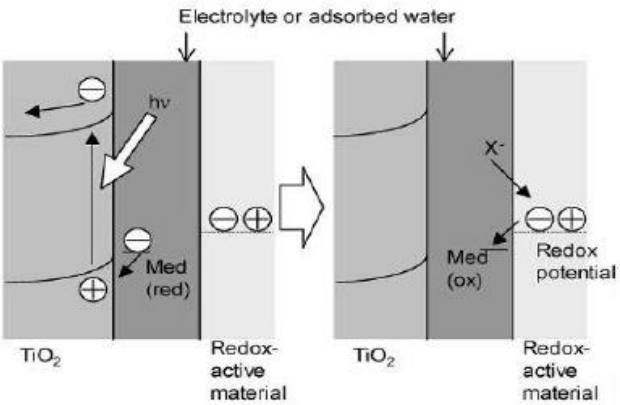

Figure 2. 14 Mediation model for the oxidative energy storage photocatalysts (Takahashi and Tatsuma, 2005).

Takahashi and Tatsuma (2005) studied oxidative energy storage ability of a TiO_2-$Ni(OH)_2$ bilayer photocatalyst. The TiO_2 and $Ni(OH)_2$ are reported to be an n-type and p-type semiconductor, respectively, hence, a p-n junction forms at the interface. They found that under UV light, electrons in the TiO_2 valence band are excited to the conduction band, and holes generate in the valence band. The oxidative energy storage, $Ni(OH)_2$ is oxidized to $NiO_x(OH)_{2-x}$ by the holes, and it could be turned from colorless to brown. After that, the brown-colored film could be turned back to colorless by electrochemical reduction. They suggested that the efficiency would be improved by increasing the junction area. And the stored oxidative energy can be discharged electrochemically or used for the chemical oxidation of various species.

Shifu *et al*. (2008) studied photocatalytic activity of p-n junction photocatalyst p-ZnO/n-TiO_2, which was evaluated by photocatalytic reduction of $Cr_2O_7^{2-}$ and photocatalytic oxidation of methyl orange (MO). The experiment results showed that the photoreduction activity of p-ZnO/TiO_2 increased with the increase in the amount of doped p-ZnO up to 2.0 wt%. When the amount of doped was higher than the optimal amount, the activity decreased as the amount of doped p-ZnO increased. On the other hand, the photocatalytic oxidation activity of p-ZnO/TiO_2 decreases rapidly with the increased in the amount of doped p-ZnO. They concluded that the p-n junction photocatalyst p-ZnO/TiO_2 had higher photocatalytic reduction activity, but lower photocatalytic oxidation activity. As the p-ZnO species can trap the hole, the photocatalytic reduction activity was enhanced greatly.

Yang *et al*. (2010) investigated oxidation and mineralization of methanol and formaldehyde by the stored oxidative energy and used TiO_2-$Ni(OH)_2$ as a photocatalyst. The results showed that the bilayer film turned brown after electrochemical oxidation to $NiO_x(OH)_{2-x}$ and bleaching of the film due to reduction of $NiO_x(OH)_{2-x}$. Then, the methanol can be oxidized to CO_2 by the stored oxidative energy. When the initial methanol concentration was increased, the mass conversion efficiency decreased because stored charges were consumed during the methanol oxidation. For the oxidation of formaldehyde, since it was easier to oxidize than methanol, hence, it was also oxidized to CO_2 by photoelectrochemically stored oxidative energy like methanol.

Lian *et al*. (2011) studied oxidative energy behavior of a porous nanostructured TiO_2-$Ni(OH)_2$ bilayer photocatalyst under UV light. They reported that the oxidative energy storage performance could be enhanced, resulting from its porous structure and nanostructured $Ni(OH)_2$ particles that may provide high specific surface area, fast redox reactions, and shortened diffusion path in solid phase. And the electrolytes with relatively high OH^- concentration facilitated the oxidative energy storage because it led to high crystal nucleation rate of $Ni(OH)_2$, thus the nanostructured particles were obtained. But, if the nucleation rate was too high, the particle sizes increased.

Dai *et al*. (2013) studied photoelectrocatalytic (PEC) activity of p-n junction Co_3O_4/TiO_2 nanotube arrays (NTs) that was evaluated by degradation of

methyl orange (MO). The results showed that the decrease in the MO concentration in the presence of unmodified TiO_2 NTs was small. On the contrary, 92% of MO was degraded by Co_3O_4/ TiO_2 thus it exhibited significantly enhanced PEC activity. The degradation rate of Co_3O_4/ TiO_2 was also faster than that over TiO_2 NTs. They discussed that Co_3O_4 is a p- type semiconductor, while TiO_2 is an n- type semiconductor. Therefore, the p- n junction is formed, which can improve separated efficiency of photogenerated carriers and inhibit their recombination.

2.6 Sol-gel Method for Thin Film Preparation

A number of methods, films such as sol-gel, sputtering, chemical vapor deposition, have been employed for the fabrication of TiO_2 thin. Each of these methods has its own advantages and disadvantages (Oshani *et al*., 2014).

For large area films preparation, the sol-gel method is apparently superior to vapor deposition methods. This scheme not only provides simplicity, low cost, and feasibility, but also proving as a precise approach to control doping concentrations (Lu *et al*., 2016b). This method is particularly attractive because of the following reasons: good homogeneity, ease of composition control, low processing temperature, large area coatings, low equipment cost and good optical properties and it allows the tuning of the refractive index and thickness of the film by varying synthesis parameters (Znaidi *et al*., 2012). Particularly, the sol-gel processes are efficient in producing thin film with high purity, transparent, multi-component oxide layers of many compositions on various substrates, including silica/glass plate, stainless steel plates, and aluminaplates (Oshani *et al*., 2014).

Sol-gel is a process, in which dispersions of a colloidal suspension, known as the sol, is formed in a liquid by the hydrolysis of inorganic or metal organic precursors, which is then followed by gel formation (Gaya, 2014). Normally, precursors such as titanium alkoxide, titanium tetrachloride, and titanium halogenide are heated under very high calcination temperature to obtain the desired crystal properties and a good adherence on the support. During heating, OH groups from the catalyst surface and the support can react and evaporate a molecule of water, creating an oxygen bridge, thus increasing the adherence of the catalyst to the support.

To immobilize uniform catalyst film on a substrate by sol-gel method, dip-coating or spin-coating technique is employed. Automated coaters are commercially available, to keep operator error minimal and accurately maintain dipping speed of substrate and duration. In general, a dip coating apparatus equipped with an adjustable motor is used to immerse the support into a solution (gel form) and then withdrawn it at a certain speed. Therefore, this route is suitable for the production of a thin film photocatalyst. However, some drawbacks of the sol-gel method include the wide variation in the particle size distribution and the necessity of a calcination step for crystallization, which may result in the melting of the substrate. To improve the drawbacks of substrate, there are many researches that studied sol-gel with dip-coating over fiberglass, woven fiberglass, aluminum plate, and glass slide as a substrate of thin film catalyst (Shan *et al*., 2010).

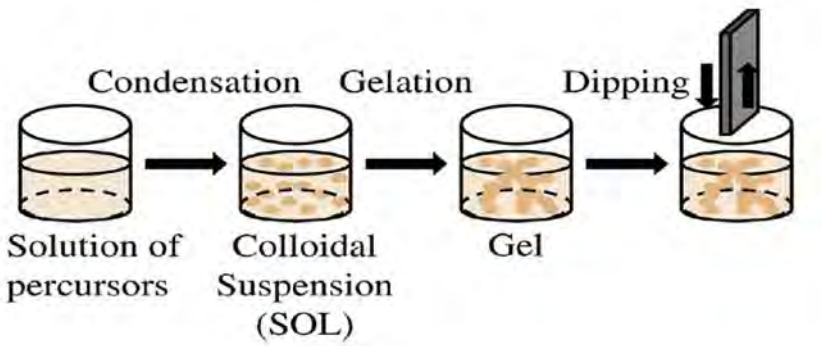

Figure 2.15 Schematic simplify diagram of sol-gel method associate with dip-coating (Angelo *et al*., 2013).

In regarding to spin-coating, it is a very convenient technique widely applied to uniform thin film deposition. As it is shown in Figure 2.16, an amount of solution is dropped on the substrate, which is fixed on the spin-coater, and then it is rotated at high speed in order to spread the fluid by centrifugal force. It can be considered as a special case of solution crystal growth, which allows the formation of highly oriented layered perovskites on a substrate, while the solvent is evaporating off. On the other hand, spin-coating enables deposition of hybrid perovskites on various substrates, including glass, plastic, quartz, silicon and sapphire. Selection of the substrate, the

solvent, the concentration of the hybrid in the solvent, the substrate temperature, and the spin speed are relevant parameters for this technique. In addition, post deposition low-temperature annealing (T < 250°C) of the hybrid films are sometimes employed to improve crystallinity and phase purity. David (2001) compared the traditional deposition technique for inorganic semiconductors with the spin-coating method and reported that the latter, spin-coating method does not require cumbersome equipment and gives high-quality films in quite short time (several minutes) in room environment.

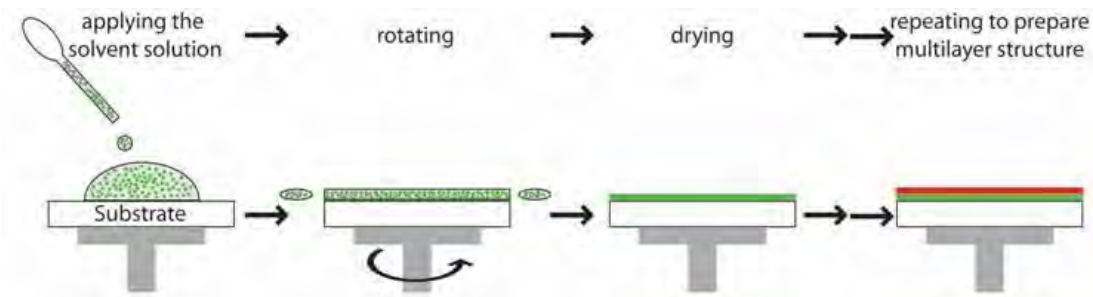

Figure 2.16 Schematic of the spin coating process (Sohrab *et al*., 2016).

Actually, in order to realize a layer with the desired thickness, the concentration of perovskites solution can be adjusted and keep the other spin-coating parameters (spin speed, acceleration, and spin duration) fixed. Generally, homogeneous 2D layered perovskite films with a thickness from 10 nm to 100 nm can be obtained by carefully selecting the parameters: less concentrated solutions give thinner layers. Therefore, the choice of the solvent is important because the solubility for both organic and inorganic must be considered (Sohrab *et al*., 2016).

Bahadur *et al*. (2006) studied morphologies of spin process derived thin films of ZnO using zinc nitrate and zinc acetate as precursor materials. The experiment showed that the films of ZnO prepared by using zinc acetate were smoother and more uniform than the zinc nitrate. Both of films were found to be crystalline in nature. The crystallite size of the nanograins in the zinc nitrate derived films was found to be smaller than the films grown by zinc acetate. They concluded that zinc acetate was the precursor material, which was suitable for preparation of ZnO films using sol-gel process or spray pyrolysis.

Lewkowicz *et al*. (2014) studied surface morphology and optical properties of TiO_2 thin films deposited on glass with the sol-gel spin coating technique. In the experiment, they used different annealing temperatures (380-900°C). The results showed that the TiO_2 thin films without annealing were amorphous but their structure shifted through the anatase to rutile phases. The amorphous nature of TiO_2 was obtained using the sol-gel methods, and the step of heat-treatment was required. The increasing of the annealing temperature, the porosity of the TiO_2 thin films decreased because of shrinkage and densification of the films. The TiO_2 films crystallize was the anatase phase between 380-700°C, while the rutile phase existed above 800°C.

Leonard *et al*. (2016) studied photocatalytic performance of SiO_2 and Ag-SiO_2 doped TiO_2 films by dip-coating process and powders to degrade methylene blue under UV light. The result showed that in the case of powders, crystallization was hindered by SiO_2 and Ag particles incorporation into the TiO_2 matrix, resulting to a decrease of the photocatalytic activity. In the case of thin film, crystallization was not influenced by the presence of SiO_2 and Ag particles. And the result also showed that films were slowly degraded due to surface contamination with carbon but both of SiO_2 and Ag can improve this problem. They concluded that the thin film can fully play their role of electron traps leading to an enhanced photocatalytic activity.

CHAPTER III
EXPERIMENTAL

3.1 Chemicals and Equipment

3.1.1 Chemicals

1. Bis(2,4-pentanedionato)-titanium (IV) oxide (reagent grade, $TiO(C_5H_7O_2)_2$, TCI Co., Ltd, Japan)
2. Zinc oxide (99%, ZnO, analytical grade, Ajax, Australia)
3. Isopropanol (99.7%, analytical grade, Carlo Erba Reagents, Italy)
4. Polyethylene glycol (100%, MW = 1000, $(H(OCH_2CH_2)_nOH$, Wako, Japan)
5. Sodium hydroxide (analytical grade, NaOH, Merck, Germany)
6. Hydrochloric acid (37%, HCl, analytical grade, Labscan, Thailand)
7. Ethanol (99.8%, C_2H_5OH, analytical grade, Merck, Germany)
8. Nitric acid (65%, HNO_3, Merck, Germany)
9. Cleaning solution (MICRO-90, Cole-Parmer, USA)
10. Deionized water

3.1.2 Equipments

1. Photocatalytic reactor
2. Spin coater (WS-650Mz-23NPPB)
3. pH meter
4. Vacuum pump (GAST0523-101Q-SG588DX)

3.2 Experimental Procedures

3.2.1 ZnO doped on TiO_2 Bilayer Films

A glass slide plate as the substrate was ultrasonically cleaned with the cleaning solution (MICRO-90) before coating. The TiO_2 film was coated on the glass plate with the solution containing 3 g of bis(2,4-pentanedionato)-titanium(IV) oxide and 3 ml ethanol by spin coating technique at 1,500 rpm for 20 s and calcined at 400ºC for 1 h. For the second layer, the ZnO layer was prepared by spin coating technique at the same conditions as above. TiO_2-sol was systhesized by sol-gel technique using titanium isopropoxide (TIPP) as a precursor. Firstly, 1.4 ml of 70% HNO_3 was diluted with 200 ml deionized water then added to 16.7 ml of TIPP under vigorous stir for a couple of days until clear solution was obtained. The resulting solution was dialyzed by a membrane to obtain TiO_2 sol at a pH condition of 3.5 ± 0.1. The solution containing TiO_2-sol with ZnO and polyethylene glycol was prepared. ZnO particles were obtained from the calcination temperatures at 400, 500 and 600ºC for 1 h, and denoted as 400ZnO, 500ZnO and 600ZnO, respectively. Then, the ZnO layer was coated on the TiO_2 layer and was calcined at 350ºC (heating rate 10ºC min^{-1}) for 1 h to obtain a ZnO/TiO_2 bilayer film.

3.2.2 Photocatalytic Activity

A 200 ml of a 100 ppm isopropanol solution was for the photocatalytic activity experiments. Adsorption of isopropanol on the bilayer films was allowed before the start of each experiment. An experiment started by turning on the uv-light source. The solution was subject to 2 h illumination before the light source is turned off for 2 h. The uv-light was then turned on for another 2 h before off for 2 h. The experiment setup was blocked from any interference from other light sources by using black box throughout the experiment. The solution samples were taken every hour for quantitative analysis by using gas chromatography (Agilent, 6890N).

3.2.3 Physical Characterization

The morphology of ZnO/TiO_2 bilayer films was examined by scanning electron microscope (SEM, Hitashi, S-4800). The crystalline structure and crystal size

was determined by X-ray diffraction measurement (XRD, Rigaku, Smartlab). The surface area, pore size, and pore volume are measured by Brunauer–Emmett–Teller surface area analysis (Quantachrome, Autosorb-1) and particle size diameter is analyzed by particle size analyzer (Malvern, Mastersizer X).

3.3 Analytical Technique

3.3.1 Gas Chromatography with Flame Ionization Detection (GC-FID)

The solution was tested every hour for quantitative analysis by using gas chromatography with flame ionization detection, (Agilent 6890N, DB-WAX column, 30 m × 0.32 mm, ID of 0.53 μm) which operated at 80°C and was connected to a flame ionization detector with H_2 as the carried gas, that use to determine the amount of product, the degradation of isopropanol was calculated by Eq 3.1.

$$\%Degradation = \frac{C_n - C_{n-2}}{C_n} \times 100\% \qquad (3.1)$$

Where C_n was a concentration at time (2,4,6,8 hr)

3.3.2 XRD Spectrometer

TiO_2 film, ZnO powder, and ZnO/TiO_2 bilayer films were detected X-ray diffractometer (XRD, Rigaku, Smartlab), with Cu-k_α radiation (λ = 1.5406 Å), 40 Kv, 30 mA) in the 2θ range of 20-80° with 3º/min scanning rate and step interval was 0.02º, to analyze crystal structure, chemical composition, and physical properties of thin films.

The Crystallite size (L) of selected sample were estimated using Scherrer's equation (Eq. 3.2).

$$L = \frac{0.9\lambda}{B\cos\theta} \qquad (3.2)$$

Where k = constant (k = 0.9)

λ = wavelength of the X-ray

B = FWHM (Full Width at Half Maximum) width of the diffraction peak

θ = diffraction angle

3.3.3 SEM Spectrometer

Surface characterization of TiO_2 film, ZnO powder, and ZnO/TiO_2 bilayer films were carried out by scanning electron microscopy (SEM, Hitashi, S-4800).

3.3.4 Brunauer–Emmett–Teller Surface Area Analysis

ZnO particles at different calcination temperature were characterized by BET surface area analyzer with N_2 adsorption at liquid nitrogen temperature (Quantachrome, Autosorb-1) to measure surface area, pore size, and pore volume of ZnO particles.

3.3.5 Particle Size Analyzer

The particle sizes of the ZnO powder at different calcination temperature were measured by Malvern's mastersize-2000 particle size analyzer (Malvern, Mastersizer X).

CHAPTER IV
RESULT AND DISCUSSION

4.1 Catalyst Characterization

The activity of ZnO/TiO_2 bilayer films for the photocatalytic degradation of isopropanol with and without UV illumination was investigated. In order to explain the properties of bilayer films, the photocatalyst films were characterized by scanning electron microscopy, Brunauer-Emmett-Teller surface area analysis**,** particle size analyzer, and X-ray diffractometer.

4.1.1 Scanning Electron Microscopy

The surfaces ZnO/TiO_2 photocatalyst bilayer films were studied from the SEM micrographs by using scanning electron microscopy (SEM, Hitashi, S-4800). The results are shown in Figures 4.1-4.2. Figure 4.1 shows the SEM micrographs of first TiO_2 layer, which shows the uniform surface. TiO_2 solution seems to cover well over the glass plate substrate. Figure 4.2 shows the SEM micrographs of ZnO/TiO_2 bilayer films, ZnO calcined at 600°C, which are denoted as $600ZnO/TiO_2$. From Figure 4.2a, it can be seen that the ZnO particles disperse on the TiO_2 layer. Figure 4.2b shows the porous structure of ZnO particles resulted from the removal of PEG in the preparation step. However, using PEG as a template, the well-ordered network pattern with a large specific surface area can be obtained as reported by Liu *et al*. (2005). It is the porosity of the second layer that allows isopropanol to adsorb on the first layer.

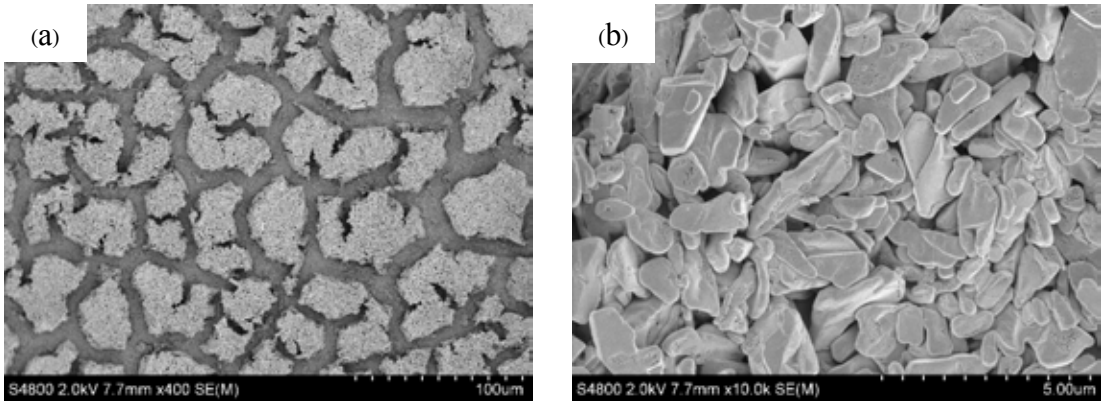

Figure 4.1 SEM micrographs of TiO_2 film at (a) 400X and (b) 10,000X magnification, respectively.

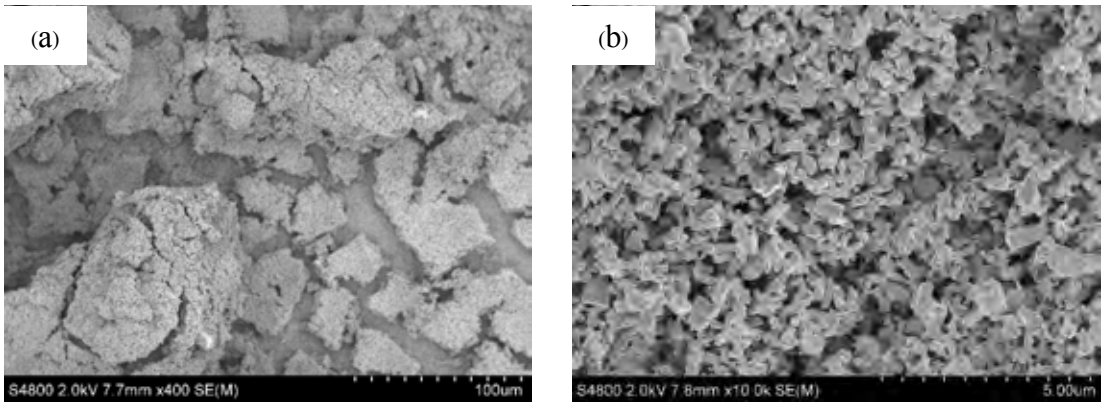

Figure 4.2 SEM micrographs of ZnO/ TiO_2 film at (a) 400X and (b) 10,000X magnification, respectively.

4.1.2 Particle Size Analysis

The particle size of ZnO was studied by the particle size analyzer (Malvern, Mastersizer X). The effect of the calcination temperature on the particle size diameter of ZnO is shown in Figure 4.3. It can be seen that by increasing the temperature, the particle size increases, which can be ascribed by the agglomerated particles. The results are consistent with those from the SEM micrographs, as shown in Figure 4.4. The ZnO particles are in the shape of hexagonal, which can be classified as wurtzite ZnO.

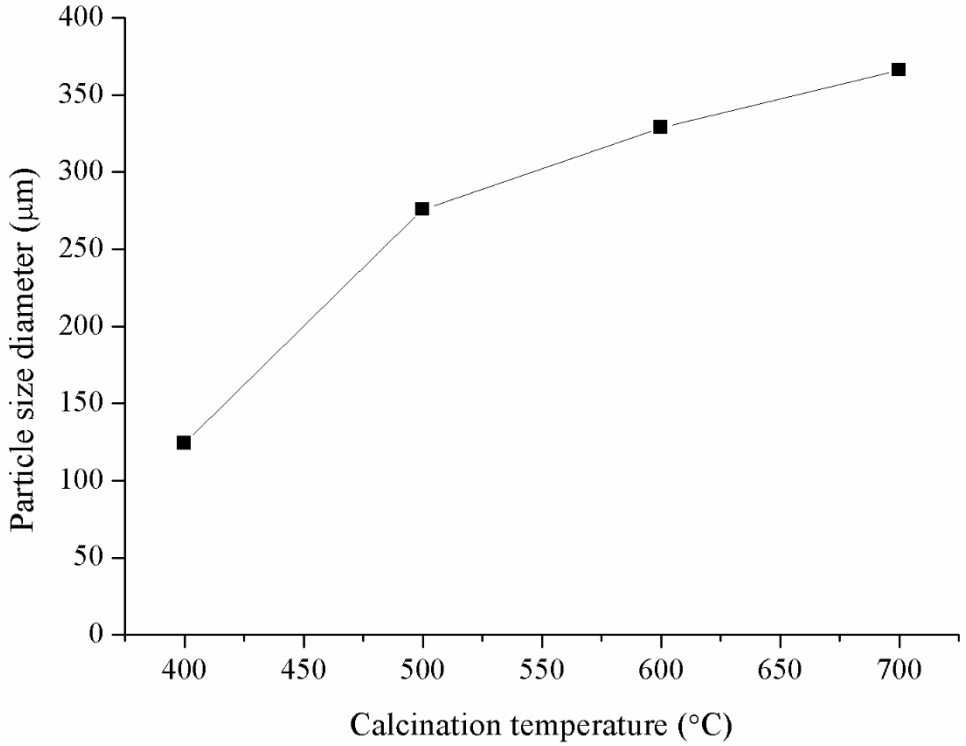

Figure 4.3 ZnO particle size diameters with different calcination temperature.

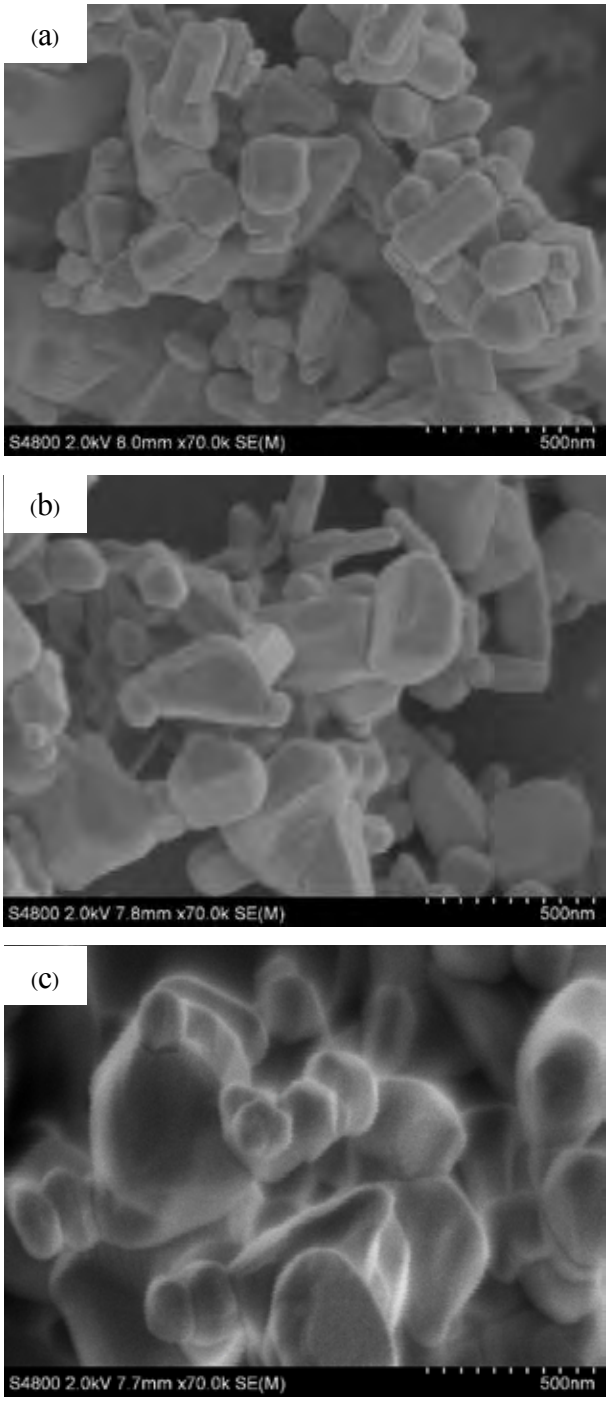

Figure 4.4 SEM micrographs of (a) 400ZnO, (b) 500ZnO, and (c) 600ZnO at 70,000X magnification.

4.1.3 Brunauer–Emmett–Teller Surface Area Analysis

The specific area, pore volume, and pore size of ZnO powder at various calcination temperature were measured (Table 4.1). The decrease in the surface area, pore volume, and pore size of ZnO can be observed when the calcination temperature is increased. That may be due to the collapse of the porous framework. However, the specific area, pore volume and pore size of 500ZnO, 600ZnO and 700ZnO are not significantly different.

Table 4.1 Effect of calcination temperatures on the physical properties of ZnO

Temperature (°C)	S_{BET} (m^2g^{-1})	Pore volume (cm^3g^{-1})	Pore size (Å)
400	10.59 ± 0.95	$2.31x10^{-2}$ ± 0.12	81.35 ± 0.61
500	5.66 ± 0.38	$0.99x10^{-2}$ ± 0.03	69.79 ± 1.11
600	5.14 ± 0.36	$0.92x10^{-2}$ ± 0.02	71.82 ± 0.35
700	4.32 ± 0.35	$0.81x10^{-2}$ ± 0.02	69.13 ± 0.41

4.1.4 X-ray Diffraction

The photocatalysts were studied by XRD technique. Figure 4.5 shows the XRD patterns of ZnO/TiO_2 bilayer films compared with TiO_2 and ZnO. TiO_2 in the thin films is of anatase form (with main peak at (101)). In addition, it is clear from the XRD pattern that ZnO is well crystallized and can be classified as hexagonal wurtzite modification, with dominating (101) peak. The XRD pattern of the ZnO/TiO_2 bilayer films is composed of TiO_2 and ZnO structures. The intensity of the main peaks of TiO_2 and ZnO in the bilayer films are more or less the same with those of TiO_2 and ZnO films. And it can be seen that, there is no indication for formation of any mixed compound.

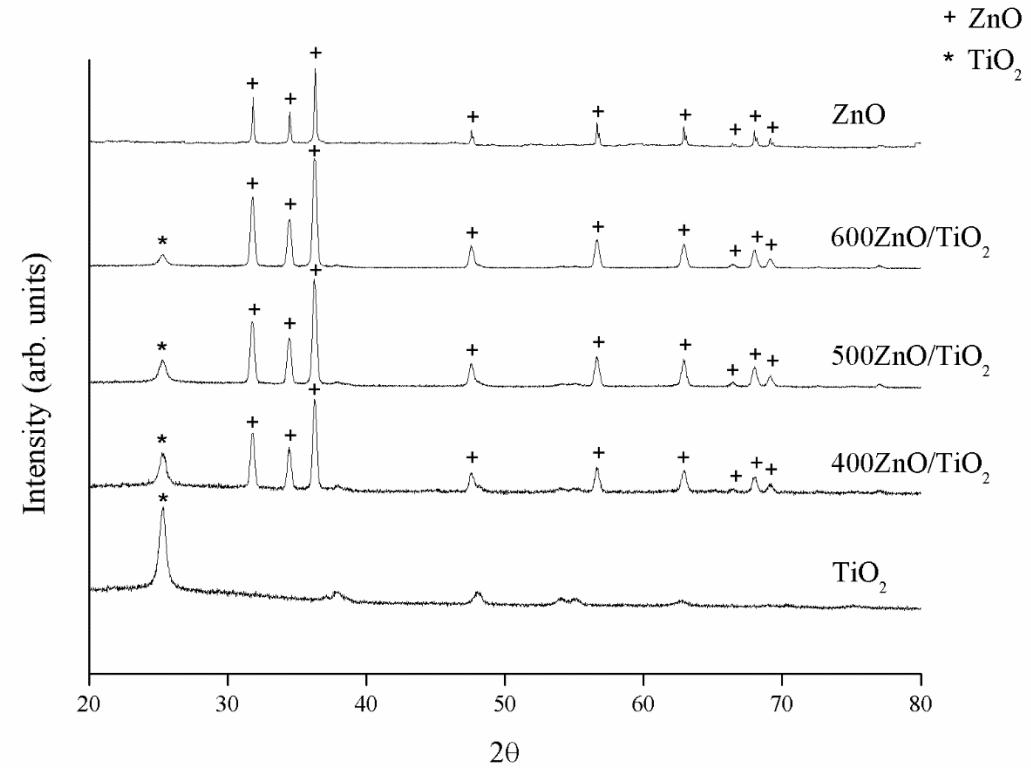

Figure 4.5 XRD patterns of TiO_2, ZnO and ZnO/TiO_2 bilayer films.

When the calcination temperature of ZnO/TiO_2 increases, the crystallinity of catalyst increases as indicated by the increase of the diffraction peak sharpness, Figure 4.6. The diffraction peak sharpness and narrowness improve with respect to the calcination temperature, and the full-width at half-maximum (FWHM) values are decreased with the increase in the calcination temperature (Rohani *et al*., 2010).

The XRD patterns of ZnO/TiO_2 with different ZnO loadings are shown in Figure 4.7 indicating that the peak patterns of all ZnO loadings are similar.

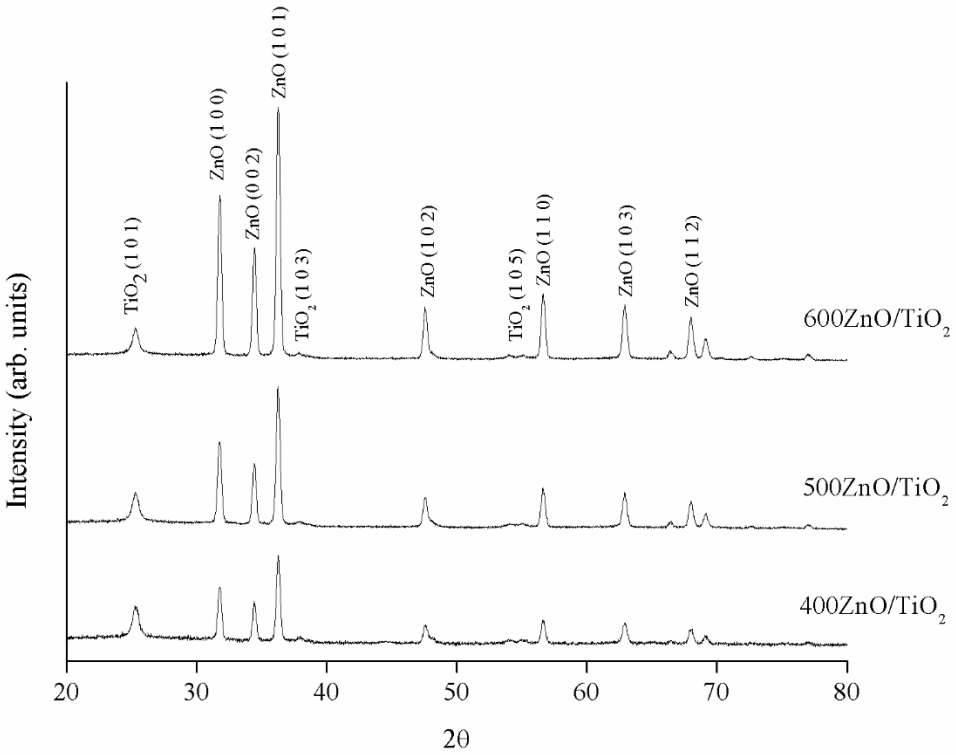

Figure 4.6 XRD patterns of 400, 500 and 600ZnO/TiO_2 bilayer films.

The average crystallite size of ZnO was calculated according to Scherrer's equation. The three highest peaks ((100), (002), and (101) planes) of ZnO were selected for this calculation. The results are given in Table 4.2. It is clear that there is an improvement in the crystallinity of ZnO by increasing the calcination temperature (Zulkiflee *et al*., 2016).

Table 4.2 Crystallite size of ZnO/TiO_2 bilayer films estimated using the XRD technique and Scherrer's equation

Temperature (°C)	400	500	600
Crystallite size (nm)	25.29	25.95	26.22

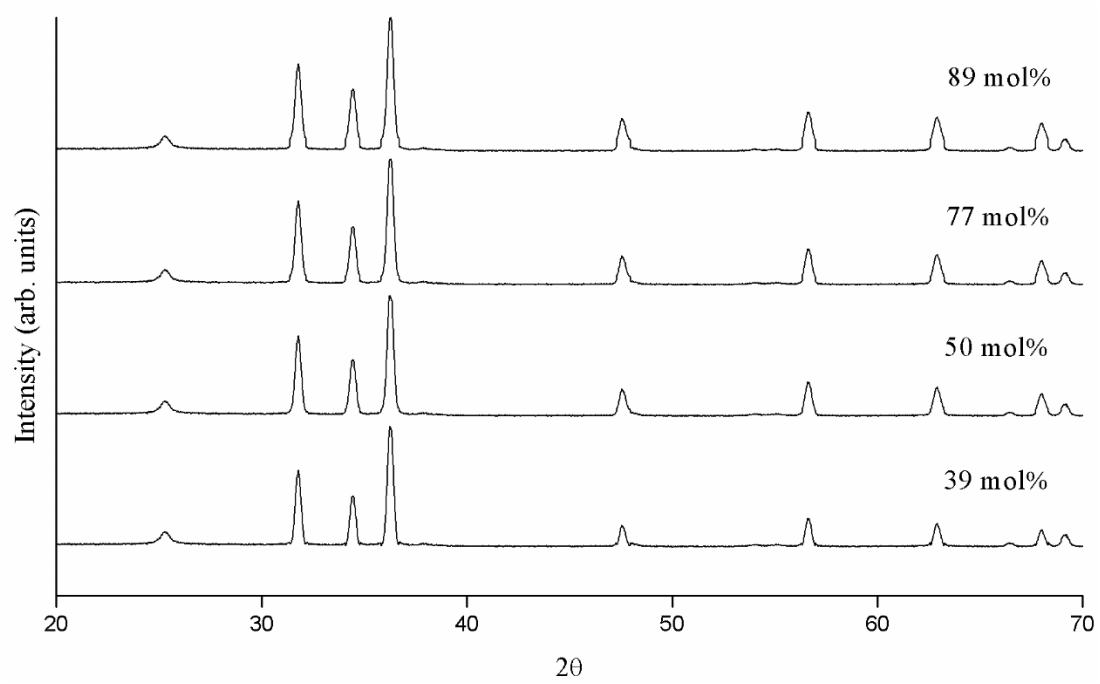

Figure 4.7 XRD patterns of ZnO/TiO_2 bilayer films with different ZnO loading.

4.2 Photocatalytic Activity

ZnO/TiO_2 was used as a bilayer film catalyst for the photocatalytic degradation of isopropanol (IPA). The first layer was coated by TiO_2 and then covered by the mixture of ZnO/TiO_2 as the second layer. The effect of adsorption was eliminated by immersing the film in the isopropanol solution for 12 h. The reactor was blocked from any disturbance from other light sources by using a black box. The conditions for the photocatalytic reaction were 30°C, 150 rpm of stirred speed, 5 lamps of UV light, 200 ml of 100 ppm isopropanol solution, and reaction time for 8 h. The amounts of either TiO_2 on the first layer or TiO_2 alone are 0.004 ± 0.001 g, and the amount of ZnO alone on the glass plate is 0.003 ± 0.001 g.

4.2.1 Photocatalytic Activity of TiO_2, ZnO, 400ZnO/TiO_2, 500ZnO/TiO_2, and 600ZnO/TiO_2 Films

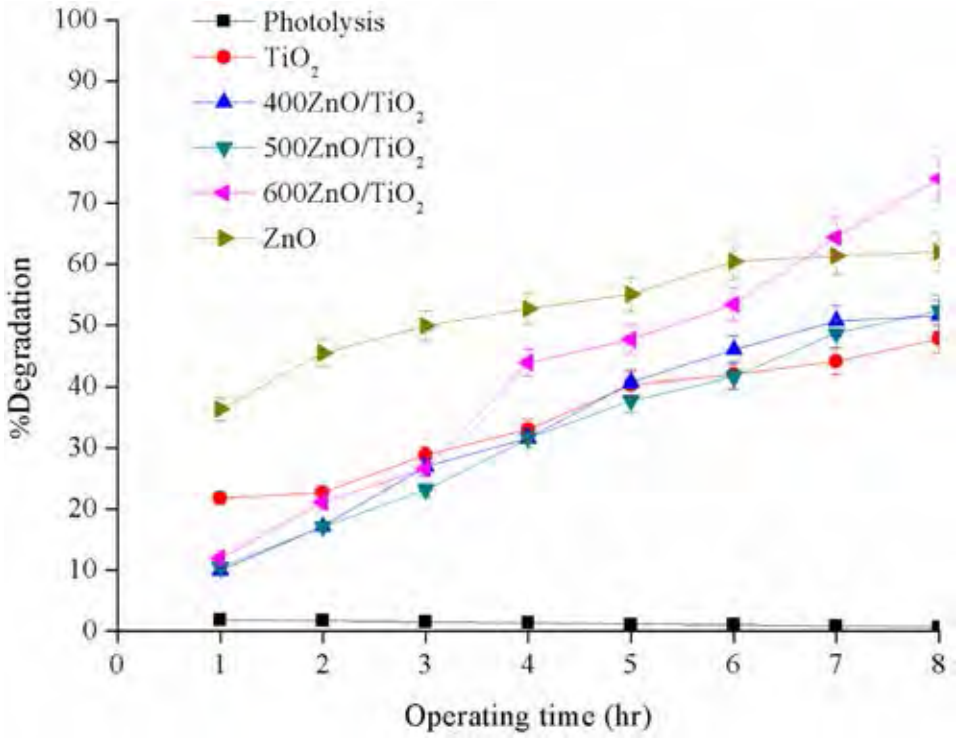

Figure 4.8 Photocatalytic degradation of isopropanol in unadjusted pH as a function of operating time by the TiO_2, ZnO, 400ZnO/TiO_2, 500ZnO/TiO_2, and 600ZnO/TiO_2 films with the UV illumination for 8 h.

100 ppm of isopropanol solution with the unadjusted pH of 6.3 are subject to UV light alone and with the presence of photocatalysts (Figure 4.8). The illumination in the absence of photocatalysts results in very little degradation of isopropanol at 8 h, whereas, in the presence of photocatalysts, higher degradation of isopropanol can be observed at 8 h up to 47.8-74.0%.

Figure 4.8 shows that the degradation of isopropanol increases with the increase in the operating time. At 8 h, TiO_2 shows the lowest activity, 47.8% degradation of isopropanol. In addition, the ZnO film shows higher degradation than TiO_2, up to 61.9%. The reason for the higher activity of ZnO is due to the absorption of more light quanta because the band gap of ZnO is 3.3 eV, and the quantum

efficiency is significantly larger than TiO_2 (3.2 eV). Other than that, the lower activity of TiO_2 results from recombination occurred at the interface due to fewer electron and hole scavengers present in the photocatalyst (Amalina *et al*., 2017). And 600ZnO/TiO_2 shows the highest photodegradation activity, 74.0%. The activity of 500ZnO/TiO_2 and 400ZnO/TiO_2 activity is about the same, 52.3% and 51.5%, respectively. At the beginning, the activity of 400, 500, and 600ZnO/TiO_2 are the same, but the activity of 400ZnO/TiO_2 and 500ZnO/TiO_2 becomes lower than 600ZnO/TiO_2 after 4 h. This might be ascribed to the photocorrosion phenomenon in the ZnO particles that results in the reduction the availability of surface active sites for the reaction to take place (Kodihalli and Timmappa, 2012). The activity of 600ZnO/TiO_2 works more effectively corresponding to the maximum formation of hydroxyl radicals on the ZnO/TiO_2 surface resulted from low recombination of electron-hole pairs, resulting in the destruction of the target organic pollutant (Yu *et al*., 2006). When the bilayer film is contacted with the UV-irradiation, the photogenerated electrons of the ZnO conduction band will be transferred to the conduction band of TiO_2, while the photogenerated electrons of TiO_2 will remain in the conduction band of TiO_2. Since the holes move in the opposite direction from the electrons, the photogenerated holes of the TiO_2 valence band will be transferred to the valence band of ZnO, which makes charge separation more efficient. Furthermore, according to the band edge position, as the conduction band of TiO_2 is lower than that of ZnO, the former can act as a source for the photogenerated electrons (Shifu *et al*., 2008). On the other hand, ZnO can increase concentration of free electrons in the conduction band of TiO_2, which implies that the charge recombination is reduced in the process of electron transport (Zhang *et al*., 2007).

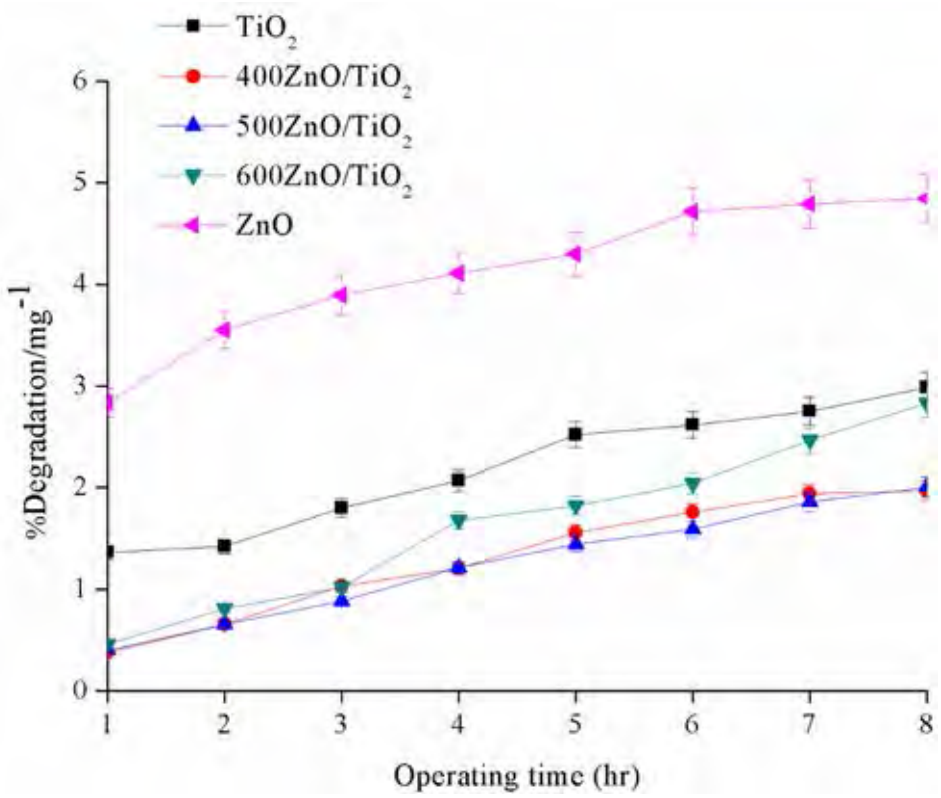

Figure 4.9 Photocatalytic degradation of isopropanol per catalyst loading weight in unadjusted pH as a function of operating time by the TiO_2, ZnO, 400ZnO/TiO_2, 500ZnO/TiO_2, and 600ZnO/TiO_2 films with the UV illumination for 8 h.

Figure 4.9 shows the photocatalytic degradation of isopropanol per weight of loading of TiO_2, ZnO, 400ZnO/TiO_2, 500ZnO/TiO_2, and 600ZnO/TiO_2 films. It can be seen that the degradation per weight of loading of 400ZnO/TiO_2, 500ZnO/TiO_2, and 600ZnO/TiO_2 bilayer films are lower than TiO_2 and ZnO alone, which is possible that the bilayer films have more thickness and weight of catalyst than TiO_2 and ZnO alone that resulted in cannot allow light to go through and activate radicals from the first TiO_2 layer; thus, the lower degradation efficiency.

Under light irradiation, isopropanol is gradually oxidized through an acetone intermediate, and the concentration of isopropanol and acetone changes as shown in Figure 4.10. It is clear that the concentration of acetone increases continually, while the concentration of isopropanol decreases with the long-term irradiation. Isopropanol photocatalytic degradation mechanisms are shown in Figure 4.11.

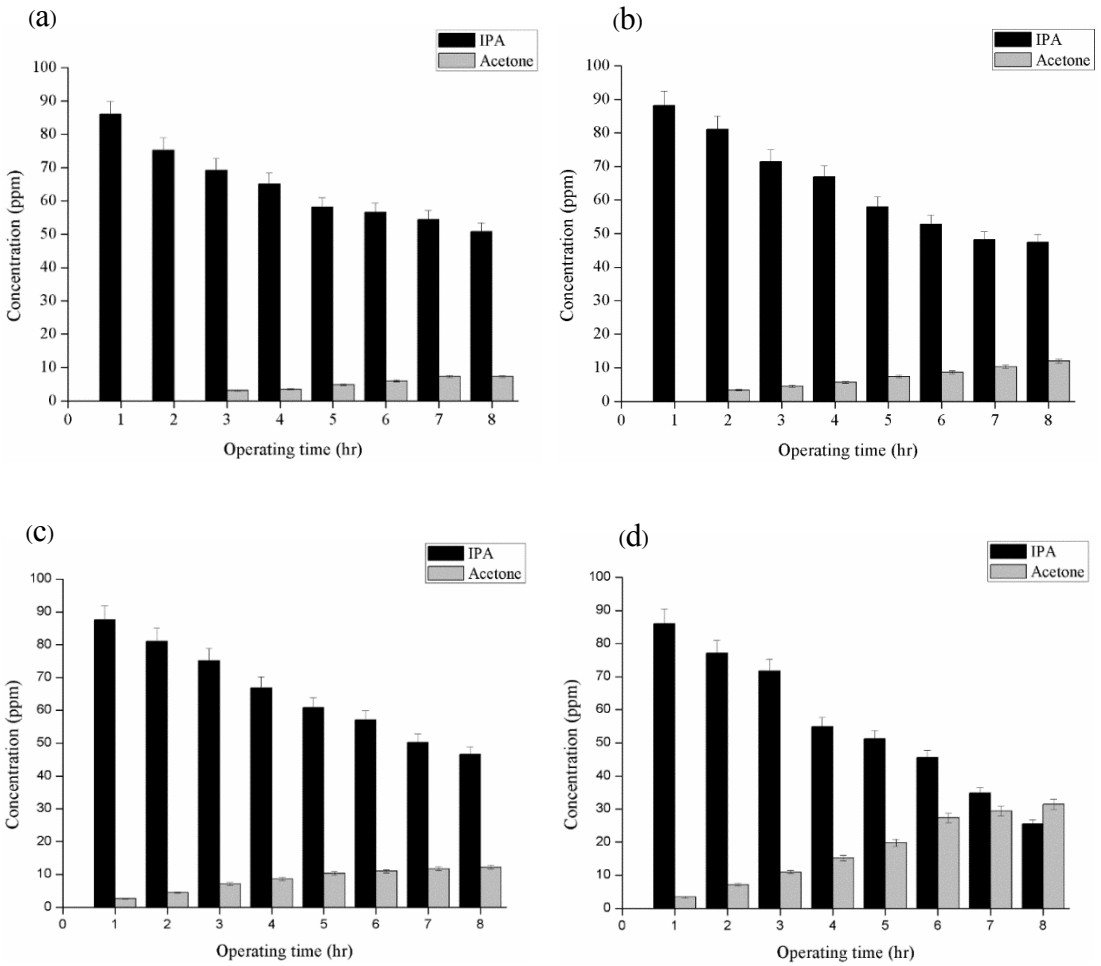

Figure 4.10 Changes of isopropanol concentration and acetone from isopropanol degradation as a function of operating time over the (a) TiO_2, (b) 400ZnO/TiO_2, (c) 500ZnO/TiO_2 and (d) 600ZnO/TiO_2 films with the UV illumination for 8 h.

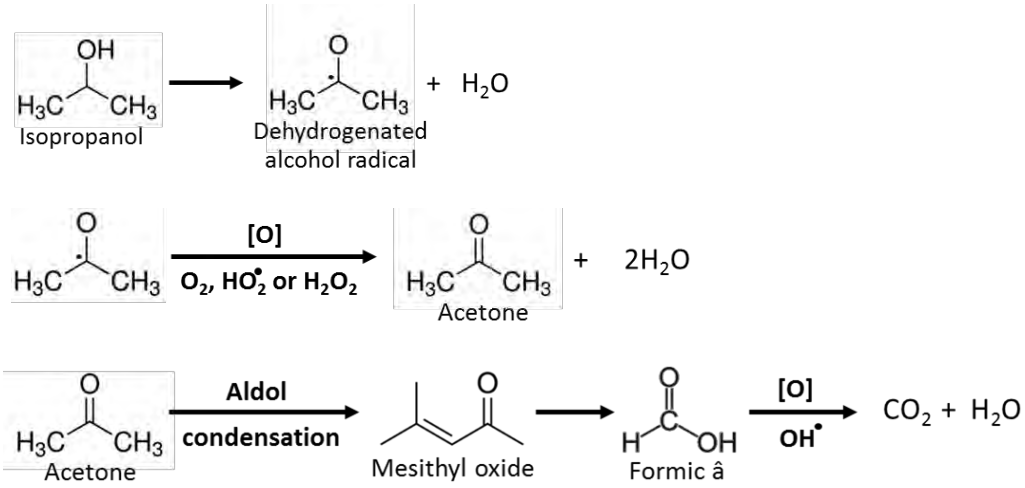

Figure 4.11 Isopropanol photocatalytic degradation mechanism (Kimball and Dowden, 1978).

4.3 Energy Storage

4.3.1 Energy Storage of TiO_2 Films

To set a baseline for energy storage of photocatalyst films, the TiO_2 film was first used. TiO_2 used for the film preparation was calcined at 400°C. The conditions for the photocatalytic reaction were 30°C, 150 rpm of stirred speed, 5 lamps of UV light, 200 ml of 100 ppm isopropanol solution at unadjusted pH. The UV light was turned on for 2 h and turned off for 2 h until 8 h operating time. From Figure 4.12, the result indicates that the degradation of isopropanol is about 16.5% after the first illumination and 14.1% after the second illumination. The reduction in the degradation of isopropanol is possibly caused by the low activity of TiO_2 alone. Furthermore, TiO_2 activity is limited by two main factors: the inability to absorb light and the fast recombination of photogenerated electron and hole (Adriana, 2008). Furthermore, intermediate products might be there, which are not desorbed from the catalyst surface; therefore, isopropanol cannot adsorb on the surface that causes low degradation efficiency. Thus, TiO_2 shows low photocatalytic activity even the photocatalytic system is under illumination. Without illumination, the highest degradation rate is about 2.6%. It possible that the amount of isopropanol may adsorb on the catalyst

surface. Moreover, the n-type TiO_2 first layer cannot form the p-n catalyst; thus, the degradation is very low.

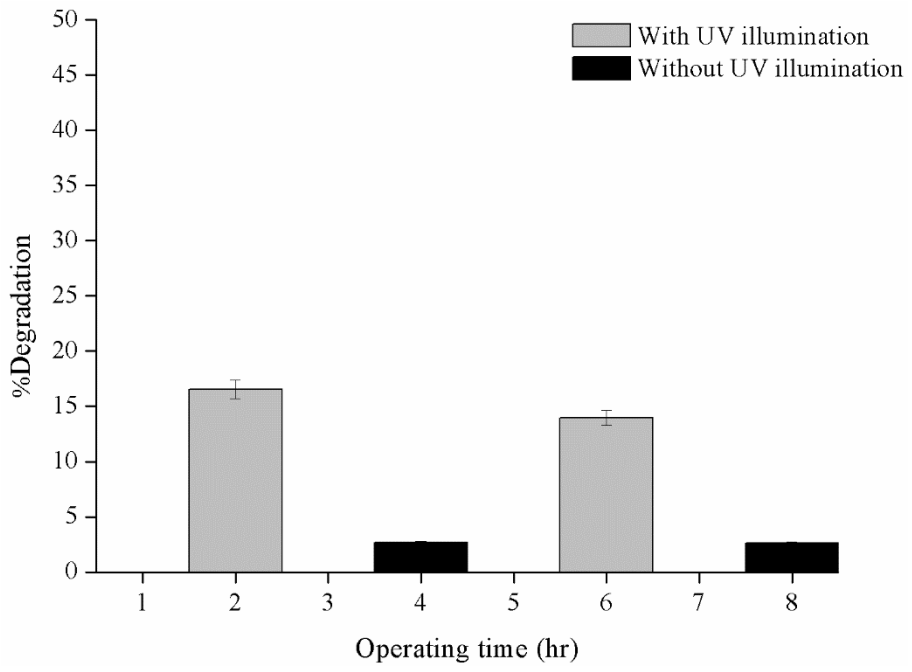

Figure 4.12 Photocatalytic degradation of isopropanol in unadjusted pH as a function of operating time by the TiO_2 film with and without UV illumination.

4.3.2 Energy Storage of ZnO Films

From Figure 4.13, the result shows that the degradation of isopropanol is about 17.0% after the first illumination and 16.5% after the second illumination. This indicates that ZnO has higher activity than TiO_2 under UV illumination. However, without illumination, the highest degradation rate is about 1.9%. Like the TiO_2 films, it possible that the amount of isopropanol may adsorb on the catalyst surface. Moreover, the p-type ZnO first layer cannot form the p-n catalyst; thus, the degradation is very low.

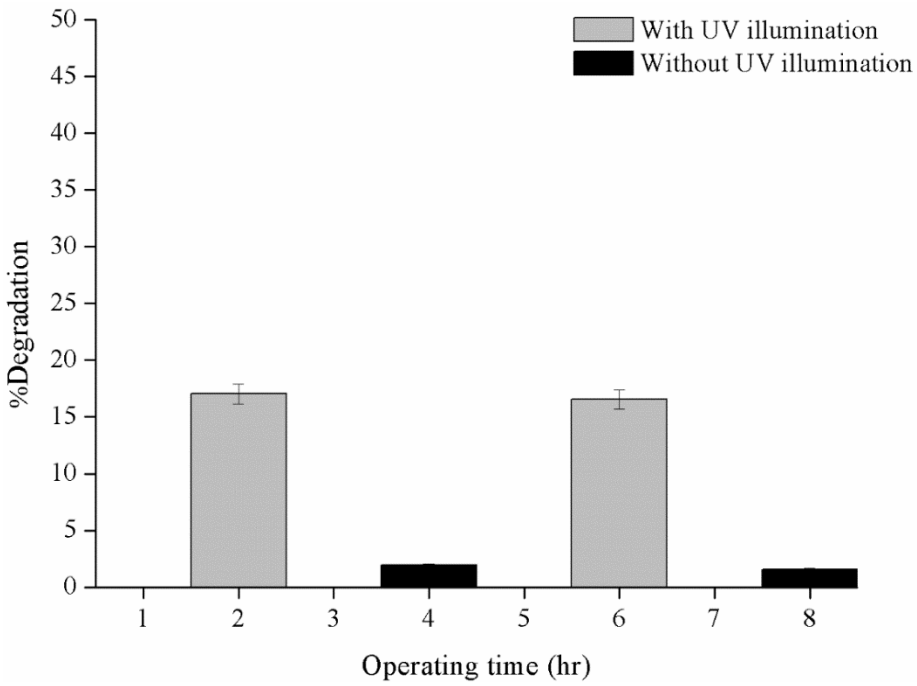

Figure 4.13 Photocatalytic degradation of isopropanol at unadjusted pH as a function of operating time by the ZnO film with and without UV illumination.

4.3.3 Effects of UV Exposure Time of the 600ZnO/TiO_2 Bilayer Film on the Oxidation Energy Storage

Exposure time of the 600ZnO/TiO_2 bilayer film to UV irradiation was also studied. The UV light was turned on 1 h and turned off 1 h until 8 h, turned on 2 h and turned off 2 h until 8 h, and turned on 3 h and turned off 3 h until 12 h.

The results show that the reaction by exposure time of 2 h has higher energy storage efficiency than the reaction by exposure time of 3 h. For the UV exposure for 1 h, the degradation without illumination is lower than zero. It may be possible that having too short of the exposure time does not have enough electrons and holes resulting in a lower extent of isopropanol degradation, and the adsorbed isopropanol could desorb from the catalyst. Thus, the UV exposure time for 1 h is not suitable for energy storage.

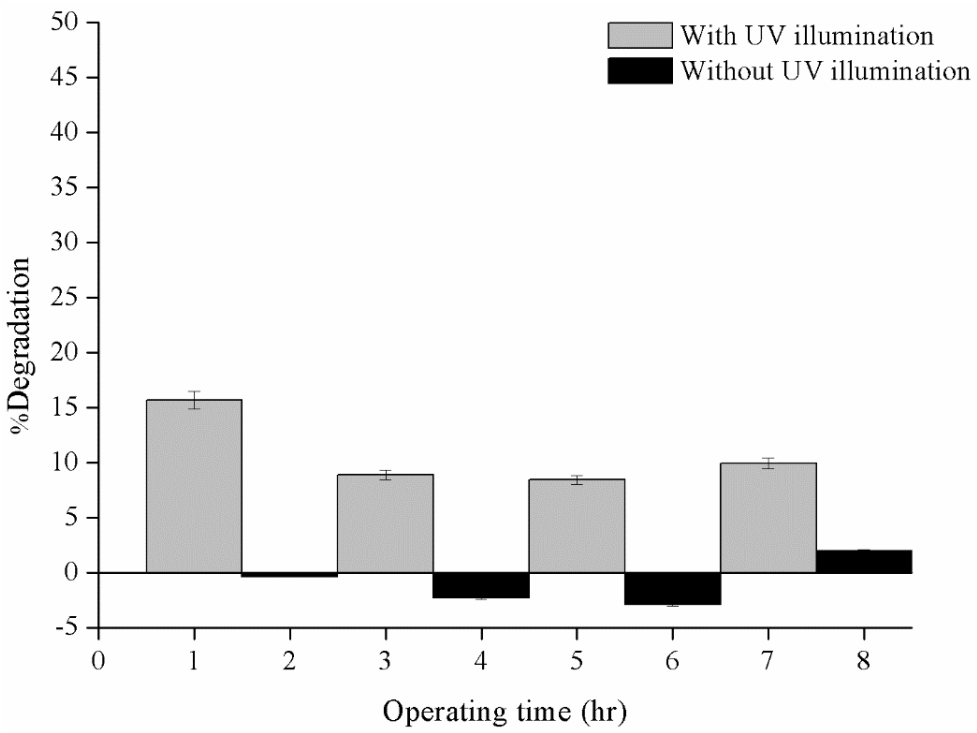

Figure 4.14 Photocatalytic degradation of isopropanol at unadjusted pH by the 600ZnO/TiO_2 film, UV irradiation for 1 h and turn off 1 h until 8 h.

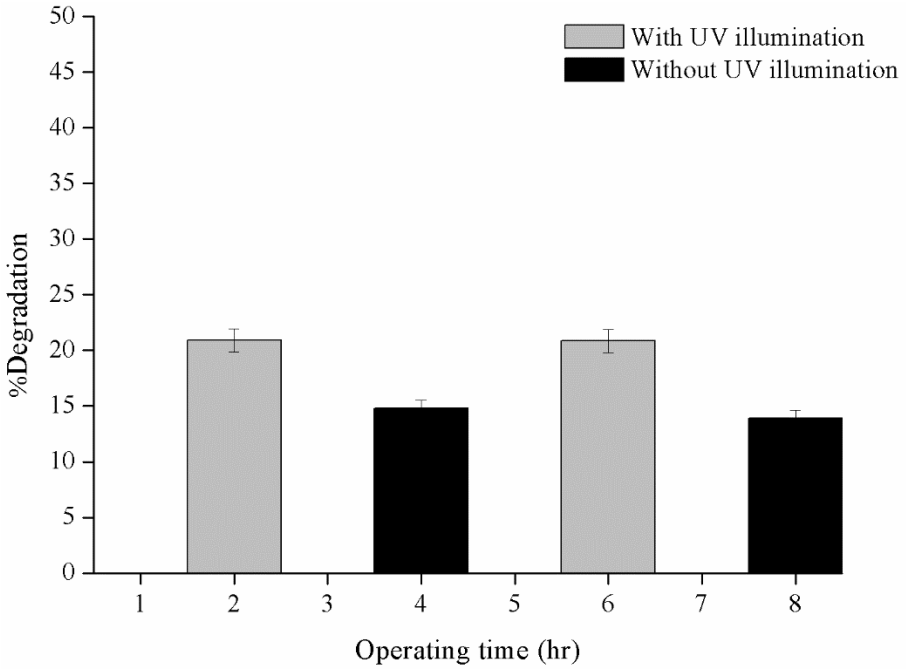

Figure 4. 15 Photocatalytic degradation of isopropanol at unadjusted pH by the 600ZnO/TiO_2 film, UV irradiation for 2 h and turn off 2 h until 8 h.

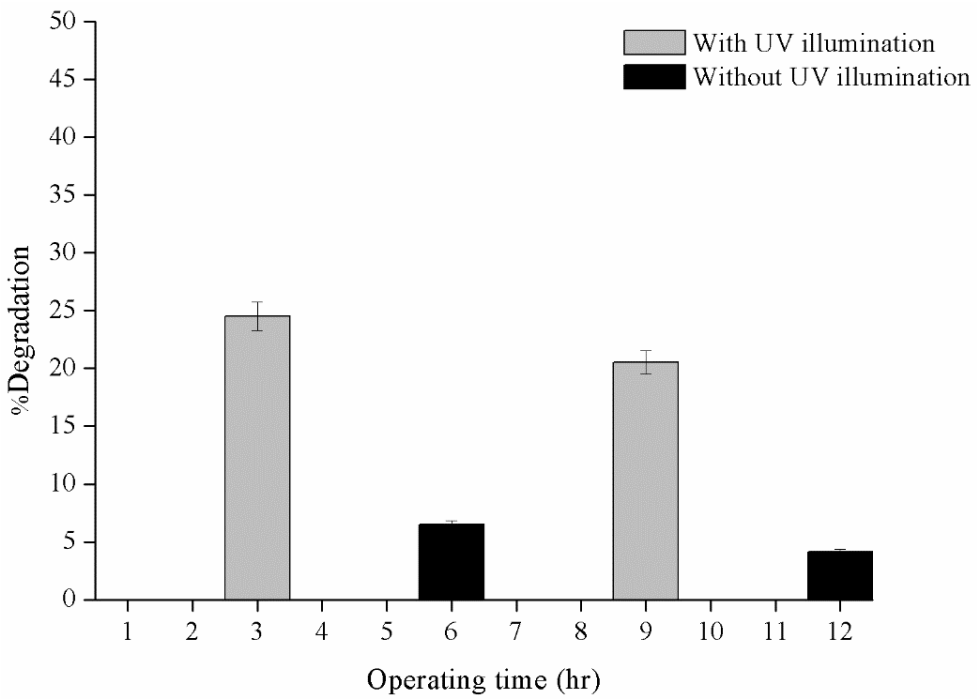

Figure 4. 16 Photocatalytic degradation of isopropanol at unadjusted pH by the 600ZnO/TiO_2 film, UV irradiation for 3 h and turn off 3 h until 12 h.

4.3.4 <u>pH Effects on the ZnO/TiO_2 Bilayer Film Activity on the Photocatalytic Reaction</u>

In this study, the effect of pH of isopropanol solution on the photodegradation was examined at pH 3.0, which was adjusted by HCl, and the unadjusted pH (pH 6.3).

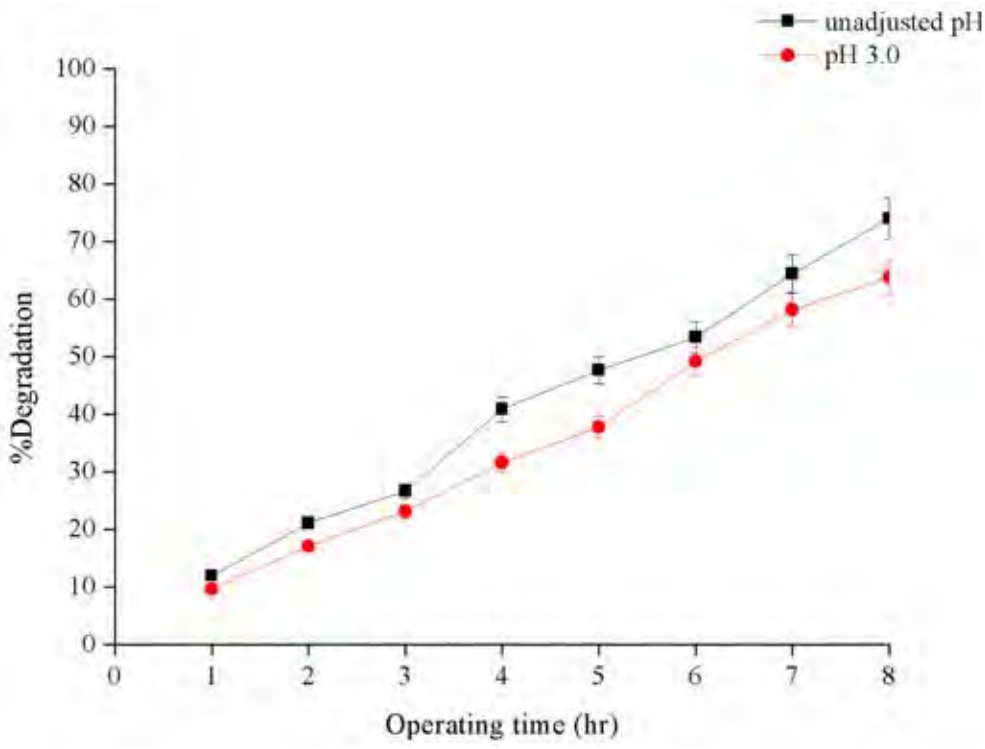

Figure 4.17 pH effect of 600ZnO/TiO_2 film on the photocatalytic degradation of isopropanol at various pH with the UV illumination for 8 h.

It was observed that the degradation efficiency with ZnO/TiO_2 decreases with the decrease in the pH exhibiting maximum of degradation at unadjusted pH, 74.0% (Figure 4.17). pH simply influences the surface charge of the photocatalyst, affecting the adsorption of the substrate onto the surface charge of the photocatalysts known as reaction site as well as the hydroxyl radical ($OH^{\bullet}$) formation (Chavadej *et al*., 2009). The pH effect on the photodegradation of isopropanol in the presence of ZnO/TiO_2 can be explained by using zero point charge (pH_{pzc}). The pH_{pzc} of ZnO is approximately 8.5 and that for TiO_2 is about 5.3; therefore, about 7.0 could be the resultant pH_{pzc} of bilayer films. Thus, the surface of the photocatalyst becomes positively charged at lower pH, but at higher pH, it becomes negatively charged (Habib *et al*., 2013). Although isopropanol can adsorb preferentially on the positively charged surface in the acidic condition, the degradation at pH 3.0 is less than at the unadjusted pH as the photocorrosion of ZnO may take place at lower pH. Bahnemann *et al*. (1987)

mentioned that ZnO is unstable due to incongruous dissolution to yield $Zn(OH)_2$ on the ZnO particle surfaces and thus leading to catalyst inactivation.

4.3.5 pH Effects on the ZnO/TiO_2 Bilayer Film Activity on the Oxidation Energy Storage

ZnO/TiO_2 bilayer films were used as a photocatalyst to study the effect of oxidation energy storage on the photocatalytic activity with and without UV illumination. Isopropanol solution was adjusted to pH 3.0 by HCl. Figure 4.18 indicates the concentration of isopropanol at various times compared with isopropanol initial concentration by different pH, which shows the degradation rate of the isopropanol solution at unadjusted pH is higher than at pH 3.0 for both with and without light illumination.

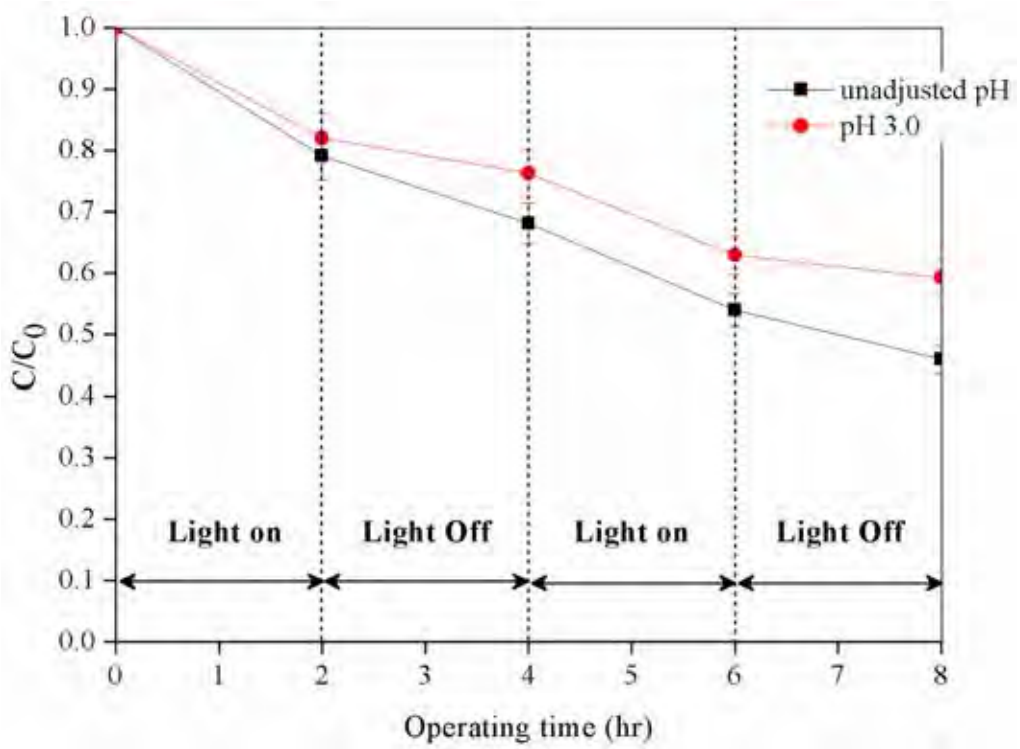

Figure 4.18 Concentration of isopropanol at various time compared with isopropanol initial concentration by the ZnO/TiO_2 bilayer films with different pH.

From Table 4.3, with UV illumination, the degradation rate of isopropanol solution at unadjusted pH by using ZnO/TiO_2 bilayer films shows the highest rate. As described before, unadjusted pH can improve the reaction site more than at pH 3.0. Other than that, at pH 3.0, might be occurred the presence of inhibition on the surface of catalyst could occur. However, the result without UV illumination shows that the degradation rate of isopropanol at unadjusted pH by ZnO/TiO_2 is also higher than at pH 3.0. Therefore, we will focus on the degradation of isopropanol at unadjusted pH by ZnO/TiO_2 to find the other optimum factors.

Table 4.3 Reaction rates of isopropanol by the ZnO/TiO_2 bilayer films with different pH

	Reaction rate ($x10^5$ s^{-1})			
	Operating time (h)*			
	2	**4**	**6**	**8**
Unadjusted pH	2.90	1.53	1.97	1.11
pH 3.0	2.50	0.79	1.85	0.51

* The UV illumination was on for two hours (2 h operating time). Then, the illumination was off for two hours (4 h operating time). After that, turning it on for two more hours (6 h operating time) and off for the last two hours (8 h operating time).

4.3.6 <u>Effects of ZnO Loading of the 600ZnO/TiO_2 Bilayer Film on the Oxidation Energy Storage</u>

Figures 4.19-4.22 show the degradation of isopropanol from ZnO/TiO_2 at various ZnO loadings. The results show that the isopropanol solution can be degraded with every ZnO loading with and without UV illumination. That be due to the p-n junction of ZnO/TiO_2, with ZnO and TiO_2 as a p-type semiconductor (p-ZnO) and n-type semiconductor (n-TiO_2), respectively. When doping p-ZnO into n-TiO_2, a number of micro p-n junction are formed. At equilibrium, the p-ZnO region is negatively charged, while the n-TiO_2 is positively charged. Under UV irradiation, electron-hole pairs are generated, then the holes flow into the negative field p-ZnO,

and the electrons flow into the positive field n-TiO_2. Thus, the electron-hole pairs are separated effectively by the p-n junction. Moreover, the p-ZnO can act as a source for photogenerated electrons that are transferred to the conduction band of n-TiO_2, while the photogenerated electrons of n-TiO_2 remain in the conduction band of n-TiO_2. In addition, the holes move in the opposite direction from the electrons, the valence band of p-ZnO (Shifu *et al*., 2008). It was reported that the holes could be trapped by p-ZnO into the Zn^{2+} form (Jing and Lu, 2003). Takahashi and Tatsuma (2005) reported that the photogenerated holes are transported into the p-semiconductor for the oxidative energy storage. From this reason, the p-n junction of ZnO/TiO_2 contributes to energy storage.

In order to examine the effect of ZnO loading on the 600ZnO/TiO_2 bilayer films, ZnO/TiO_2 was prepared at 4, 8, 15, and 19 mol% ZnO loadings (per total film). Figures 4.19-4.22 show the photocatalytic degradation of isopropanol with various ZnO loadings at unadjusted pH. When the ZnO loading is increased from 4 mol% to 15 mol%, the degradation activity with and without UV illumination increases until the loading hits 15 mol% and then decreases when the loading is increased to 19 mol%. Moreover, the ZnO has higher activity than TiO_2 because it has wide energy band gap; thus, it can harvest wide UV region. Chavadet *et al*. (2008) mentioned that increasing the catalyst loading resulted in increasing the generation of active species to react with organic molecules, consequently increasing the reaction rate, as shown in Table 4.4. And, with higher loading, the dispersion of ZnO particle on TiO_2 surface may decrease, resulting in larger ZnO particle. Bansal *et al*. (2009) mentioned that, with the high dose of catalyst, there was a decrease in the UV light penetration; hence, the photoactivated electron-hole pairs decrease. Therefore, the light masking effect by ZnO particles on the TiO_2 surface also has a negative factor on the photocatalytic activity.

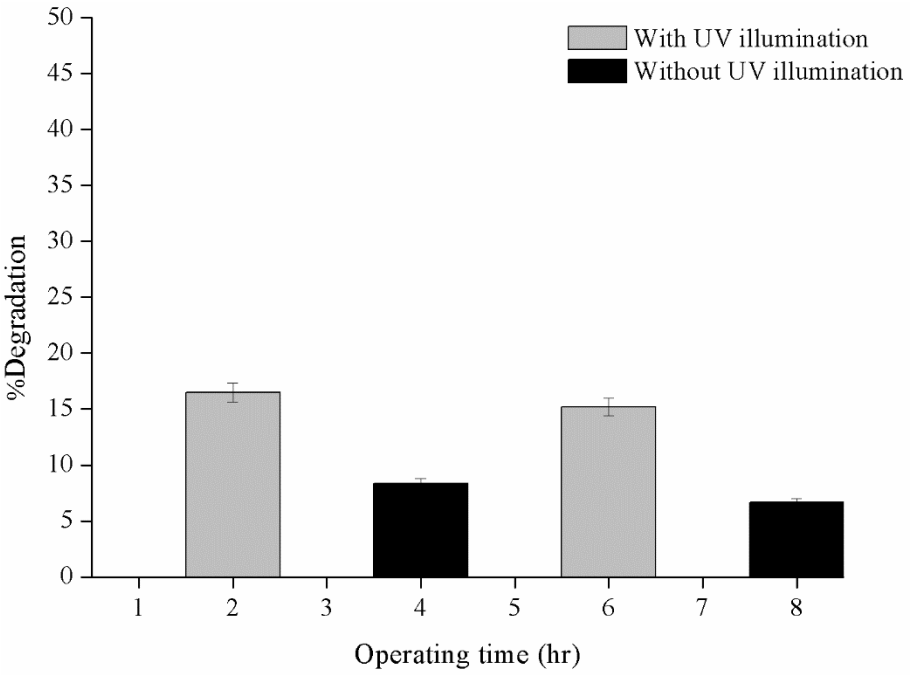

Figure 4.19 Photocatalytic degradation of isopropanol at unadjusted pH by the 600ZnO/TiO_2 film, 4 mol% ZnO, with and without UV illumination.

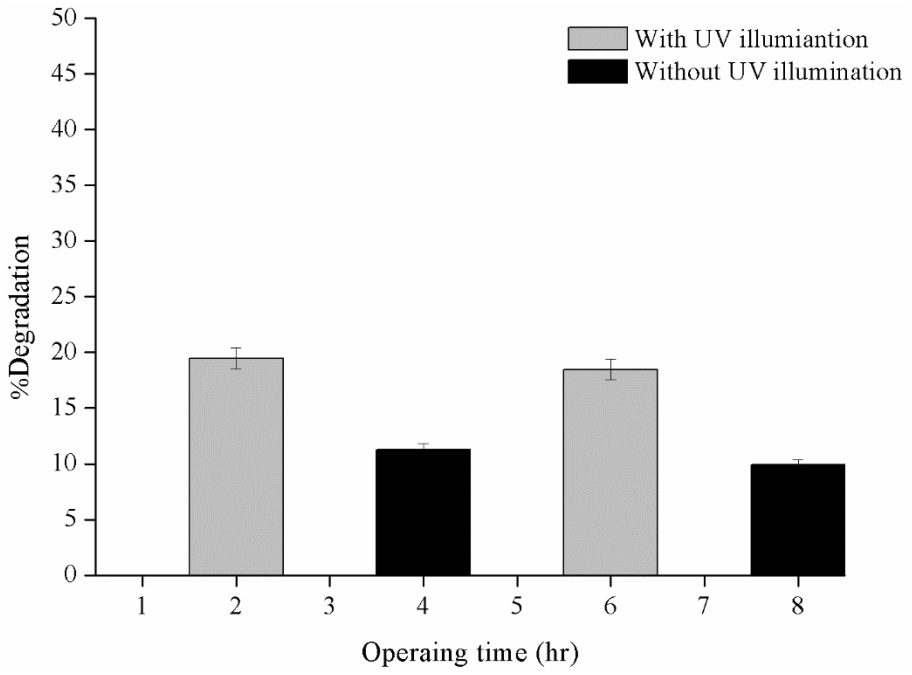

Figure 4.20 Photocatalytic degradation of isopropanol at unadjusted pH by the 600ZnO/TiO_2 film, 8 mol% ZnO, with and without UV illumination.

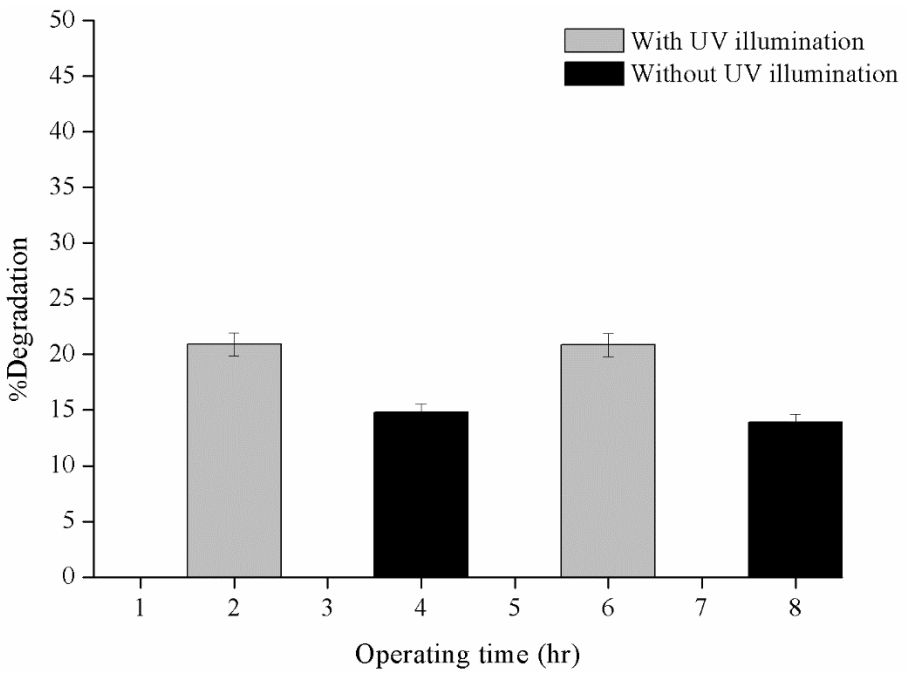

Figure 4.21 Photocatalytic degradation of isopropanol at unadjusted pH by the 600ZnO/TiO_2 film, 15 mol% ZnO, with and without UV illumination.

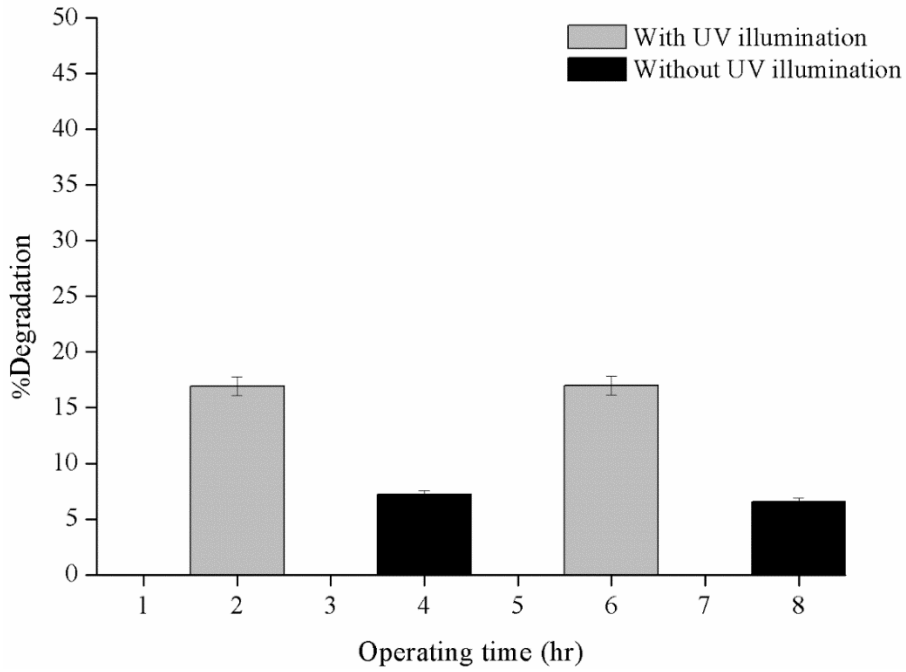

Figure 4.22 Photocatalytic degradation of isopropanol at unadjusted pH by the 600ZnO/TiO_2 film, 19 mol% ZnO, with and without UV illumination.

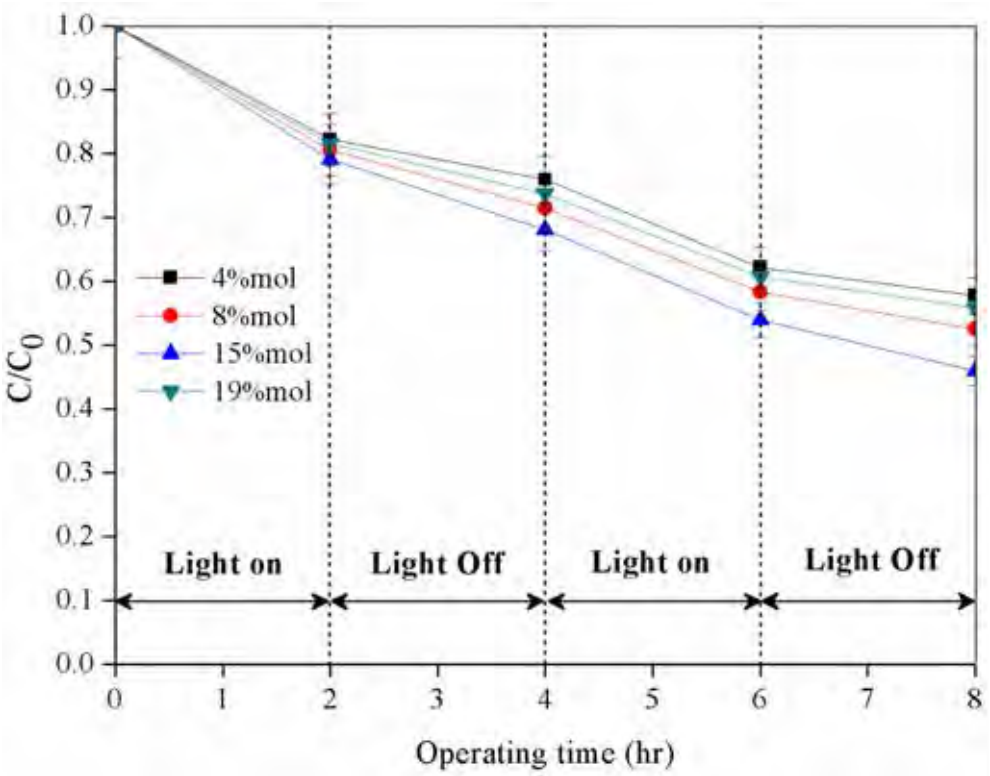

Figure 4.23 Concentration of isopropanol at various time compared with isopropanol initial concentration by the ZnO/ TiO_2 bilayer films with different ZnO loading with and without UV illumination.

Figure 4.23 shows the concentration of isopropanol at various time compared with isopropanol initial concentration and the reaction rate of isopropanol by ZnO/TiO_2 bilayer films with different ZnO loadings, also shown in Table 4.4.

Table 4.4 Reaction rates of isopropanol by the ZnO/TiO_2 bilayer films with different ZnO loading

	Reaction rate ($x10^5$ s^{-1})			
	Operating time (h)*			
	2	**4**	**6**	**8**
4 mol% ZnO	2.47	0.87	1.91	0.61
8 mol% ZnO	2.70	1.26	1.83	0.80
15 mol% ZnO	2.90	1.53	1.97	1.11
19 mol% ZnO	2.57	1.09	1.81	0.67

*The UV illumination was on for two hours (2 h operating time). Then, the illumination was off for two hours (4 h operating time). After that, turning it on for two more hours (6 h operating time) and off for the last two hours (8 h operating time).

The rate of photocatalytic degradation can be expressed by Eq (4.1).

$$r = \frac{d\left(\frac{C}{C_0}\right)}{dt} \qquad (4.1)$$

where r is the rate of reaction (s^{-1}), C is the isopropanol concentration at various times (ppm), C_0 is the isopropanol initial concentration (ppm), and t is the operating time (s). Table 4.4 shows the rate of photocatalytic degradation of isopropanol by using the ZnO/TiO_2 bilayer films with different ZnO loading. It can be clearly seen that the reaction rate with using 15 mol% ZnO is the highest followed by 8, 19, and 4 mol%, respectively.

4.3.7 Effects of ZnO Calcination Temperature of the ZnO/TiO_2 Bilayer Film on the Oxidation Energy Storage

To investigate the optimum oxidation energy storage, ZnO particles were calcined at 400, 500, and 600°C, denoted as 400ZnO/TiO_2, 500ZnO/TiO_2, and 600ZnO/TiO_2, respectively. And the bilayer films were prepared at 15 mol% ZnO loading. Figures 4.24-4.26 show the photocatalytic degradation of isopropanol with the tested catalysts. These experimental results indicate that higher photocatalytic degradation activity is observed in the early stage of reaction, and become lower until at 8 h. This can be ascribed to the photocorrosion phenomenon on the surface of catalyst during the photocatalytic reaction contributed to low degradation efficiency (Feng *et al*., 2014). Moreover, the lower efficiency of photocatalytic degradation can be explained by the low photo-generated electrons and holes precipitated in the reaction (Wang *et al*., 2005).

The results also show that 600ZnO/TiO_2 has the highest photodegradation efficiency. This may be corresponding to the maximum formation of hydroxyl radicals on the ZnO/TiO_2 surface resulted from low recombination of electron-hole pairs, resulting in the destruction of the target pollutant. The hydroxyl radicals are known to be powerful and non-selective oxidizing agent, which are responsible for partial or complete mineralization of several organic chemicals (Pardeshi and Patil, 2009). The 600ZnO/TiO_2 photocatalyst shows the highest crystallite size and high particle size, but low BET surface area. Generally, the BET surface area is considered as a key parameter but, in this research, although the 400ZnO/TiO_2 has the highest surface area, it has the lowest photocatalytic degradation of isopropanol. Di and Haneda (2003) reported that the photocatalytic activity rises with the increase in the crystallinity, but decrease with the BET surface area indicating that crystallinity, rather than BET surface area, played a more important role on the photocatalytic activity. Kodihalli and Timmappa (2012) indicated that the increase in the calcination temperature resulted in the increase in the particle size and in crystallinity, which was helpful to enhance the photocatalytic activity. Muhammad *et al*. (2015) also reported that the nanomaterials, which had higher crystallinity, may provide direct path for the transfer of electron and decrease the charge recombination, thus increasing the efficiency. Furthermore, the higher crystallinity had more

conductive zone in contact with the degrading organic compound to produce a better photocatalytic activity.

Moreover, the photocatalytic degradation from the bilayer films is also higher than TiO_2 and ZnO films. Without illumination, the optimum condition is 600°C, and the highest photocatalytic degradation of isopropanol can be as high as 14.8%. The photocatalytic activity of ZnO/TiO_2 prepared in any other preparation condition is lower than that of 600°C heat treatment.

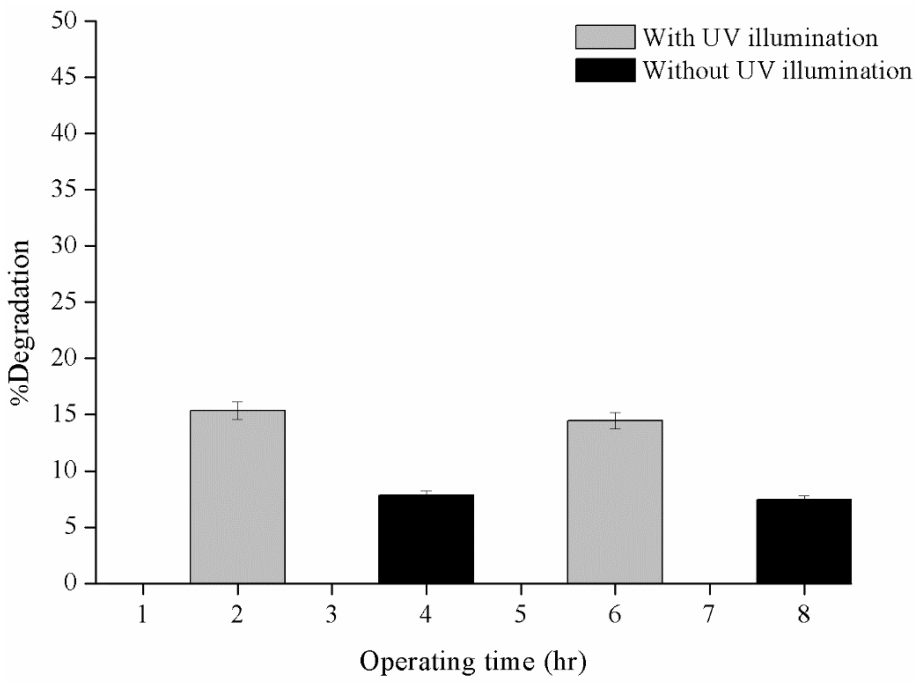

Figure 4.24 Photocatalytic degradation of isopropanol at unadjusted pH by the $400ZnO/TiO_2$ film, 15 mol% ZnO, with and without UV illumination.

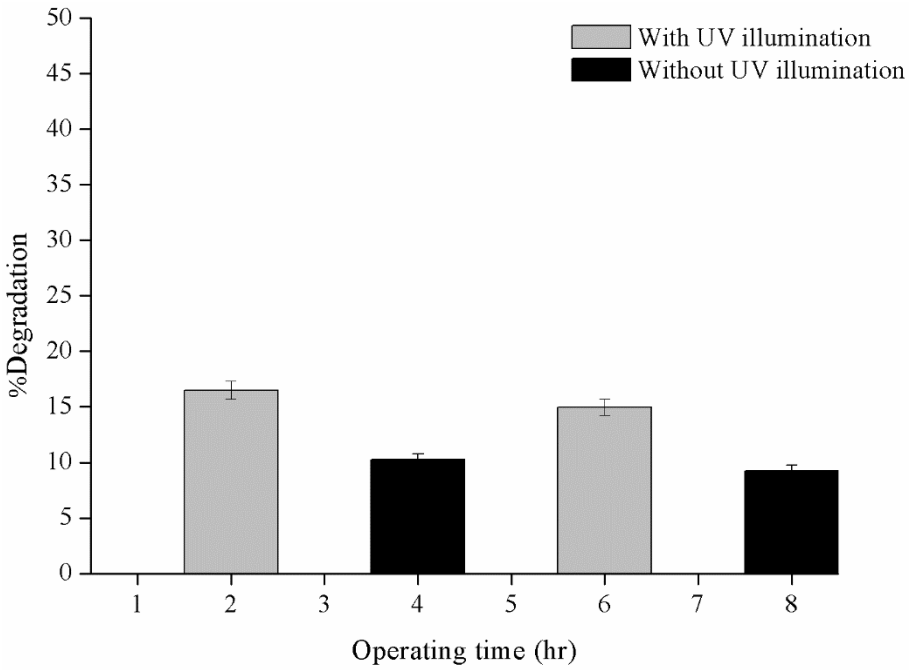

Figure 4.25 Photocatalytic degradation of isopropanol at unadjusted pH by the 500ZnO/TiO_2 film, 15 mol% ZnO, with and without UV illumination.

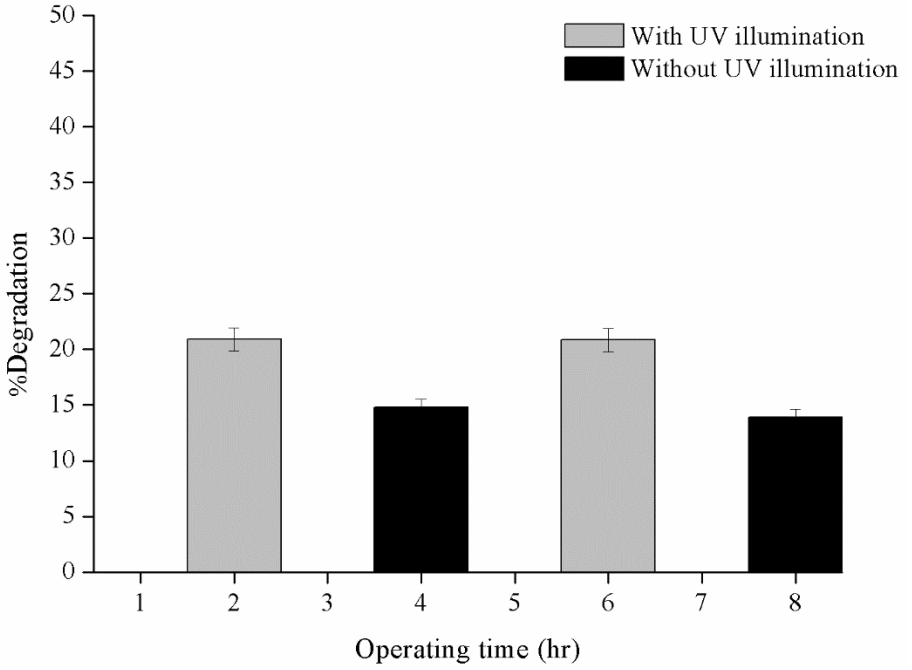

Figure 4.26 Photocatalytic degradation of isopropanol at unadjusted pH by the 600ZnO/TiO_2 film, 15 mol% ZnO, with and without UV illumination.

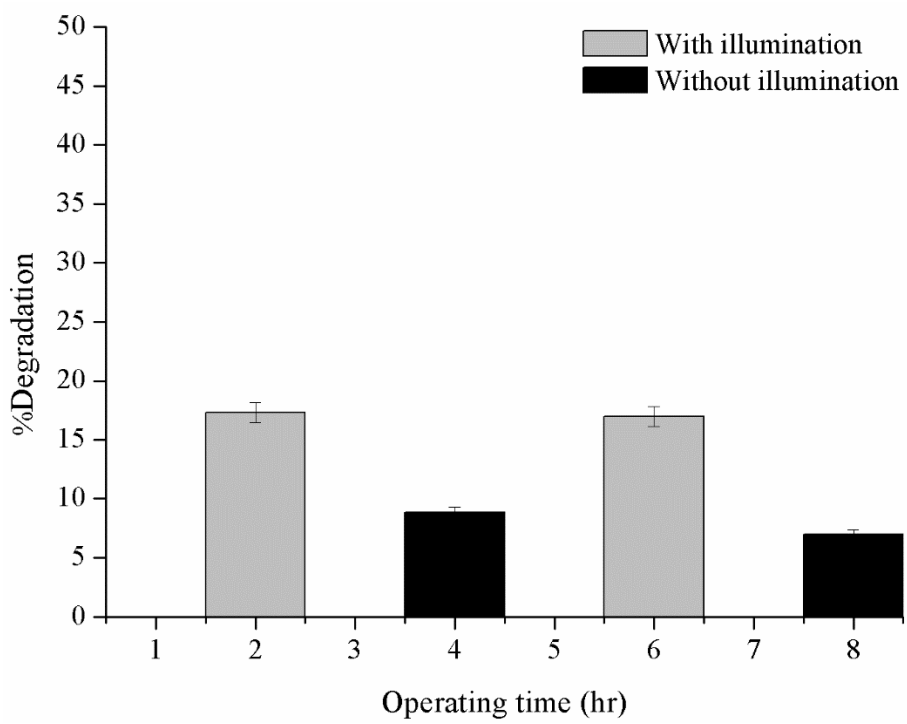

Figure 4.27 Photocatalytic degradation of isopropanol at unadjusted pH by the 700ZnO/TiO_2 film, 15 mol% ZnO, with and without UV illumination.

Figure 4.27 shows the photocatalytic degradation of isopropanol with 700ZnO/TiO_2, it can be seen that when the calcination temperature increases up to 700°C, the degradation becomes lower, which is possibly due to the decrease in specific surface area, pore size and pore volume, and the increase of particle size; hence, the reduction of active sites for the reaction.

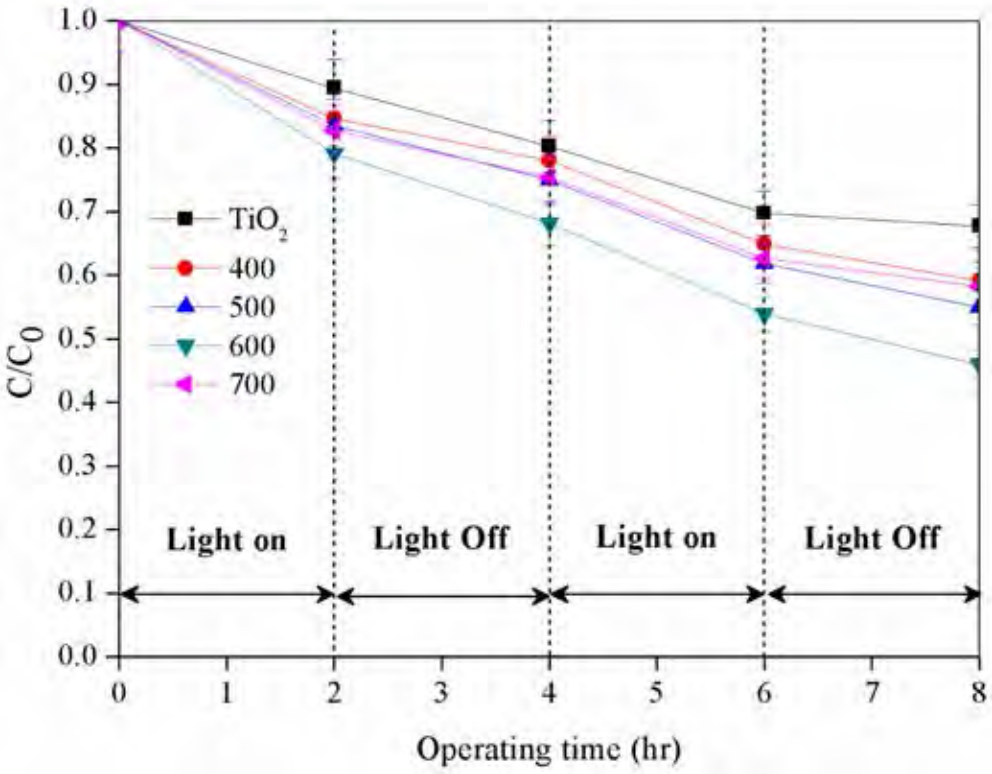

Figure 4.28 Concentration of isopropanol at various time compared with isopropanol initial concentration by the ZnO/TiO_2 bilayer films with different ZnO calcination temperature with and without UV illumination.

Furthermore, Figure 4.28 shows the concentration of isopropanol at various times compared with its initial concentration and the reaction rate of isopropanol by ZnO/TiO_2 bilayer films with different ZnO calcination, also shown in Table 4.5.

Table 4.5 Reaction rates of isopropanol by the ZnO/TiO_2 bilayer films with different ZnO calcination temperatures

	Reaction rate ($x10^5$ s^{-1})			
	Operating time (h)*			
	2	**4**	**6**	**8**
$400ZnO/TiO_2$	2.13	0.92	1.82	0.80
$500ZnO/TiO_2$	2.29	1.19	1.82	0.96
$600ZnO/TiO_2$	2.90	1.53	1.97	1.11
$700ZnO/TiO_2$	2.40	1.02	1.77	0.61

*The UV illumination was on for two hours (2 h operating time). Then, the illumination was off for two hours (4 h operating time). After that, turning it on for two more hours (6 h operating time) and off for the last two hours (8 h operating time).

4.3.8. Photocatalytic degradation of TiO_2, $400ZnO/TiO_2$, $500ZnO/TiO_2$, $600ZnO/TiO_2$, and ZnO Films on the Oxidation Energy Storage

Figure 4.29 shows the photocatalytic degradation on the oxidative energy storage ability of TiO_2, $400ZnO/TiO_2$, $500ZnO/TiO_2$, $600ZnO/TiO_2$, and ZnO films. It can be seen that when the lights are off, the degradation per weight of catalyst loading of $400ZnO/TiO_2$, $500ZnO/TiO_2$, and $600ZnO/TiO_2$ are higher than TiO_2 and ZnO alone. Therefore, the bilayers films contribute to energy storage ability. And, the degradation per weight of loading of $600ZnO/TiO_2$ is higher than $500ZnO/TiO_2$ and $400ZnO/TiO_2$, respectively.

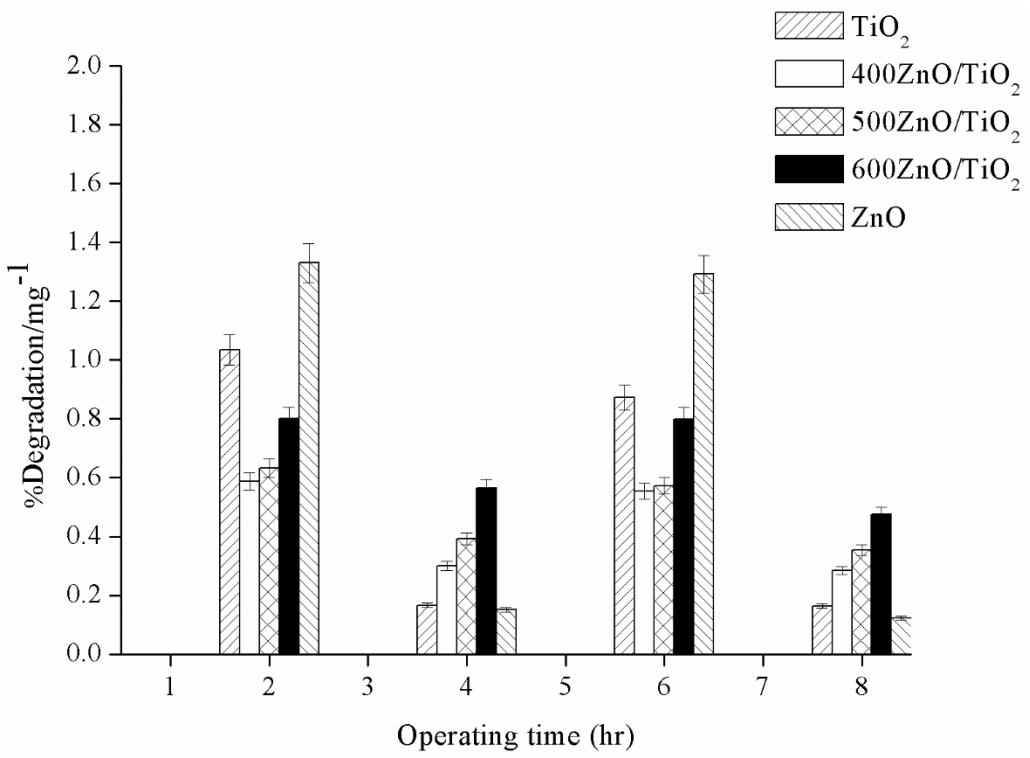

Figure 4.29 Photocatalytic degradation of isopropanol per catalyst loading weight on the oxidation energy storage in unadjusted pH as a function of operating time by the TiO_2, $400ZnO/TiO_2$, $500ZnO/TiO_2$, $600ZnO/TiO_2$, and ZnO films with the UV irradiation for 2 h and turn off 2 h until 8 h.

CHAPTER V
CONCLUSIONS AND RECOMMENDATIONS

5.1 Conclusions

ZnO/TiO_2 bilayer photocatalyst films were prepared by spin coating method to test the photocatalytic degradation of isopropanol and their energy storage. From the photocatalytic activity study, ZnO/TiO_2 showed the highest isopropanol degradation about 74.0%. However, that was not the case when the weight of the film was taken into consideration. Furthermore, the degradation of ZnO/TiO_2 in the unadjusted pH solution was higher than at pH 3.0. From the investigation on the energy storage, 2-hour exposure time showed the best time to store energy to degrade isopropanol without illumination. 15 mol% of $600ZnO/TiO_2$ was found to be optimum and exhibited the best activity in isopropanol degradation at unadjusted pH when there was no illumination. The highest degradation of isopropanol without illumination was about 14.8%. Moreover, when the weight of the films was included, the bilayer films still had the highest activity when there was no illumination.

5.2 Recommendations

From this study, the following recommendations are suggested:

1. Find other p-type semiconductors that could improve the efficiency of photocatalyst to degrade organic compounds during the reaction without illumination.
2. Use ZnO/TiO_2 bilayer films to degrade other organic compounds.
3. Use mixed of TiO_2 and ZnO in one layer to degrade organic compound

REFERENCES

Adriana, Z. (2008) Doped-TiO_2: A Review. Recent Patents on Engineering, 2(3), 157-164.

Akpan, U.G. and Hameed, B.H. (2009) Parameters affecting the photocatalytic degradation of dyes using TiO_2-based photocatalysts: A review. Hazardous Materials, 170(1), 520-529.

Amalina, A., Sulfan, S., and Jaganatthan, K. (2017) Effect of calcination temperature on ZnO/TiO_2 composite in photocatalytic treatment of phenol under visible light. Analytical Sciences, 21(1), 173-181.

Amini, M. and Ashrafi, M. (2016) Photocatalytic degradation of some organic dyes under solar light irradiation using TiO_2 and ZnO nanoparticles. Nanochemistry Research, 1(1), 79-86.

Angelo, J., Andrade, L., Madeira, M.L., and Mendes, A. (2013) An overview of photocatalytic phenomena applied to NO_x abatement. Environmetal Management, 129(11), 522-539.

Bahadur, H., Srivastava, A.K., Sharma, R.K., Chandra, S. (2006) Morphologies of sol–gel derived thin films of ZnO using different precursor materials and their nanostructures. Nanoscale Research Letters, 2(4), 469-475.

Bahnemann, D.W., Kormann, C., and Hoffmann, M.R. (1987) Preparation and characterization of quantum size zinc oxide: a detailed spectroscopic study, Physical Chemistry, 91(14), 3789-3798.

Bansal, P., Bhullar, N., and Sud, D. (2009) Studies on photodegradation of malachite green using TiO_2/ZnO photocatalyst. Desalination and Water treatment, 12(5), 108-113.

Barakat, N.A.M., Kanjwai, M.A., Chronakis, I.S., and Kim, H.Y. (2013) Influence of temperature on the photodegradation process using Ag-doped TiO_2 nanostructures: negative impact with the nanofibers. Molecular Catalysis A Chemical, 366(12), 333-340.

Bhatkhande, D.S., Pangarkar, V.G., and Beenackers, A. (2001) Photocatalytic degradation for environmental applications - a review Chemical Technology and Biotechnology, 77(1), 102-116.

Bickley, R.I., Munuera, G., and Stone, F.S. (1973) Photoadsorption and photocatalysis at rutile surfaces. Part II: Photocatalytic oxidation of isopropanol. Catalysis, 3(3), 398-407.

Boroski, M., Rodrigues, A.C., Garcia, J.C., Sampaio, L.S., Nozaki, J., and Hioka, N. (2009) Combined electrocoagulation and TiO_2 photoassisted treatment applied to wastewater effluents from pharmaceutical and cosmetic industries. Hazardous Materials, 162(4), 448-454.

Braslavsky, S.E. (2007) Glossary of terms used in photochemistry. International union of pure and applied chemistry, organic and biomolecular chemistry division, subcommittee on photochemistry. Pure Applied Chemistry, 79(3), 293-465.

Burkhart, K. and Kulig, K. (1990) The other alcohols: methanol, ethylene glycol, and isopropanol. Emergency Medicine Clinics of North America, 8(4), 913-928.

Cao, Y., Cao, Y., Yu, Y., Zhang, P., Zhang, L., and He, T. (2013) An enhanced visible-light photocatalytic activity of TiO_2 by nitrogen and nickel-chlorine modification. Separation and Purification Technology, 104(2), 256-262.

Chavadej, S., Phuaphromyod, P., Gulari, E., Rangsunvigit, P., and Sreethawong, T. (2008) Photocatalytic degradation of 2-propanol by using Pt/TiO_2 prepared by microemulsion technique. Chemical Engineering Journal, 137(3), 489-495.

Chen, X. and Mao, S.S. (2007) Titanium dioxide nanomaterials: synthesis, properties, modifications, and applications. Chemical Reviews, 107(8), 2891-2959.

Chen, D., Ouyang, S., and Ye, J. (2009). Photocatalytic degradation of isopropanol over $PbSnO_3$ nanostructure under visible light irradiation. Nanoscale Research Letters, 4(1), 274-280.

Coronado, J., Fresno, F., Hernandez, A., M.D., and Portela, R. (Eds). (2008) Design of advanced photocatalytic materials for energy and environmental applications. Green Energy and Technology, 8(2), 1-3.

Dai, G., Liu, S., Liang, Y., and Luo, T. (2013) Synthesis and enhanced photoelectrocatalytic activity of p-n junction Co_3O_4/TiO_2 nanotube arrays. Applied Surface Science, 264(3), 157-161.

David, B.M. (2001) Thin-film deposition of organic-inorganic hybrid materials. Chemistry of Materials, 13(10), 3283-3298.

Di, L. and Haneda, H. (2003) Morphologies of zinc oxide particles and their effects on photocatalysis. Chemosphere, 51(9), 129-137.

Feng, C., Li, G., Ren, P., Wang, Y., Huang, X., and Li, D. (2014) Effect of photo-corrosion of Ag_2CO_3 on visible light photocatalytic activity of two kind of Ag_2CO_3/TiO_2 prepared from different precursors. Applied Catalysis B: Environmental, 158(10), 224-232.

Fujishima, X. and Zhang, C.R. (2006) Titanium dioxide photocatalyst: present situation and future approaches. Comptes Rendus Chimie, 9(5-6), 750-760.

Garcia, M.J., Domenech X., Garcia H.J.A., Torrades F., and Peral J. (2008) The testing of several biological and chemical coupled treatments for Cibacron Red FN-R azo dye removal. Hazardous Material, 154(1-3), 484-490.

Gaya, U.I. and Abdullah, A.H. (2008) Heterogeneous photocatalytic degradation of organic contaminants over titanium dioxide: A review of fundamental, progress and problems. Photochemistry and Photobiology C: Photochemistry Reviews, 9(1), 1-12.

Gianluca, L.P., Bono, A., Krishnaiah, D., Collin, JG. (2008) Preparation of titanium dioxide photocatalyst loaded onto activated carbon support using chemical vapor decomposition: A review paper. Hazardous Material, 157(4), 209-219.

Giuseppe, M., Vincenzo, A., Maria, J. L.M., Cristina, M., Leonardo, P., Vicente, R., Mario, S., Richard, J.D.T., and Anna, M.V. (2001) Preparation characterization and photocatalytic activity of polycrystalline ZnO/TiO_2 systems. Physical Chemistry, 105(11), 1033-1040.

Gnanaprakasam, A., Sivakumar, V. M., and Thirumarimurugan, M. (2015) Influencing parameters in the photocatalytic degradation of organic effluent via nanometal oxide catalyst: A review. Materials Science, 4(1), 1-16.

Hoffmann, M.R., Martin, S.T., Choi, W., and Bahnemann, D.W. (1995) Environmental applications of semiconductor photocatalysis. Chemical Reviews, 95(12), 69-96.

Huang, M., Xu, C., Wu, Z., Huang, Y., Lin, J., and Wu, J. (2008) Photocatalytic discolorization of methyl orange solution by Pt modified TiO_2 loaded on natural zeolite. Dyes and Pigments, 77(2), 327-334.

Jian, R.S., Wang, T.Y., Song, L.Y., Kuo, C.Y., Tian, W.C., Lo, E.W., and Lu, C.J. (2015) Field investigations and dynamic measurements of process activity induced VOCs inside a semiconductor cleanroom. Building and Environmental, 94(4), 287-295.

Jing, L.Q., and Xu, Z.L. (2003) Photoactivity of ZnO and TiO_2 particles and their deactivation and regeneration. Catalyst, 24(6), 175-180.

Kimball, C., and Dowden, D.A. (1978) Specialist periodical reports "Catalysis volume 2. Royal Society of Chemistry.

Kisch, H. (2013) Semiconductor photocatalysis-mechanistic and synthetic aspects. Angewandte Chemie International Edition, 52(8), 12-47.

Kodihalli, G.C. and Thimmappa, V.V. (2012) Electrochemical synthesis and photocatalytic property of zinc oxide nanoparticles. Nano-Micro Letter, 4(1), 14-24.

Konstantinou, K.I. and Albanis, A.T. (2004) TiO_2-assisted photocatalytic degradation of azo dyes in aqueous solution: kinetic and mechanistic investigations. Applied Catalysis, 49(2), 1-14.

Konyar, M., Yatmaz, H.C., and Ozturk, K. (2012) Sintering temperature effect on photocatalytic efficiencies of ZnO/TiO_2 composite plates. Applied Surface Science, 258(11), 7440-7447.

Lan, Y., Lu, Y., and Ren, Z. (2013) Mini review on photocatalysis of titanium dioxide nanoparticles and their solar applications. Nano Energy, 2(5), 1031-1045.

Leonard, G.L.M., Malengreaux, C.M., Melotte, Q., Lambert, S.D., Bruneel, E., Driessche, I.V., and Heinrichs, B. (2016) Doped sol-gel films vs. powders TiO2: on the positive effect induced by the presence of a substrate. Environmental Chemical Engineering, 4(13), 449-459.

Lewkowicz, A., Synak, A., Grobelna, B., Bojarski, P., Bogdanowicz, B., Karczewski, J., Szczodrowski, K., and Behrendt, M. (2014) Thickness and structure change of titanium(IV) oxide thin films synthesized by sol-gel spin coating method. Optical Material, 36(8), 1-6.

Liao, S., Donggen, H., Yu, D., Su, Y., and Yuan, G. (2004) Preparation and characterization of ZnO/TiO_2, $SO_4^{2-}/ZnO/TiO_2$ photocatalyst and their photocatalysis. Photochemistry and Photobiology A: Chemistry, 168(1),7-13.

Lian, H.Q., Wang, J.-M., Xu, L., Zhang, L.Y., Shao, H.B., Zhang, J.Q., and Cao, C.N. (2011) Oxidative energy storage behavior of a porous nanostructured TiO_2-$Ni(OH)_2$ bilayer photocatalysis system. Electrochimica Acta, 56(2), 2074-2080.

Lin, S.H. and Kiang, C.D. (2003) Combined physical, chemical and biological treatments of wastewater containing organics from a semiconductor plant. Hazardous Materials, 97(5), 159-171.

Liu, X., Jin, Z., Bu, S., and Yin, T. (2005) Influences of solvent on properties of TiO_2 porous films prepared by a sol-gel method from the system containing PEG. Sol-Gel Science and Technology, 36(7), 103-111.

Lu, K.T., Nguyen, V.H., Yu, Y.H., Yu, C.C., Wu, J.C.S., Chang, L.-M., and Lin, A.Y.C. (2016a) An internal-illuminated monolith photoreactor towards efficient photocatalytic degradation of ppb-level isopropyl alcohol. Chemical Engineering Journal, 296(1), 11-18.

Lu, Y., Khan, S., Song, C.L., Wang, K.K., Yuan, G.Z., Li, W., Han, G.R., and Liu, Y. (2016b) Doping concentration effects upon column-structured $Nb:TiO_2$ for transparent conductive thin films prepared by a sol-gel method. Alloys and Compounds, 663(15), 413-418.

Luo, Q., Li, X., Wang, D., and An, J. (2011) Photocatalytic activity of polypyrrole/TiO_2 nanocomposites under visible and uv light. Material Science, 46(3), 1646-1654.

Meacock, G., Taylor, K.D.A., Khowles, and Himonides M., A. (1997) The improved whitening of minced cod fish using dispersed titanium dioxide. Science of Food and Agriculture. 73(2), 221-225.

Mills, A., Davies, R.H., and Worsley, D. (1993) Water purification by semiconductor photocatalysis. Chemical Society Reviews, 22(3), 417-425.

Ming, G.E., Changsheng, G.., Xingwang, Z., Liki, M.A., Zhenan, H., Wei, H., and Yuqiu, W. (2009) Photocatalytic degradation of methyl orange using ZnO/TiO_2 composites. Frontiers of Environmental Science & Engineering in China, 3(3), 271-280.

Muhammad, A.J., Rana, A.A., Abdulrahman, A.A., and Umair, M. (2015) Photocatalysis and bandgap engineering using ZnO nanocomposites. Advanced in Materials Science and Engineering, 54(4), 113-117.

Ngaotrakarnwiwat, P. (2013) Energy storage materials for use as photocatalysts in the dark: A review. Materials for Energy Storage Nanomaterials, 12(1), 1-4.

Ohtani, B. (2014) Revisiting the fundamental physical chemistry in heterogeneous photocatalysis: its thermodynamics and kinetics. Physical Chemistry Chemical Physics, 16(4), 1788-1797.

Oshani, F., Marandi, R., Rasouli, S., and FarHoud, M.K. (2014) Photocatalytic investigations of TiO_2-P25 nanocomposite thin films prepared by peroxotitanic acid modified sol-gel method. Applied Surface Science, 311(13), 308-313.

Pardeshi, S.K. and Patil, A.B. (2009) Effect of morphology and crystallite size solar photocatalytic activity of zinc oxide synthesized by solution free mechanochemical method. Molecular Catalysis A, 308(7), 32-40.

Pelaez, M., Nolan, N.T., Pillai, S.C., Seery, M.K., Falaras, P., Kontos, A.G., Dunlop, P.S.M., Hamilton, J.W.J., Byrne, J.A., OShea, K., Entezari, M.H., and Dionysiou, D.D. (2012) A review on the visible light active titanium dioxide photocatalysts for environmental applications. Applied Catalysis B: Environmental, 125(11), 331-349.

Perez-Gonzalez, M., Tomas, S.A., Morales-Luna, M., Arvizu, M.A., and Tellez-Cruz, M.M. (2015) Optical, structural, and morphological properties of photocatalytic TiO_2-ZnO thin films synthesized by the sol-gel process. Thin Solid Films, 594(15), 304-309.

Rauf, M.A., Meetani, M.A., and Hisaindee, S. (2011) An overview on the photocatalytic degradation of azo dyes in the presence of TiO_2 doped with selective transition metals. Desalination, 276(8), 13-27.

Rohani, A.A., Salehi, A., Tabrizi, M., Manafi, S.A., and Fardafshari, A. (2010) Synthesis of ZnO nanostructures via gel-casting method. Chemical, Molecular, Nuclear, Material and Metallurgical Engineering, 4(11), 720-723.

Roland, M. (2014) Semiconductor composites: strategies for enhancing charge carrier separation to improve photocatalytic activity. Advanced Functional Material, 24(3), 2421-2440.

Sakthivel, S., Neppolian, B., Shankar, M.V., Arabindoo, B., Palanichamy, M., and Murugesan, V. (2003) Solar photocatalytic degradation of azo dye: comparison of photocatalytic efficiency of ZnO and TiO_2. Solar Energy Materials and Solar Cell, 77(6), 65-82.

Salazar, C. and Nanny, M.A. (2010) Influence of hydrogen bonding upon the TiO_2 photooxidation of isopropanol and acetone in aqueous solution. Journal of Catalysis, 269(2), 404-410.

Sathishkumar, P., Mangalaraja, R.V., Anandan, S., and Ashokkumar, M. (2013) $CoFe_2O_4/TiO_2$ nanocatalysts for the photocatalytic degradation of Reactive Red 120 in aqueous solutions in the presence and absence of electron acceptors. Journal of Chemical Enigineering, 16(4), 844-849.

Serpone, N. and Salinaro, A. (1999) Terminology, relative photonic efficiencies and quantum yields in heterogeneous photocatalysis. Part I: suggested protocol. Pure Applied Chemistry, 71(2), 303-320.

Shan, Y.A., Ghazi, I.T., and Rashid, A.S. (2010) Immobilisation of titanium dioxide onto supporting materials in heterogeneous photocatalysis: A review. Applied Catalysis A: General, 389(1-2), 1-8.

Shifu, C., Wei, Z., Wei, L., and Sujuan, Z. (2008) Preparation, characterization and activity evaluation of p-n junction photocatalyst p-ZnO/n-TiO_2. Applied Surface Science, 255(4), 2478-2484.

Sun, J., Qiao, L., Sun, S., and Wang, G. (2008) Photocatalytic degradation of Orange G on nitrogen-doped TiO_2 catalysts under visible light and sunlight irradiation. Hazardous Materials, 155(2), 312-319.

Takahashi, Y., Ngaotrakanwiwat, P., and Tatsuma, T. (2004) Energy storage ability TiO_2-MoO photocatalysts. Electrochemica Acta, 49(5), 2025-2029.

Takahashi, Y. and Tatsuma, T. (2005) Oxidative energy storage ability of a TiO_2-$Ni(OH)_2$ bilayer photocatalyst. Langmuir, 21(26), 12357-12361.

Tatsuma, T., Saitoh, S., Ohko, Y., and Fujishima, A. (2001) TiO_2-WO_3 photoelectrochemical anti-corrosion system with an energy storage ability. Chemistry of Materials, 13(2), 2838-2842.

Tatsuma, T., Saitoh, S., Ngaotrakanwiwat, P., Ohko, Y., and Fujishima, A. (2002) Energy storage of TiO_2-WO_3 photocatalysis systems in the gas phase. Langmuir, 18(7), 7777-7779.

Tian, B., Li, C., Gu, F., Jiang, H., Hu, Y., and Zhang, J. (2009) Flame sprayed V-doped TiO_2 nanoparticles with enhanced photocatalytic activity under visible light irradiation. Chemical Engineering Journal, 151(13), 220-227.

Vinita, M., Dorathi, R.P.J., and Palanivelu, K. (2010) Degradation of 2,4,6-trichlorophenol by photo Fenton's like method using nano heterogeneous catalytic ferric ion. Solar Energy, 84(9), 1613-1618.

Wang, Z-P., Xu, J., Cai, W-M., Zhou, B-X., He, Z-G., Cai, C-G., and Hong, X-T. (2005) Visible light induced photodegradation of organic pollutants on nitrogen and fluorine co-doped TiO_2 photocatalyst. Environment Sciences, 17(1), 76-80.

Wang, L. and Egerton, T.A. (2013) The influence of chromium on photocatalysis of propan-2-ol and octadecanoic acid oxidation by rutile TiO_2. Photochemistry and Photobiology A: Chemistry, 252(21), 211-215.

Wu, Y., Xing, M., Tian, B., Zhang, J., and Chen, F. (2010) Preparation of nitrogen and fluorine co-doped mesoporous TiO_2 microsphere and photodegradation of acid orange 7 under visible light. Chemical Engineering Journal, 162(2), 710-717.

Xiong, L.B., Ouyang, M.L., Yan, L.L., Li, J.L., Qiu, M.Q., and Yu, Y. (2009) Visible-light energy storage by Ti^{3+} in TiO_2/Cu_2O bilayer film. Chemistry Letters, 38(4), 1154-1155.

Yamashita, H., Harada, M., and Misaka, J. (2001) Application of ion beam techniques for preparation of metal ion-implanted TiO_2 thin film photocatalyst available under visible light irradiation: Metal ion-implantation and ionized cluster beam method. Journal Synchrotron Radical, 8(1), 569-571.

Yang, F., Takahashi, Y., Sakai, N., and Tatsuma, T. (2010) Oxidation of methanol and formaldehyde to CO_2 by a photocatalyst with an energy storage ability. Phys Chem Chem Phys, 12(19), 5166-5170.

Yasomanee, J.P. and Bandara, J. (2008) Multi-electron storage of photoenergy using Cu_2O-TiO_2 thin film photocatalyst. Solar Energy Materials and Solar Cells, 92, 348-352.

Yu, J., Yu, H., Cheng, B., Zhou, M., and Zhao, X. (2006) Enhanced photocatalytic activity of TiO_2 powder (P25) by hydrothermal treatment. Molecular Catalysis A, 253(1), 112-118.

Zelmanov, G. and Semiat, R. (2008) Phenol oxidation kinetics in water solution using iron(3)-oxide-based nano-catalysts. Water Research, 42(14), 3848-3856.

Zhang, Z., Yuan, Y., Fang, Y., Liang, L., Ding, H., and Jin, L. (2007). Preparation of photocatalytic nano-ZnO/TiO_2 film and application for determination of chemical oxygen demand. Talanta, 73(7), 523-528.

Zhao J. and Yang, X. (2003) Photocatalytic oxidation for indoor air purification: A literature review. Building and Environment, 38(5), 645-654.

Zhao, J., Chen, C., and Ma, W. (2005) Photocatalytic degradation of organic pollutants under visible light irradiation. Topics in Catalysis, 35(1), 269-278.

Znaidi, L., Tou, T., Vrel, D., Soude, N., Ben, Y.S., Brinza, O., Fischer, A. and Boudrioua, A. (2012) ZnO Thin Films Synthesized by Sol-Gel Process for Photonic Applications. Proceedings of the International Congress on Advances in Applied Physics and Materials Science, 121(1), 165-168.

Zulkiflee, N.S., Hussin, R., Halim, J., Ibrahim, M.I., Zainal, M.Z., Nizam, S., and Rahman, S.A. (2016) Characterization of TiO_2, ZnO, and TiO_2/ZnO thin films prepared by sol-gel method. Journal of Engineering and Applied Sciences, 11(12), 7633-7637.

Chemical Book. "Isopropanol." CAS DataBase List. 11 November 2014. 29 March 2016. <http://www.chemicalbook.com/ChemicalProductProperty_EN_CB8854102.htm>

New Jersey Department of Health. "Isopropyl Alcohol." Hazardous Substance Fact Sheet. April 2011. 14 March 2016. <http://nj.gov/health/eoh/rtkweb/documents/fs/1076.pdf>

Physics and Radio-Electronics. "P-N Junction." Semiconductor diodes. June 2013. 29 March 2016. <http://www.physics-and-radio-electronics.com>

Sohrab, A.K., Soghra, M., and Arash, N. "Solar Cells-New Approaches and Reviews." Chapter8: Inorganic-Organic Perovskite Solar Cells. July 2010. 29 May 2016. <http://www.intechopen.com/books/solar-cells-new-approaches-andreviews /inorganic-organic-perovskite-solar-cells>

The Dow Chemical Company. "Isopropanol, Material Safety Data Sheet." Product Safety Assessment. January 2008. 8 November 2011. 14 March 2016. <www.dow.com /webapps/msds/ msdssearch.aspx>

Umar, M. and Aziz, H.A. "Photocatalytic degradation of organic pollutants in water." Chapter 8: Organic pollutants-monitoring, risk and treatment. March 2013. 9 June 2016. <http://dx.doi.org/10.5772/53699>

APPEDICES

Appendix A Standard X-ray Diffraction Powder Patterns of TiO_2

PDF Card No.: 00-001-0562 Quality:B

Sub-File Name:	Inorganic, Mineral, Alloy&Metal, Pharmaceutical,
Formula:	Ti O2
Name:	Anatase I/Ic (RIR)= —
Crystal System:	Tetragonal Space Group: I41/amd(141) Dmeas: 3.900
Cell Parameters:	a= 3.7300 b= 3.7300 c= 9.3700
	Alpha= 90.000 Beta= 90.000 Gamma= 90.000
	Volume= 130.364 Z= 4
Reference:	Hanawalt, J., et al. Anal. Chem. 10(1938)475.
Radiation:	MoKalpha1 Wavelength= 0.70930
2Theta range:	25.28 - 119.00
Database comments:	Additional Patterns: See PDF 00-004-0477. Color: Brown. Deleted Or Rejected By: Deleted by NBS card 00-021-1272. General Comments: T.P. to alpha-anatase at 642 C. To rutile at 915.

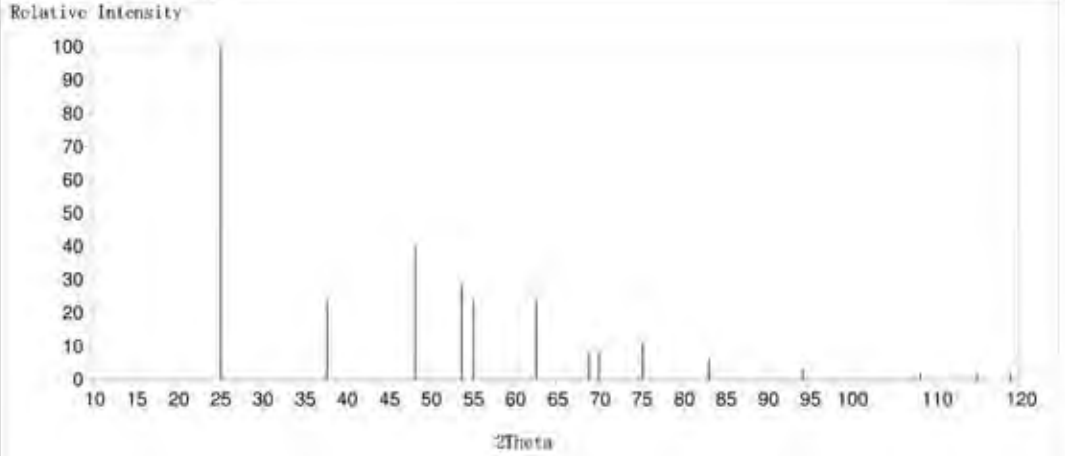

No.	2Theta	d-Value	Intensity	h	k	l	No.	2Theta	d-Value	Intensity	h	k	l
1	25.28	3.520	100.0	1	0	1							
2	37.93	2.370	24.0	1	0	3							
3	48.38	1.880	40.0	2	0	0							
4	53.89	1.700	28.0	1	0	5							
5	55.30	1.660	24.0	1	0								
6	62.73	1.480	24.0	2	1	3							
7	69.00	1.360	8.0	1	1	6							
8	70.18	1.340	8.0	1	1								
9	75.37	1.260	11.0	1	0	7							
10	83.22	1.160	6.0	3	0	3							
11	94.38	1.050	3.0	3	1	4							
12	108.36	0.950	2.0	3	1	6							
13	115.07	0.913	2.0	4	0	2							
14	119.00	0.894	2.0	4	1	1							

Note: 2theta are calculated with wavelength = 1.54059

2017-May-24 10:48:52 Page-1/1

Appendix B Standard X-ray Diffraction Powder Patterns of ZnO

PDF Card No.: 00-003-0888 Quality:B

Sub-File Name: Inorganic, Alloy&Metal, Common Phase, Forensic, Pharmaceutical, Pigment&Dye,

Formula: Zn O

Name: Zinc Oxide I/Ic (RIR)= —

Crystal System: Hexagonal Space Group: P63mc(186) Dmeas:

Cell Parameters: a= 3.2489 b= 3.2489 c= 5.2062

Alpha= 90.000 Beta= 90.000 Gamma= 120.000

Volume= 47.591 Z= 2

Reference: United Steel Companies, Sheffield, England, UK. Private Communication().

Radiation: CoKalpha Wavelength= 1.79020

2Theta range: 31.82 - 116.27

Database comments: Deleted Or Rejected By: Deleted by NBS Set 5. General Comments: Analytical reagent. D-values corrected for absorption.

Relative Intensity

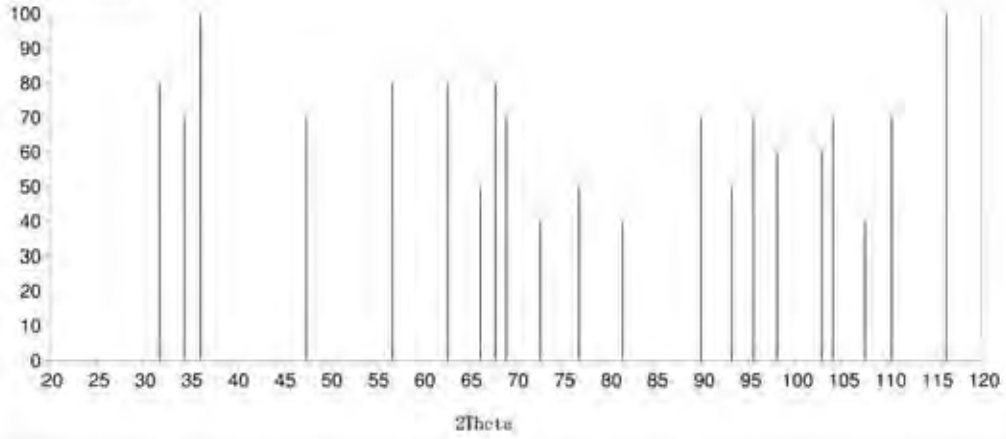

No.	2Theta	d-Value	Intensity	h	k	l	No.	2Theta	d-Value	Intensity	h	k	l
1	31.82	2.810	80.0	1	0	0	21	116.27	0.907	100.0	2	1	3
2	34.47	2.600	70.0	0	0	2							
3	36.19	2.480	100.0	1	0	1							
4	47.57	1.910	70.0	1	0	2							
5	56.78	1.620	80.0	1	1	0							
6	62.73	1.480	60.0	1	0	3							
7	66.29	1.410	50.0	2	0	0							
8	67.88	1.380	80.0	1	1	2							
9	69.00	1.360	70.0	2	0	1							
10	72.67	1.300	40.0	0	0	4							
11	76.81	1.240	50.0	2	0	2							
12	81.51	1.180	40.0	1	0	4							
13	89.93	1.090	70.0	2	0	3							
14	93.22	1.060	50.0	2	0								
15	95.58	1.040	70.0	2	1	1							
16	98.08	1.020	60.0	2	1								
17	102.89	0.985	60.0	2	1	2							
18	104.08	0.977	70.0	1	0	5							
19	107.53	0.955	40.0	2	0	4							
20	110.41	0.938	70.0	3	0	0							

Note: 2theta are calculated with wavelength = 1.54059

2017-May-24 10:50:04 Page-1/1

Appendix C Calculation sample of ZnO loadings on TiO_2 layer

The calculation of ZnO on TiO_2 layer can be calculated by

$$\%\, mol\ ratio = \frac{mol\ ZnO}{mol\ ZnO + mol\ TiO_2}$$

For example;

Weight of the second layer = 0.00125 g

TiO_2 sol (on the second layer) = 0.0015 g

∴ ZnO on the second layer = 0.0015 – 0.00125 = 0.00025 g

TiO_2 (on the first layer) = 0.004 g

∴ The amount of TiO_2 total film = 0.0015 + 0.004 = 0.0055 g

From the mol ratio equation;

Mw of TiO_2 = 79.866

Mw of ZnO = 81.408

$$\text{Mol ratio} = \frac{\frac{0.00025}{81.408}}{\frac{0.00025}{81.408}+\frac{0.0055}{79.866}} = 0.0427 = 4\ \text{mol\% of ZnO per total film}$$

And the other mol% of ZnO per total film can be calculated by the same with this equation.

CURRICULUM VITAE

Name: Ms. Ratchawan Jarumanee

Date of Birth: November 25, 1992

Nationality: Thai

University Education:

2011-2014 Bachelor Degree of Industrial Chemistry, Faculty of Science, Chiang Mai University, Chiang Mai, Thailand

Work Experience:

2013-2013	Position:	Internship Student (Quality Assurance)
	Company name:	Thai Parkerizing Company Limited, Rayong, Thailand

Proceedings:

1. Jarumanee, R., Rangsunvigit, P., and Ngaotrakanwiwat, P. (2017, May 23) Study on energy storage ability of ZnO/TiO_2 for photocatalytic degradation of isopropanol. Proceedings of The 8th Research Symposium on Petrochemical and Material Technology and The 23rd PPC Symposium on Petroleum, Petrochemicals, and Polymers, Bangkok, Thailand.

Presentation:

1. Jarumanee, R., Rangsunvigit, P., and Ngaotrakanwiwat, P. (2017, June 12-15) Synthesis of bilayer films for photocatalytic degradation of isopropanol in the absence of light. Poster Presented at 2nd International Conference on Applied Surface Science (ICASS), Dalian, China.